Two-Color/Two-Dye Planar Laser-Induced Fluorescence Thermography for Temperature Measurements at an Evaporating Meniscus

Zwei-Farb/Zwei-Farbstoff planare laserinduzierte Fluoreszenzthermographie für Messungen an einem verdampfenden Meniskus

Zur Erlangung des akademischen Grades Doktor-Ingenieur (Dr.-Ing.)
genehmigte Dissertation von M.Sc. Andreas J. C. Fenner aus Frankfurt am Main
Tag der Einreichung: 07.08.2017, Tag der Prüfung: 15.11.2017
Darmstadt 2017 — D 17

1. Gutachten: Prof. Dr.-Ing. P. Stephan
2. Gutachten: Prof. Dr. rer. nat. A. Dreizler

TECHNISCHE
UNIVERSITÄT
DARMSTADT

Fachbereich Maschinenbau
Fachgebiet Technische Thermodynamik

Two-Color/Two-Dye Planar Laser-Induced Fluorescence Thermography for Temperature Measurements at an Evaporating Meniscus
Zwei-Farb/Zwei-Farbstoff planare laserinduzierte Fluoreszenzthermographie für Messungen an einem verdampfenden Meniskus

Genehmigte Dissertation von M.Sc. Andreas J. C. Fenner aus Frankfurt am Main

1. Gutachten: Prof. Dr.-Ing. P. Stephan
2. Gutachten: Prof. Dr. rer. nat. A. Dreizler

Tag der Einreichung: 07.08.2017
Tag der Prüfung: 15.11.2017

Darmstadt 2017 — D 17

Danksagung

Diese Arbeit entstand während meiner Tätigkeit als Stipendiat des DFG Graduiertenkollegs 1114 und anschließend als wissenschaftlicher Mitarbeiter am Fachgebiet für Technische Thermodynamik der Technischen Universität Darmstadt unter der Leitung von Herrn Prof. Dr.-Ing. Peter Stephan. Herrn Prof. Dr.-Ing. Peter Stephan gilt mein besonderer Dank für das mir entgegengebrachte Vertrauen und die Schaffung der hervorragenden finanziellen und technischen Ausstattung des Fachgebiets für Technische Thermodynamik. Insbesondere möchte ich mich für die Möglichkeit der Einrichtung eines ausgezeichneten Laserlabors bedanken, in dem ich meiner Forschung nachgehen konnte. Dies hat maßgeblich zum Erfolg meiner wissenschaftlichen Arbeit beigetragen. Herrn Prof. Dr. rer. nat. Andreas Dreizler danke ich für seine sehr guten Vorlesungen *Lasermesstechnik* und *Einführung in die Quantenmechanik und Laserspektroskopie*, welche mir Anstoß zu neuen Lösungsansetzen gaben, sowie für die freundliche Übernahme des Koreferates. Herrn Prof. Dr.-Ing. Cameron Tropea danke ich in seiner Funktion als Sprecher des Graduiertenkollegs 1114 für seine Unterstützung und die Aufnahme als Stipendiat. Für die finanzielle Unterstützung meiner Forschung danke ich der Deutschen Forschungsgemeinschaft.

Für die jederzeit sehr gute Zusammenarbeit möchte ich den Mitarbeitern der mechanischen Werkstatt (Roland Berntheisel, Dirk Feldmann und Matthias Felter) unter der Leitung von Roland Berntheisel danken, die mit ihrer Arbeit zu meiner Forschung beigetragen haben. Danken möchte ich ebenfalls Gaby Gunkel und Heike Kagerbauer für ihre Unterstützung in Verwaltungsangelegenheiten und dem IT Team (Marcus Keiner, Volker Bartsch, Denis Schinko und Marcel Nürnberger) unter der Leitung von Marcus Keiner für ihre schnelle und erfolgreiche Unterstützung in IT Angelegenheiten. Mein besonderer Dank gilt Robert Schrod für seine technische und moralische Unterstützung, die maßgeblich zum Gelingen meiner Arbeit beigetragen hat. Boris Schulmann, Andreas Preusche, Till Pfeiffer, Felix Hromatka, Manuel Winter und Matthias Schäfer möchte ich für ihre Beiträge die sie zu meiner Forschung im Rahmen ihrer Abschlussarbeiten geleistet haben danken.

Meiner Frau Andrea, meinem Vater Thomas und Daniel Ross möchte ich für das Korrekturlesen der vorliegenden Arbeit danken. Meiner Frau Andrea, meiner Mutter Gabriele und meinem Vater Thomas danke ich für ihre moralische Unterstützung, ihre jederzeit offenen Ohren und ihr Verständnis.

–Andreas Fenner
03. August 2017

Contents

Nomenclature

Latin Symbols

Symbol	Description	Unit
C	Dye concentration	molL^{-1}
I	Intensity	Wm^{-2}
l	Path length	cm
R	Ratio of fluorescence signals	-
r	Ratio of fluorescence signals for a single pixel	-
S	Fluorescence signal	arb. unit
s	Fluorescence signal for a single pixel	arb. unit
SNR	Signal-to-noise ratio	-
T	Temperature	K
t	Temperature for a single pixel	K
u	Laser fluence	Jm^{-2}

Greek Symbols

Symbol	Description	Unit
β	Temperature coefficient	K
ε	Molar absorption coefficient	$\mathrm{Lmol}^{-1}\mathrm{cm}^{-1}$
λ	Wavelength	nm
σ	Standard deviation	
Φ	Quantum yield	-
χ^2	Weighted sum of squared deviations	-

Subscripts and Superscripts

Subscript	Description
R	Ratio of fluorescence signals
ref	Reference signal
rel	Relative to reference signal
sat	Saturation
sens	Temperature sensitive signal
T	Temperature

List of Figures

List of Tables

1 Introduction

1.1 Motivation

Evaporation is an interesting technical way to transfer heat, because of the low temperature differences needed to transfer high amounts of heat. Evaporation is widely used as a heat transfer mechanism in technical applications ranging from cooling of microelectronic devices to the generation of electrical power. Therefore evaporation plays a vital role for modern civilization.

Although evaporation processes have been intensively studied in the past decades physical principles underlying the processes are not yet fully understood. Therefore they are not described in a way that allows a prediction of the heat transfer for an arbitrary system. Many correlations can be found in literature which allow a prediction of the heat transfer for special evaporation processes within a limited parameter range in an operating map manner.

In technical applications the performance limits are approached more closely than ever before, because of the need for performance, efficiency, and cost optimization. Therefore predictive tools are needed on the basis of physical principles. In order to gain the needed understanding of the physical principles and to validate numerical modeling and simulation, generic experiments are required.

In the past these experiments were focused on the measurement of temperature distribution on the surface of a heated wall on which the evaporation process takes place. For the understanding of evaporation processes additionally the knowledge of temperature fields in the liquid phase close to the interfaces is of major importance. Measuring such temperature distributions contactlessly with high spatial and temporal resolution is a challenge for measurement technology.

1.2 Objectives

By means of two-color/two-dye planar laser-induced fluorescence thermography (2c/2d PLIF-Thermography), it is possible to measure temperature fields in transparent liquids contactlessly. 2c/2d PLIF-Thermography is an optical measurement technique which utilizes the temperature dependence of the fluorescence intensity of fluorescent dyes dissolved in a liquid. So far, 2c/2d

PLIF-Thermography has mainly been used in the investigation of single-phase processes, e.g. convection and mixing. The extent to which 2c/2d PLIF-Thermography can also be applied to two-phase processes, in particular those in which evaporation takes place and the temperature field near the liquid boundaries is to be measured, has not yet been clarified. Clarifying this is the objective of this work.

1.3 Structure

The work is structured as follows. In chapter two an introduction to the basics of 2c/2d PLIF-Thermography is given followed by a brief summary of the state of the art. The chapter concludes with a summary of open scientific questions arising from the literature study, which form the starting point of this work. In the third chapter the experimental setups and materials used for this work are described along with the procedures used for the experiments and the data evaluation. In chapters four and five the results of the conducted investigations are presented and discussed. In chapter six a summary of the conducted work and the main results are given followed by an outlook concerning open scientific questions arising from the results of this work.

2 State of the Art

In the first two sections of this chapter the basics and the concept of two-color/two-dye planar laser-induced fluorescence thermography are explained along with its application to evaporation processes which can be found in literature. In the following an overview of other spatially resolved temperature measurement techniques regarding their application to stationary evaporating liquid menisci is given. The chapter is concluded with a summary of the open scientific questions this work is dealing with.

Readers who are interested in the basics of quantum mechanics and molecular spectroscopy kindly refer to Atkins and Paulo (2013) – *Physikalische Chemie* [2], chapters 8–13. A detailed overview of fluorescence spectroscopy is given by Valeur (2013) – *Molecular Fluorescence: Principles and Applications* [56], chapters 1–4. Details about the structure and properties of fluorescent dyes can be found in Schäfer (1973) – *Dye Lasers* [49], chapter 5.

2.1 Two-Color/Two-Dye Planar Laser-Induced Fluorescence Thermography

In this section the basics of two-color/two-dye planar laser-induced fluorescence thermography are explained. First an introduction to the measurement method is given. Afterwards the origin of temperature dependence, possible spectral conflicts, linearity assumptions, and photobleaching are examined more closely. Finally overviews of common materials used as well as reported measurement uncertainties and temporal and spatial resolutions are given.

Measurement Method

Planar laser-induced fluorescence thermography (PLIF-Thermography) is based on the temperature dependence of a fluorescence signal of a dissolved fluorescent dye excited by laser light. According to Sakakibara, Hishida, and Maeda [48] the fluorescence intensity I of such dye solutions can be described by

$$I = I_0 \, \varepsilon \, A \, L \, C \, \Phi \tag{2.1}$$

where I_0 is the laser intensity; ε, the molar absorption coefficient at the wavelength of the laser; A, the fraction of light collected; L, the sampling length; C, the concentration of the fluorescent dye; Φ, the temperature-dependent quantum yield. This model contains the assumption that the fluorescence intensity is linear to both concentration and laser intensity. These assumptions are only valid for low laser intensities and low dye concentrations, i.e. low absorption of fluorescence by the dyes on its way to the detector [13, 40, 50, 55].

To eliminate the influence of the laser intensity, Sakakibara and Adrian [46] introduced a ratiometric approach of PLIF-Thermography, where a fluorescent reference signal almost insensitive to temperature is used. Most often, a fluorescence spectrum with a temperature-sensitive part and a temperature-insensitive part is created by the combination of two fluorescent dyes. This kind of PLIF-Thermography is called two-color/two-dye (2c/2d) PLIF-Thermography. In this approach the ratio R which is dependent on temperature is

$$R = \frac{I_{\text{sens}}}{I_{\text{ref}}} = \frac{\varepsilon_{\text{sens}} C_{\text{sens}} \Phi_{\text{sens}}}{\varepsilon_{\text{ref}} C_{\text{ref}} \Phi_{\text{ref}}} \tag{2.2}$$

where the index "sens" is associated with the temperature-sensitive part and the index "ref" with the temperature-insensitive part of the fluorescence spectrum. Fig. 2.1 shows a qualitative illustration of the principles of the 2c/2d PLIF-Thermography. The ratio is independent of the laser intensity if the initial assumption, that the fluorescence intensity is linear to the laser intensity, is valid. With the additional assumption that the fluorescence intensity is linear to the dye concentration the ratio is also independent of the individual dye concentrations C_{sens} and C_{ref} as long as the concentration ratio $C_{\text{sens}}/C_{\text{ref}}$ is constant [46].

Typically a dye with high temperature sensitivity is combined with a dye with low temperature sensitivity. The selection rules for dye combinations based on the overlap of absorption and emission spectra are given by Coppeta and Rogers [14]. In the theoretical ideal case the emission and absorption bands are completely separated spectrally. The absorption bands of the two dyes need to overlap to allow excitation by the same laser. Fig. 2.2a qualitatively illustrates this theoretical case. However, in practice the emission and absorption bands partially overlap with each other. Fig. 2.2b qualitatively shows the common emission and absorption spectra of dye combinations used for 2c/2d PLIF-Thermography.

Spectral Conflicts

Coppeta and Rogers [14] identified three categories of spectral conflicts of absorption and emission bands which could lead to erroneous measurements. The first kind of spectral conflict is

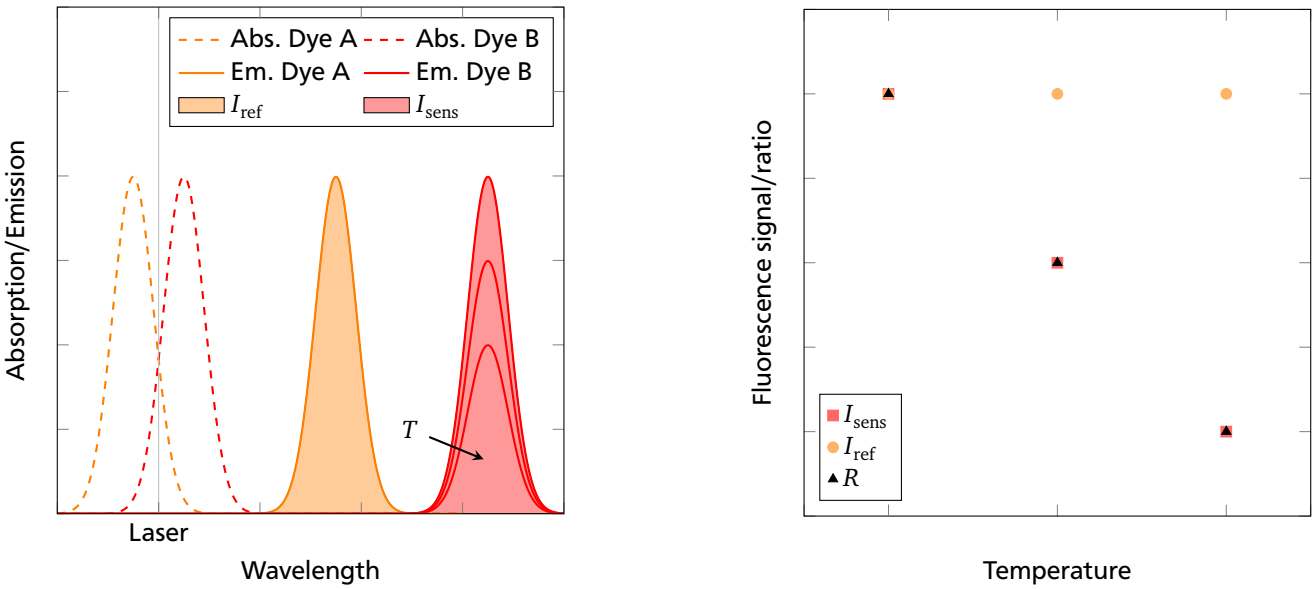

(a) Spectral **(b)** Integral

Figure 2.1: Qualitative illustration of the principles of 2c/2d PLIF-Thermography.

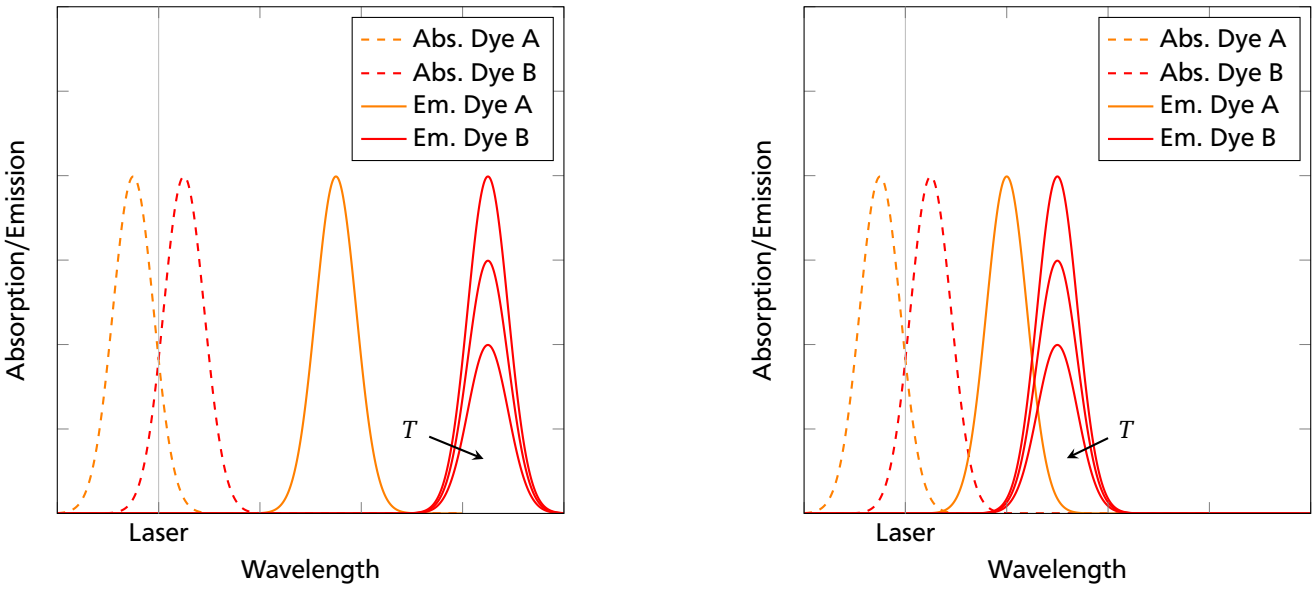

(a) Theoretical **(b)** Practical

Figure 2.2: Qualitative typical emission and absorption spectra for the theoretical and practical case of 2c/2d PLIF-Thermography.

the overlap of emission bands of the two dyes. The fluorescent dyes need to be excitable with the same laser wavelength and usually have broad emission spectra. Thus a certain amount of overlap is observed for all known dye combinations used for 2c/2d PLIF-Thermography. The overlap can make it difficult to separate the fluorescence signals sensitive and insensitive to temperature. The resulting crosstalk can lead to a reduction of the temperature sensitivity. This kind of spectral conflict can be minimized by the choice of the spectral regions used for 2c/2d PLIF-Thermography.

The second kind of spectral conflict is an overlap of the emission and the absorption spectra. For fluorescent dyes a certain amount of overlap of the absorption and emission spectrum is common [56]. This conflict results in a dependence of the fluorescence signal on the amount of absorption in the overlapping region. In this region the validity of the assumption of linear dependence of the fluorescence signal on the dye concentration is questionable and has to be verified for the used dye combination. If possible this spectral region should not be used for 2c/2d PLIF-Thermography.

The third kind of spectral conflict is similar to the second one with the difference that the amount of absorption is dependent on the value to be measured, e.g. temperature itself. Such a conflict can not be corrected and therefore a dye combination which exhibits this kind of spectral conflict can not be used for 2c/2d PLIF-Thermography.

Origin of the Temperature Dependence

Apart from some exceptions, the dependence on temperature of the fluorescence signal is attributed to the dependence of the quantum yield on temperature [1–3, 18, 26, 34, 39, 46, 49, 56, 59]. The quantum yield is the ratio of the emitted versus the absorbed photons. The quantum yield of fluorescent dyes in general is less than unity at room temperature because besides the emission of a photon, a non-radiative deactivation of the electronically excited state (S_1) is also possible. Radiative and non-radiative processes are in competition with each other. Fig. 2.3 shows possible radiative and non-radiative transitions in a Perrin–Jablonski diagram. The excited molecule can go back to the ground state (S_0) via internal conversion of the excited state to an elevated vibrational level of the ground state. From there, the molecule can transfer energy to the surrounding and move to lower vibrational levels by vibrational relaxation. During this process no photon is emitted. Another possibility is that the molecule in the excited singlet state goes to the triplet state (T_1) via intersystem crossing. At room temperature and above commonly no phosphorescence is observed. Due to the long lifetime of the triplet state it is efficiently deactivated non-radiatively by collision of the dye molecule with solvent molecules.

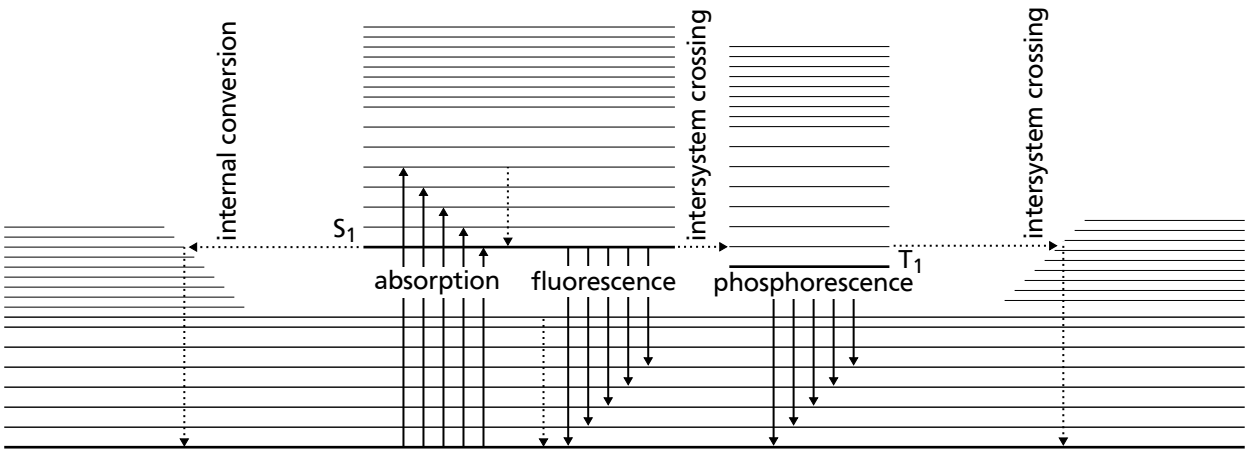

Figure 2.3: Perrin–Jablonski diagram with possible radiative and non-radiative transitions. Illustration based on [56].

Whether the amount of non-radiative deactivation is influenced by temperature or not depends on the rigidity of the dye molecule's structure [49]. The more planar and rigid the structure of the molecule, the less the quantum yield is affected by temperature. In general a higher temperature results in a lower quantum yield, because the non-radiative deactivation processes based on thermal agitation are more efficient at higher temperatures [56]. Also other properties of the surroundings than temperature like polarity, viscosity, pH or oxygen can have a significant influence on the quantum yield. Due to the many possible influencing factors and their unknown amount of influence the prediction of temperature dependence is not possible and therefore has to be determined experimentally. Because of possible simultaneous effects a careful characterization of the fluorescent dyes to be used and an in situ calibration is always necessary for 2c/2d PLIF-Thermography.

Lemoine et al. [39] proposed an equation which describes the temperature dependence of the quantum yield by an exponential function.

$$I_\mathrm{f} = K_\mathrm{opt}\,\varepsilon\,C\,\Phi = K_\mathrm{opt}\,K_\mathrm{spec}\,C\,e^{\frac{\beta}{T}} \tag{2.3}$$

where I_f is the fluorescence signal; K_opt, a constant determined by the optical system; K_spec, a constant determined by the fluorescent dye and the solvent; ε, the molar absorption coefficient at the wavelength of the laser; C, the concentration of the fluorescent dye; Φ, the quantum yield; β, the temperature coefficient; T, the temperature of the dye solution.

As mentioned above for 2c/2d PLIF-Thermography the assumption of a linear relationship between the fluorescence signal and the laser fluence is made. However this assumption is only sufficiently valid up to a certain limit of laser fluence which is dependent on the fluorescent dye and the solvent. Deviations from this assumption for 2c/2d PLIF-Thermography have been reported for various dyes dissolved in water [13, 15, 40, 50, 55]. In the context of fluorescent dyes for laser applications also the deviation from the linear relationship is observed and well known [19, 49]. In general for low laser fluence the relationship between the fluorescence signal and the laser fluence can be described by a linear equation. This region is called the linear regime. For increasing laser fluence the fluorescence signal approaches an upper saturation limit. Fig 2.4 shows the qualitative relationship between the fluorescence signal and the laser fluence of two dyes with different saturation limits.

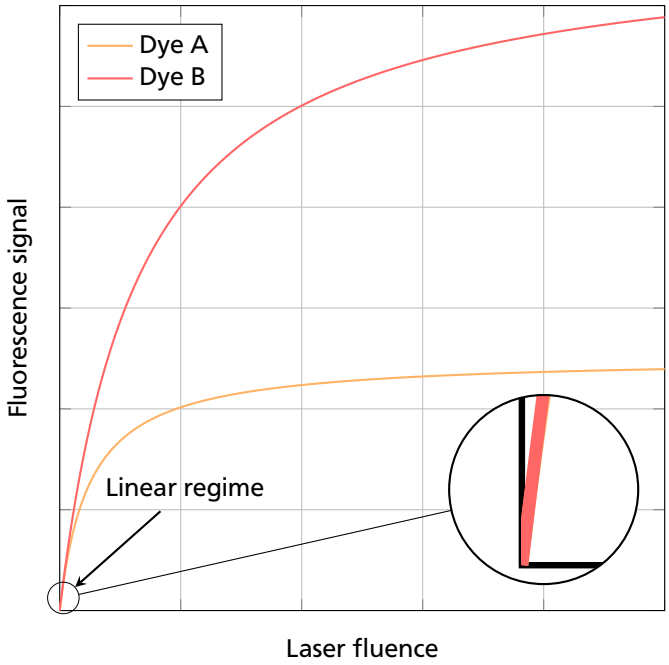

Figure 2.4: Qualitative dependence of the fluorescence signal on the laser fluence of two dyes with different saturation limits.

According to Eckbreth [20] and Lee [37] from a rate equation analysis of a two-level model the following relationship, which describes the fluorescence signal F as a function of the laser spectral irradiance I_ν, can be derived:

$$F = h\,\nu\,\frac{\Omega}{4\pi}\,A\,l\,N_1^0\,\frac{B_{12}}{B_{12}+B_{21}}\,\frac{A_{21}}{1+\frac{I_{\nu,\mathrm{sat}}}{I_\nu}} \tag{2.4}$$

where h is Planck's constant; ν, the frequency of the emitted fluorescence; Ω, the collection solid angle; A, the focal area of the laser beam; l, the axial extent along the beam from which the fluorescence is observed; N_1^0, the species population prior to excitation; B_{12}, Einstein coefficient for stimulated absorption; B_{21}, Einstein coefficient for stimulated emission; A_{21}, Einstein coefficient for spontaneous emission; $I_{\nu,\mathrm{sat}}$, saturation spectral irradiance. At low irradiances compared to the saturation irradiance the relationship can be described by the linear equation with the quenching rate constant Q_{21}:

$$F = \frac{h\,\nu}{c}\,\frac{\Omega}{4\pi} A\,l\,N_1^0\,B_{12}\,I_\nu\,\frac{A_{21}}{A_{21}+Q_{21}} \tag{2.5}$$

The saturation limit is dependent on the dye and the solvent used. Therefore in a 2c/2d PLIF-Thermography application the behavior of the fluorescence signal is not the same for both dyes outside of the linear regime. This contradicts the approach of 2c/2d PLIF-Thermography because outside of the linear regime the ratio is still dependent on the laser fluence. Since there is no predictive model available in literature the linear regime has to be determined experimentally. Furthermore, in the linear regime the behavior is only approximately linear. Therefore, the temperature deviations induced by a change of the laser fluence have to be determined in situ for 2c/2d PLIF-Thermography applications. Additionally to temperature deviations arising from the nonlinear response of the fluorescence signal to a change of the laser fluence, Chaze et al. [13] report a reduction of the dependence on temperature outside the linear regime with increasing laser fluence.

As mentioned above for 2c/2d PLIF-Thermography the assumption of a linear relationship between the dye concentration and the fluorescence signal is made. In literature for all known dyes and their combinations used for 2c/2d PLIF-Thermography a deviation from the assumed linear behavior is reported [13, 36, 38, 50, 55]. For increasing dye concentrations the fluorescence signal developed increasingly underproportional. Only for low concentrations and path lengths is a linear behavior observed. The observed behavior is attributed to the absorption of the fluorescence signal by the fluorescent dyes themselves. Since all known dye combinations used for 2c/2d PLIF-Thermography exhibit some degree of a spectral conflict of the second kind, which is an overlap of the absorption and the emission band, the assumption of a linear behavior is only valid under optically thin conditions. In other words the product of the path length through the dye solution, the dye concentration, and the absorption coefficient, i.e. the absorbance, has to be so low that absorption of the fluorescence signal is negligible.

According to Lemoine, Wolff, and Lebouche [38] the fluorescence signal S_f versus the molar dye concentration C can be described by the Beer–Lambert law:

$$S_f = K_{\text{opt}} V_c I_0 \Phi \varepsilon_1 C e^{-C \varepsilon_2 l} \tag{2.6}$$

where K_{opt} is a constant determined by the optical system; V_c, the collection volume; I_0, the intensity of the laser beam; Φ, the quantum yield; ε_1, the absorption coefficient at the laser wavelength; ε_2, the absorption coefficient for the fluorescence signal; l, the path length. The extent of the overlap is dependent on the fluorescent dyes. As stated before, the amount of absorption also depends on the choice of the spectral regions to be used for 2c/2d PLIF-Thermography [14]. This effect is also known as inner filter effect, where the fluorescence signal is dependent on the observation conditions [56]. In Tab. 2.1 the deviation from linearity between fluorescence signal and dye concentration is given for various absorbances.

Although the assumption of linearity in the relation between fluorescence signal and dye concentration is always included in the 2c/2d PLIF-Thermography theory, the validity of the assumption only becomes important for applications where the product of path length and dye concentration is not constant throughout calibration and measurement. Since the amount of deviation from the assumption of a linear relationship depends on the wavelength region observed, the ratio of the fluorescence signals becomes also a function of the dye concentration and path length if re-absorption is not negligible. Therefore the temperature deviations introduced by this have to be evaluated experimentally in situ for a given 2c/2d PLIF-Thermography application.

Table 2.1: Deviations from the assumed linear relationship between the fluorescence signal and the dye concentration depending on the absorbance [56].

Absorbance	Deviation
10^{-3}	0.1 %
10^{-2}	1.1 %
0.05	5.5 %
0.10	10.6 %
0.20	19.9 %

Photobleaching

Due to excessive irradiation with laser light it is possible that fluorescent dye molecules are destroyed and no longer contribute to the fluorescence signal. This process is called photobleaching. During photobleaching the dye molecules are irreversibly converted to a colorless leuco compound. Especially dye molecules in the triplet state are vulnerable to photobleaching because they are often highly reactive [44, 49, 51, 52]. The occurrence of photobleaching is dependent on excitation intensity, dye concentration, and exposure time [35].

For 2c/2d PLIF-Thermography applications the fluorescent dyes used have to be sufficiently photo-stable under experimental conditions [14, 55]. Otherwise the current ratio of the fluorescence signal depends on the number of already applied laser pulses which in turn lead to a drift of the temperature measured with the 2c/2d PLIF-Thermography. However, in most applications of 2c/2d PLIF-Thermography the degeneration of the fluorescent dyes is not observed because only low laser fluence can be used due to the requirement to stay inside the linear regime in order to justify the assumption of a linear relationship between the laser fluence and the fluorescence signal described above. The reason for this is that for 2c/2d PLIF-Thermography fluorescent dyes designed for dye laser application are commonly used. From their originally intended use the requirement to withstand laser irradiation is much higher than for 2c/2d PLIF-Thermography. Nevertheless, photo-stability is commonly investigated for dyes intended to be used for 2c/2d PLIF-Thermography [14, 35, 46, 55]. Because there is no predictive model available in literature which allows a calculation of the photo-stability beforehand, it has to be determined experimentally under the conditions used for the 2c/2d PLIF-Thermography.

Common Materials Used

In almost all 2c/2d PLIF-Thermography experiments the excitation of the fluorescent dyes is achieved by illumination with laser light. Laser light is used because it is monochromatic, has high radiation power, and can be formed into a thin light sheet. In the majority of the applications of PLIF-Thermography the 488 nm or the 514.5 nm line of a continuous wave argon-ion laser is used [15, 42]. In recent years pulsed frequency-doubled Nd:YAG lasers with a wavelength of 532 nm are increasingly used for PLIF-Thermography because of the high pulse energies and short pulse lengths [13]. For PLIF-Thermography the laser light has to be formed into a thin light sheet. This is commonly done by a combination of cylindrical lenses, so that the laser light is expanded into a plane. In many cases the laser light is additionally focused in a plane perpendicular to the light sheet in order to make the light sheet thinner.

The dyes used for PLIF-Thermography are in most cases dyes originally designed for the application in dye lasers. For the 2c/2d PLIF-Thermography the most common dye combination used is Rhodamine 110 and Rhodamine B dissolved in water [21, 25, 27, 32, 33, 46, 47, 54]. For other solvents than water only limited information on dyes suitable for 2c/2d PLIF-Thermography is available in literature.

For the detection of the fluorescence signal in the majority of the studies two monochrome CCD cameras are used because of their good linearity, homogeneity, and signal-to-noise ratio [15]. Two cameras are necessary to allow simultaneous detection of both parts of the fluorescence spectrum. For the selection of an appropriate camera a trade-off has to be made between the

number of pixels, bit-depth, and frame rate. The separation of the two spectral regions of the fluorescence signal necessary for 2c/2d PLIF-Thermography is normally achieved by a combination of optical filters consisting of a beamsplitter and long-, short-, and band-passes which are placed in the optical path of the two cameras [46]. This way the fluorescence signal is split up and distributed to both cameras and the desired spectral regions can be extracted. The selection of the optical filters is usually a trade-off between signal, sensitivity to temperature, and spectral conflict of the second kind. Additionally the optical filters are used to prevent the laser light from being detected together with the fluorescence signal.

Reported Measurement Uncertainties and Temporal and Spatial Resolutions

In literature comprehensive analysis of the measurement uncertainty of the temperatures measured by 2c/2d PLIF-Thermography can rarely be found. Most often it remains unclear how the uncertainty was calculated, e.g. what kind of temporal and spatial averaging was applied. Sakakibara and Adrian [46] used in their first paper two Sony XC77 ($> 50\,\mathrm{dB}$) CCD cameras. In doing so, they achieved a precision of $\pm 1.4\,^{\circ}\mathrm{C}$. In a later study Sakakibara and Adrian [47] increased the precision by using two Apogee KX85 cameras with 14 bit and low read-out noise to $\pm 0.2\,^{\circ}\mathrm{C}$. In a corresponding error analysis Sakakibara and Adrian pointed out that the noise of the cameras in combination with the low temperature sensitivity is the main part of the uncertainty. In general it can be said that a high signal-to-noise ratio and a high temperature sensitivity are desirable in order to achieve a low measurement uncertainty. Since the actual measurement uncertainty of the temperatures measured by 2c/2d PLIF-Thermography is dependent on a variety of influencing factors it has to be determined experimentally in situ.

In literature for 2c/2d PLIF-Thermography commonly CCD cameras with 12 or 14 bit with a high sensitivity, low noise, and quite low frame rates ($\leq 60\,\mathrm{Hz}$) are used [15, 47]. The temporal resolution in common 2c/2d PLIF-Thermography applications is limited by the cameras used. Typical values found in literature are in the order of $1 \times 10^{1}\,\mathrm{s}$ to $1 \times 10^{-3}\,\mathrm{s}$. Also the temporal resolution is often limited by the temporal averaging necessary to improve the signal-to-noise ratio.

The spatial resolution in common 2c/2d PLIF-Thermography applications is limited only by the optical setup used. Typical values found in literature are in the order of $1 \times 10^{-5}\,\mathrm{m}$ to $1 \times 10^{-3}\,\mathrm{m}$ [42].

2.2 2c/2d PLIF-Thermography Applications to Evaporation Processes

In literature only a few studies can be found where 2c/2d PLIF-Thermography is used to investigate evaporation processes. In the studies available the general question of the applicability of 2c/2d PLIF-Thermography is not addressed. Since the applicability is at least questionable because of the locally changing fluorescent dye concentration due to evaporation a detailed examination is needed. In all studies inhomogeneous illumination, caused by reflections of the laser light at the liquid-vapor interface, led to local deviations of the measured temperatures. The studies dealing with nucleate boiling additionally suffered from high measurement uncertainty because of the high temporal resolution needed to capture the highly dynamic processes which limited the fluorescence signal height. In the studies dealing with a stationary evaporating meniscus a lower measurement uncertainty could be achieved because temporal averaging was possible. In the following the studies available in literature are described.

Nucleate Boiling

Jones [32] used 2c/2d PLIF-Thermography to investigate the temperature distribution inside the liquid around a single vapor bubble during nucleate boiling. As fluid, water with the well-known dye combination Rhodamine B and Rhodamine 110 was used. For the excitation of the dyes a 5 W continuous wave ND:YVO_4 laser with a wavelength of 532 nm was used. The images were recorded with 1000 frames per second and 0.5 ms exposure time. His detector setup had a spatial resolution of 33.5 µm per pixel. The experiments were conducted at a reduced atmospheric pressure of 0.25 atm.

Jones was able to resolve the thermal boundary layer at the heater surface. The actual heater surface could not be observed due to the obstruction by the out-of-focus heater edge. He observed a dependence of the measured temperature on the local illumination intensity by the laser light. Brighter areas seemed to result in lower temperatures whereas areas that lie in a shadow led to higher temperatures. This is an indication for a nonlinear response of the fluorescence signals to the laser fluence which lead to a dependence of the measured temperature on the local illumination situation. The inhomogeneity of the illumination with laser light was caused by reflections at the heater and the liquid-vapor interface. Fig 2.5 illustrates the temperature deviations which occurred due to inhomogeneous illumination.

As a further improvement Jones suggested the use of a transparent heater to reduce the warming of the heater by the laser light. He identified reflections at the liquid-vapor interface as the main source of the observed measurement errors. An analysis of the temperature measurement uncertainty was not performed for the 2c/2d PLIF-Thermography. Nevertheless Jones concluded

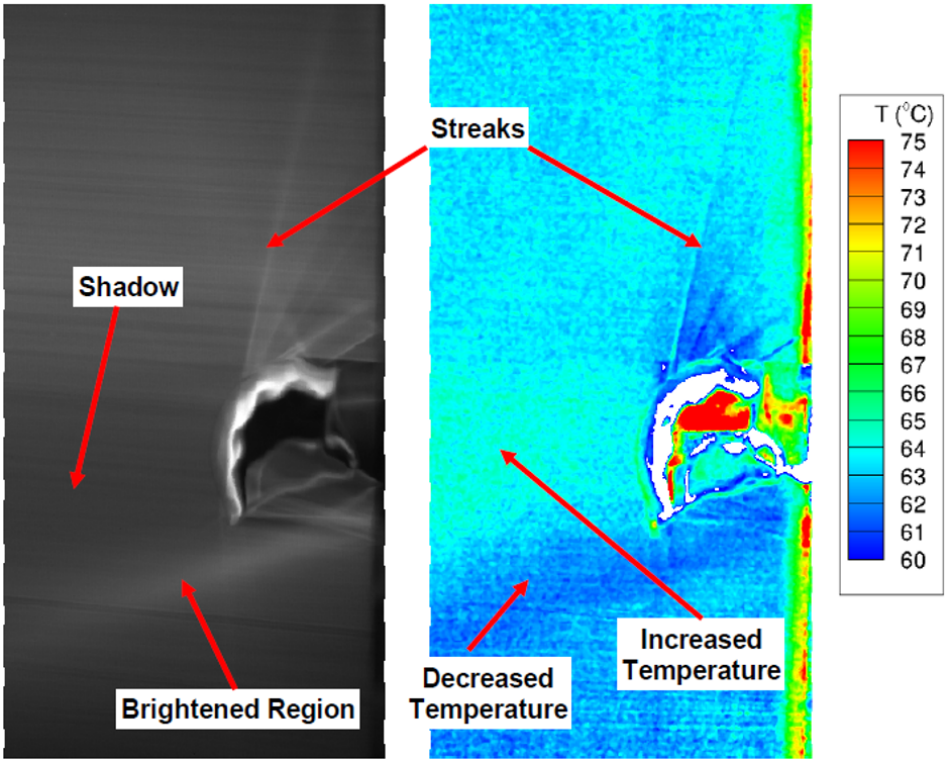

Figure 2.5: Temperature deviations due to inhomogeneous illumination occurred during 2c/2d PLIF-Thermography at a single vapor bubble growing on a heated surface. Left: image of the intensity field. Right: resulting temperature field. [32]

that 2c/2d PLIF-Thermography could yield important insights into evaporation processes like nucleate boiling.

Also Vogt [57] used 2c/2d PLIF-Thermography to measure the temperature field inside the liquid around a single growing vapor bubble during nucleate boiling. In his study acetone was used as fluid. For the 2c/2d PLIF-Thermography a combination of Rhodamine 19 and DCM was used as fluorescent dyes. The fluorescent dyes were excited by laser light generated by a pulsed frequency-doubled Nd:YAG laser with a wavelength of 532 nm and a pulse energy of 28 mJ. For the detection of the fluorescence signal two CMOS cameras were used. The experiments were performed with a frame rate of 1000 Hz and an exposure time of 1 ms. Each frame was illuminated by one laser pulse. The spatial resolution of the optical setup was 4.4 µm per pixel.

Like Jones [32] he also observed a dependence of the measured temperature on the local illumination situation caused by reflections at the liquid-vapor interface of the laser light sheet. In contrast to Jones, Vogt observed in regions with low illumination by the laser a reduction of the measured temperature and vice versa. Another drawback of his studies was the poor photo-stability of the used dye combination in acetone, which caused an increasing deviation of the measured temperatures with the number of laser pulses applied due to photobleaching.

Additionally, Vogt reported that the liquid-vapor interface could not be reconstructed from the images because it appeared blurred. At the blurred interface the measured temperature appeared to be erroneous. Fig 2.6 shows an exemplary result of a measurement performed by Vogt and illustrates optical drawbacks that occurred. As explanation, Vogt suggested that in the region of the blurred interface the fluorescence signals from two spectral regions used for the 2c/2d PLIF-Thermography were separated spatially by chromatic dispersion at the liquid-vapor interface.

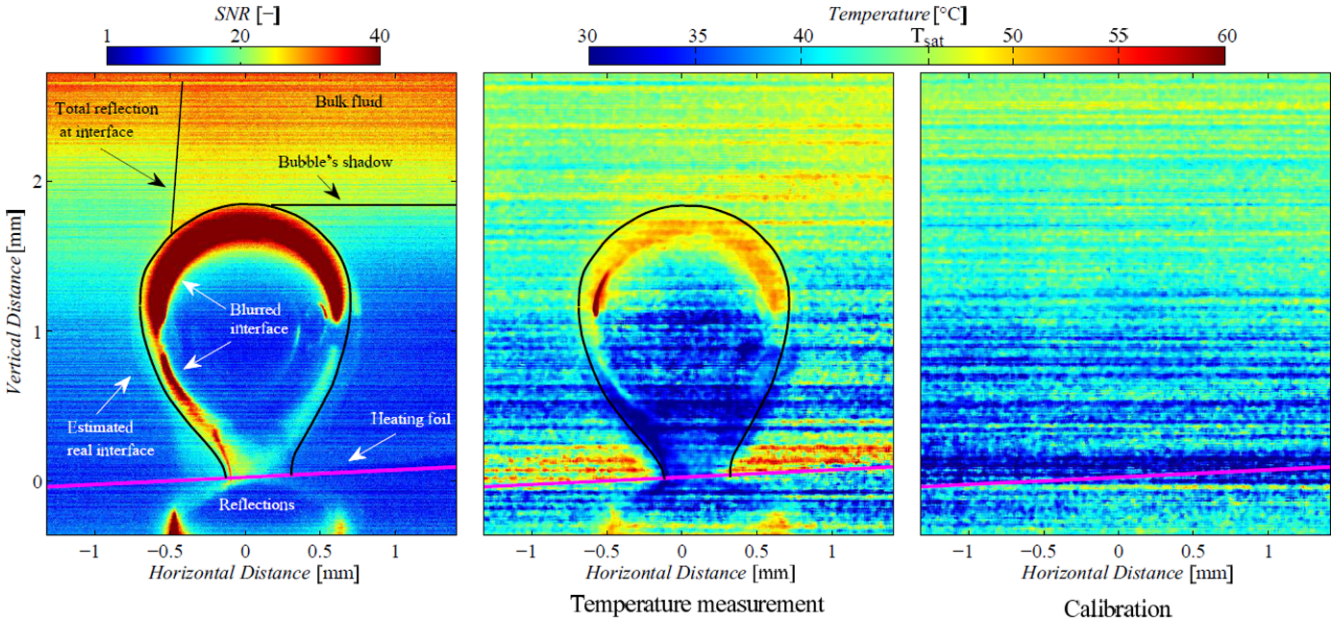

Figure 2.6: Temperature distribution measured with 2c/2d PLIF-Thermography at a growing vapor bubble and illustration of optical effects [57].

The measurement uncertainty of the 2c/2d PLIF-Thermography was calculated to be ±8.4 °C. According to Vogt the main reason for the high measurement uncertainty was the poor signal-to-noise ratio of the images because of the low fluorescence signal. A higher fluorescence signal could not be generated due to the needed temporal resolution. Apart from these drawbacks Vogt concluded that the 2c/2d PLIF-Thermography could be suitable for measurements at evaporation processes. He suggested the application of 2c/2d PLIF-Thermography to a stationary evaporating liquid meniscus as described by Song and Nobes [54] because in such a case no temporal resolution would be needed.

Evaporating Liquid Meniscus

In conjunction with a study about Marangoni convection with particle image velocimetry, Song and Nobes [53, 54] performed 2c/2d PLIF-Thermography measurements at an evaporating water meniscus. They used the well-known dye combination for water Rhodamine B and Rhodamine 110 which was excited by a semiconductor laser diode. For the detection of the fluores-

cence signal Song and Nobes used two CCD cameras. Images were recorded at a frame rate of 2 Hz with an exposure time of 0.02 s. In order to exclude that the flow pattern Song and Nobes observed near the meniscus had a buoyancy-driven component, they measured the temperature distribution below the deepest point of the meniscus to compute the density distribution. Measurements were done in a pressure range from 250 Pa to 820 Pa. The meniscus gap had a width of 10 mm and a depth of 4 mm. The meniscus was heated only at the bottom of the gap. Due to optical constraints the field of view observed covered only 8 mm around the gap's centerline. Because of reflections Song and Nobes were not able to measure the temperature distribution in the corners of the meniscus. Fig 2.7 shows the result of their 2c/2d PLIF-Thermography measurement. An analysis of the temperature uncertainties of the 2c/2d PLIF-Thermography is missing. From their research Song and Nobes concluded that the convection pattern they observed was driven by surface tension rather than by buoyancy.

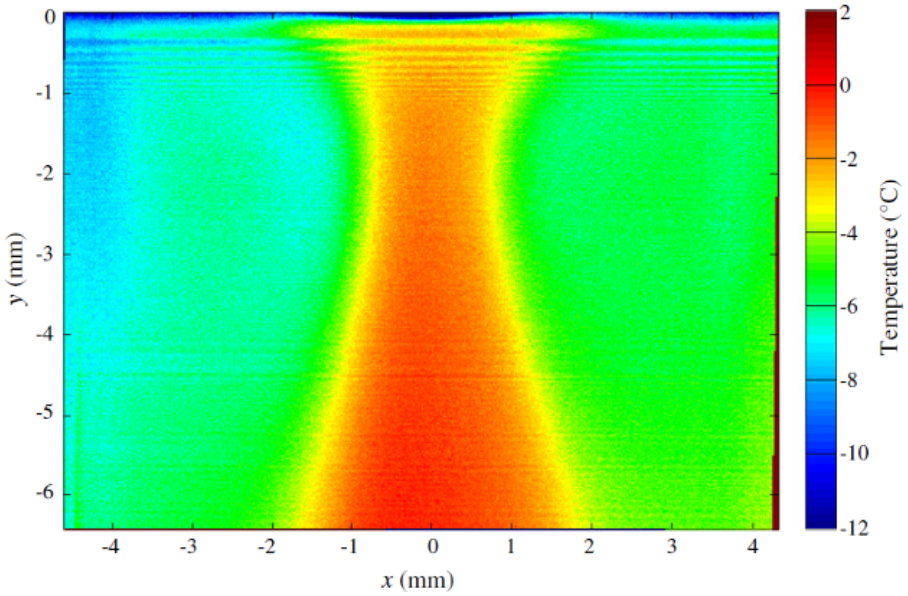

Figure 2.7: Temperature distribution measured by 2c/2d PLIF-Thermography under the deepest point of an evaporating water meniscus at 430 Pa [54].

Also in a channel with a rectangular cross section and with 1 mm edge length Wee [60] tried to measure temperatures with 2c/2d PLIF-Thermography near an evaporating water meniscus. His setup was open to the ambient and therefore influenced by the air in the laboratory. The channel was heated by a foil heater located in the region of the channel above the liquid. Because of this the heating was very inhomogeneous along the channel's height. He also used the well-known dye combination for water of Rhodamine B and Rhodamine 110. For the excitation the 488 nm line of an argon-ion laser was used. In contrast to other studies only one CCD camera was used. Therefore the fluorescence signal of the two spectral regions for 2c/2d PLIF-Thermography had to be detected subsequently. Another drawback was that the calibration was not done in situ. Due to the low spatial resolution of 200 µm and the measurement uncertainty of ±0.91 °C it was

not possible for Wee to resolve the temperature distribution near the meniscus itself. The reason for this was most likely the optical setup. Using only one camera for 2c/2d PLIF-Thermography, Wee had to acquire the two frames subsequently. This contradicts the approach of 2c/2d PLIF-Thermography because the influence of illumination which should be corrected by the 2c/2d PLIF-Thermography approach was different for the two frames. Because of the total internal reflection at the curved liquid-vapor interface the region around the meniscus was subject to an even larger error. Thus Wee had to limit his work to the temperature distribution along the channel axis. He concluded that 2c/2d PLIF-Thermography could have a great potential to be used for measurements at evaporation processes.

2.3 Spatially Resolved Temperature Measurements at an Evaporating Meniscus

In literature two techniques that are frequently used for spatially resolved temperature measurements in the context of evaporating liquid menisci can be found. In earlier studies thermochromic liquid crystals thermography (TLC-Thermography) was successfully applied to study the temperature distribution at the outside of a heated wall in the region in contact with a stationary evaporating liquid meniscus. In more recent studies TLC-Thermography was replaced by infrared thermography (IR-Thermography) because of its superior performance. Both techniques have in common that they are limited to the measurement of temperature distributions on surfaces and therefore are not able to access the temperature distribution inside of liquids. In the following an overview of the application of TLC-Thermography and IR-Thermography to the evaporation of a liquid meniscus is given.

Thermochromic Liquid Crystals Thermography

First spatially resolved temperature measurements of the outside wall temperature of a heated capillary slot with a stationary evaporating water meniscus inside were conducted by Höhmann and Stephan [28]. They developed a method to measure the temperature distribution by thermochromic liquid crystals (TLCs) with a high spatial resolution of 0.83 µm per pixel and a measurement uncertainty of ±0.51 °C. The TLCs were applied in a thin layer to the outside of a 20 µm thick stainless steel foil which was used as electrically heated wall of the capillary slot. The color play of the TLCs was used to determine the spatially resolved temperature distribution in the region where the contact line of the meniscus was located on the stainless steel foil. Fig 2.8a shows the result of their measurement. With this technique Höhmann and Stephan were able to observe a temperature drop in the region of the contact line of the evaporating water meniscus. The height of the temperature drop was in the range of 0.1 °C to 0.2 °C depending on data processing and had an extent of about 33 µm.

Buffone and Sefiane [9] used the measurement technique introduced by Höhmann and Stephan to measure the temperature distribution on the outside of a glass capillary tube from which pentane was evaporating into the air atmosphere. The capillary tube had an internal diameter of 1630 μm and a wall thickness of 235 μm. The TLCs were applied in a layer of about 15 μm thickness to the outside of the capillary tube. They achieved a spatial resolution of 16.19 μm per pixel at a frame rate of 30 Hz. Fig 2.8b shows the result of their measurement. Buffone and Sefiane observed a temperature drop in the order of 11 °C in the region of the contact line of the pentane meniscus with an extent of 8 mm.

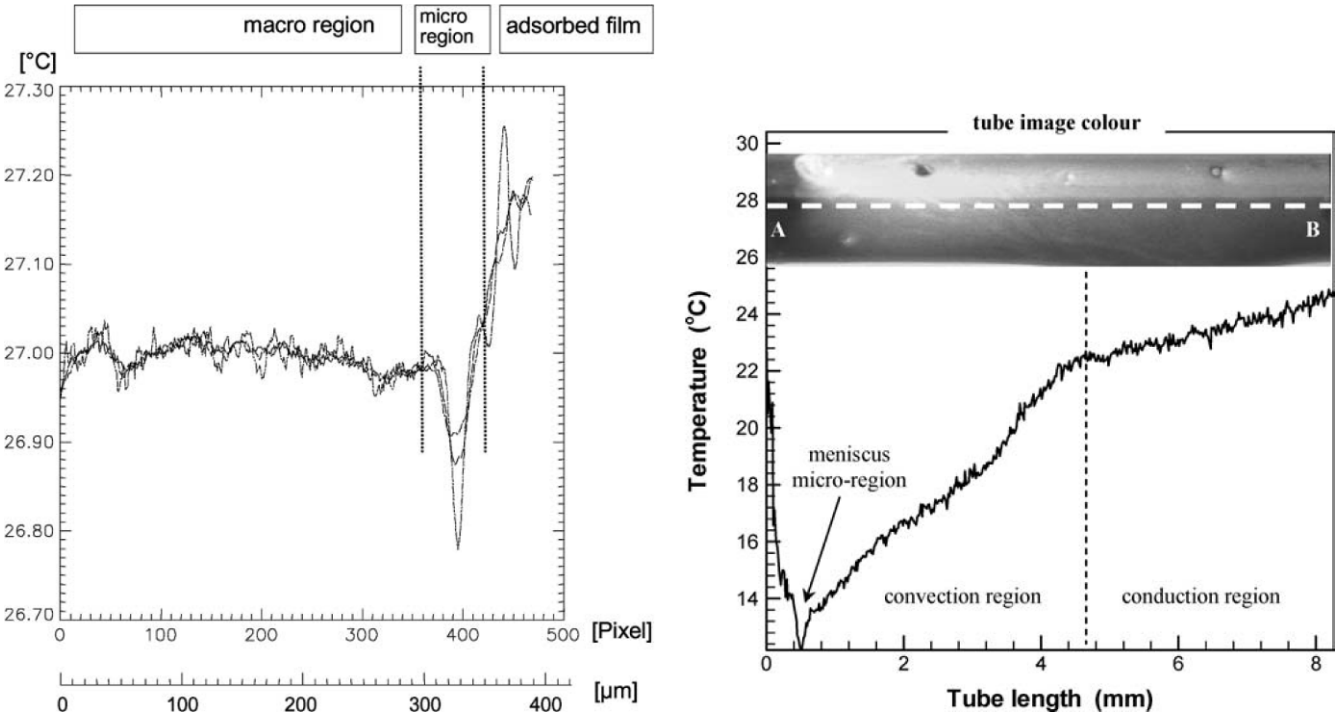

(a) Höhmann and Stephan [28] **(b)** Buffone and Sefiane [9]

Figure 2.8: Results of spatially resolved temperature measurements with TLC-Thermography of the temperature distribution on the outside of a heated capillary slot (a) and a capillary tube (b).

Infrared Thermography

Buffone and Sefiane [7, 8, 10, 11] studied the cooling effect by evaporation of volatile fluids (ethanol, methanol, acetone, and pentane) in borosilicate capillary tubes with sizes of 600 μm, 900 μm, and 1630 μm. With IR-Thermography they measured the interface temperature distribution of an evaporating meniscus by pointing the camera at the open tip of the capillary tube. They compared this temperature distribution to the one measured at the empty capillary tube. Buffone and Sefiane qualitatively found that the temperature at the wall of the tube was lower than at the center. Due to the limited depth of focus of about 100 μm the center of the menis-

cus was out of focus and the measured temperatures in this region were not reliable. Buffone and Sefiane concluded that the temperature gradient close to the wall was the reason for the Marangoni convection observed by them. Buffone and Sefiane [7, 8, 11] also investigated the temperature distribution of the side of the capillary tubes. For the side view they found that the lowest temperature was measured in the region of the liquid-vapor interface.

Buffone and Sefiane [8, 10] also conducted experiments with a heated capillary tube. Fig. 2.9 shows their results of the IR-Thermography measurements. The heating was realized by a silver coating of the tube which was not covering the area with the meniscus. The heater was located below the liquid-vapor interface. They observed that in this case also the lowest temperatures were measured close to the wall for the top view. For the side view they observed that, similar to the unheated case, the lowest temperature was measured in a region close to the liquid-vapor interface. Also the flow pattern around the meniscus was similar, but the strength of the flow was enhanced by the heating.

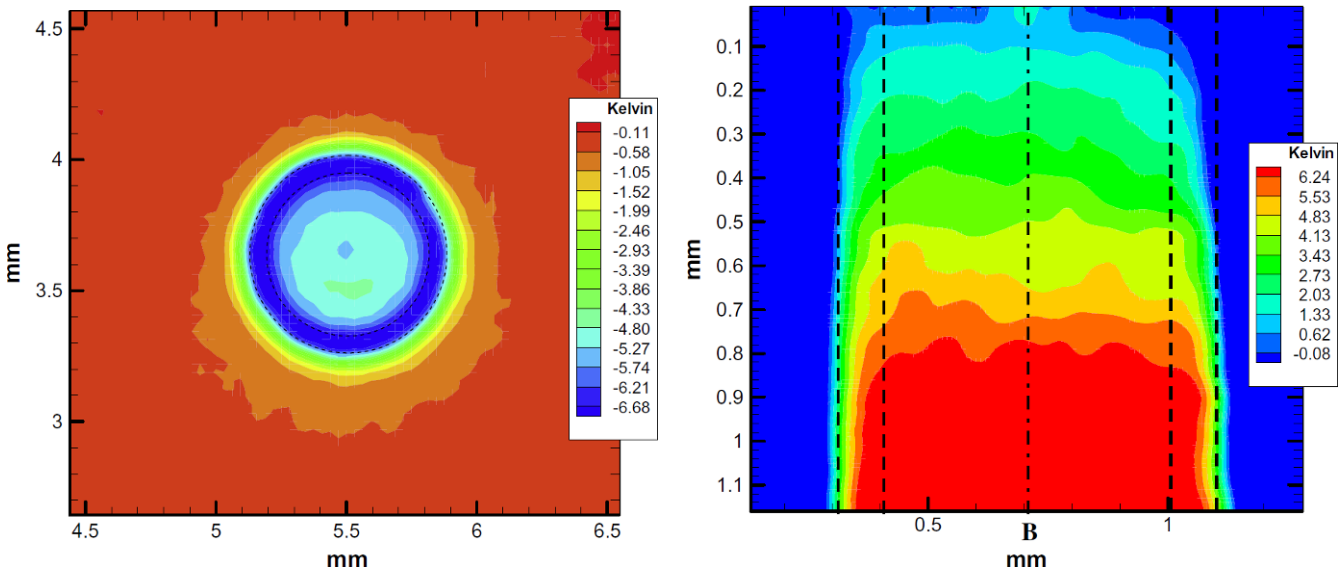

(a) Top view, unheated

(b) Side view, heated

Figure 2.9: Results of IR-Thermography measurements for ethanol inside a capillary tube [10]. The indicated temperature is the difference to the ambient temperature.

Dhavaleswarapu, Garimella, and Murthy [16] performed IR-Thermography at a stationary evaporating heptane meniscus into the air atmosphere. The meniscus was formed between a heated fused quartz wafer and an acrylic knife edge with a Teflon coating. The temperature distribution on the surface of the fused quartz wafer was measured by IR-Thermography from both sides. Fig. 2.10a shows a schematic of the setup along with the results of the IR-Thermography. The lowest temperature was measured in the region of the contact line. The temperature drop in this region was about 1 °C. The temperature drop had an extent of about 400 µm. The results of the IR-Thermography from the top and the bottom showed a significant difference. The temper-

ature drop was found to be more prominent in the IR-Thermography measurements performed from the top. This was explained by them with the thermal conduction inside the fused quartz wafer.

Migliaccio, Dhavaleswarapu, and Garimella [41] performed IR-Thermography measurements of a wetted wall of a V-groove filled with heptane with a similar setup. The measurements were only performed for the wetted side. Fig 2.10b shows the results of the IR-Thermography measurements. They also observed a temperature drop in the region of the contact line. In contrast to Dhavaleswarapu, Garimella, and Murthy the temperature drop was only 0.2 °C. The extent of the temperature drop was 300 µm.

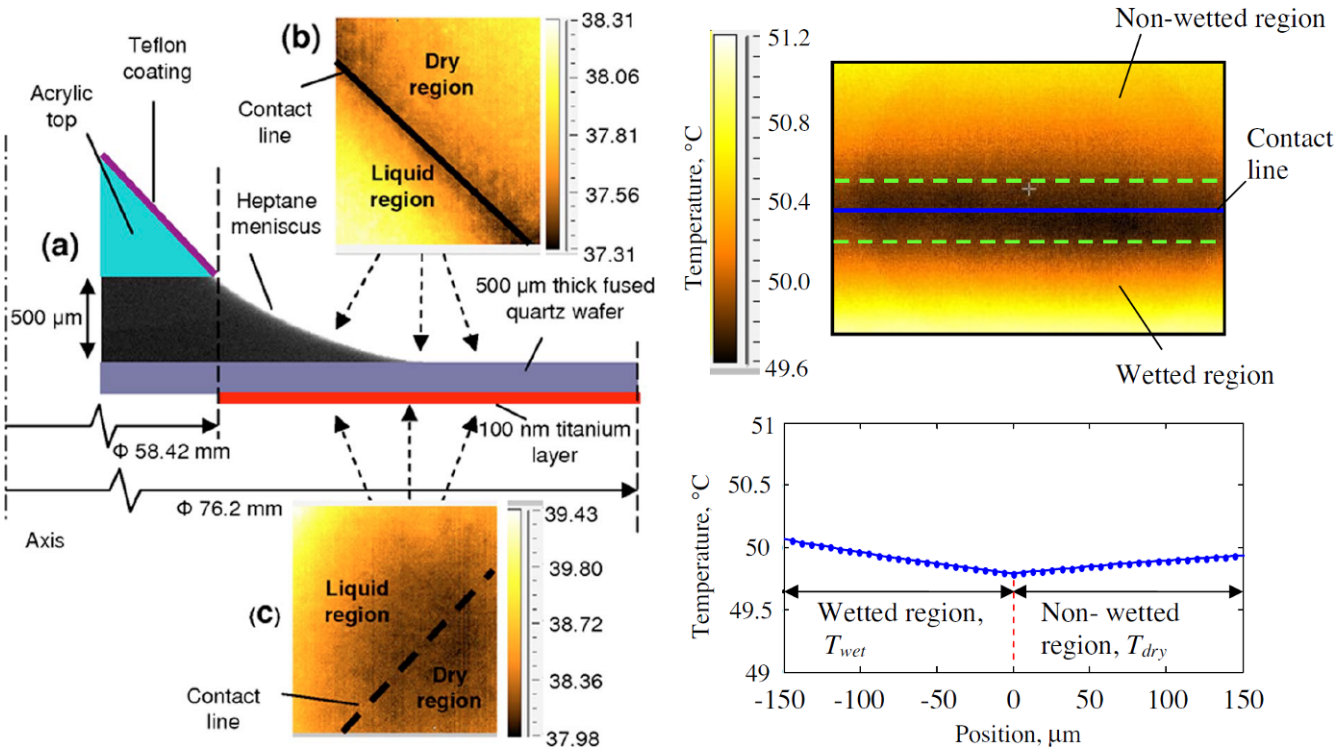

(a) Dhavaleswarapu, Garimella, and Murthy [16] **(b)** Migliaccio, Dhavaleswarapu, and Garimella [41]

Figure 2.10: Results of IR-Thermography measurements of the temperature distribution of a heated wall with an evaporating heptane meniscus on top.

Ibrahem et al. [29–31] investigated the temperature distribution on the heated wall of a capillary slot with a stationary liquid meniscus inside, in order to calculate the local heat transfer. HFE-7100 was used as fluid. The temperature distribution was measured by IR-Thermography. The capillary slot was formed by a copper plate and a 10 µm thick stainless steel foil. The stainless steel foil was used as resistive heater. The temperature distribution was measured at the outside of the stainless steel foil. The IR-Thermography measurements were performed at a frame rate of 244 Hz with a spatial resolution of 14.8 µm per pixel. Fig 2.11a shows the results of the IR-Thermography measurements. At the position of the contact line a temperature drop in the order of 0.4 °C to 12 °C was observed. The temperature drop was found to be dependent

on the heat flux and the position of the contact line on the heated stainless steel foil. With increasing heat flux also the temperature drop increased.

Fischer [24] performed similar measurements at the heated wall of a capillary slot filled with FC-72. In this case the IR-Thermography measurements were performed at a frame rate of 1000 Hz with a spatial resolution of 29.27 µm per pixel. Fig 2.11b shows the results of the IR-Thermography measurements. Fischer also observed a temperature drop at the position of the contact line, but in contrast to Ibrahem et al. it was in the order of 0.1 °C. Fischer estimated the measurement uncertainty of the IR-Thermography measurements to be ±0.125 °C.

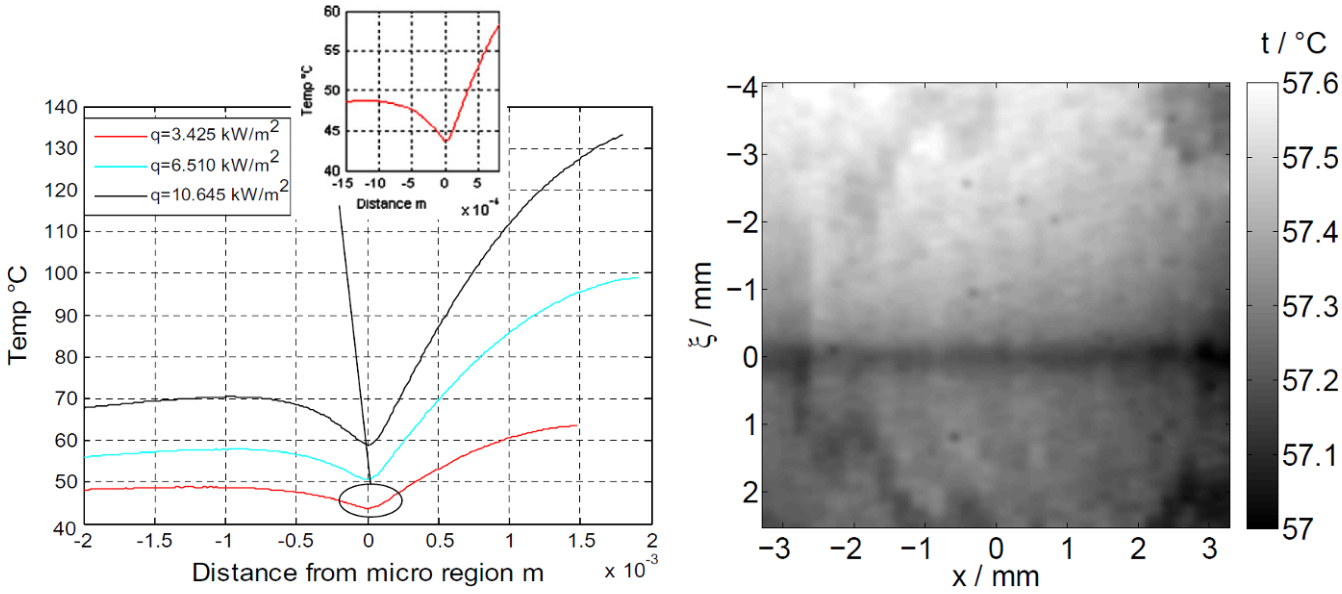

(a) Ibrahem et al. [30] **(b)** Fischer [24]

Figure 2.11: Results of IR-Thermography measurements of the temperature distribution of the back side of the heated wall of a capillary slot with a stationary liquid meniscus inside.

2.4 Open Scientific Questions

With TLC-Thermography and IR-Thermography so far only spatially resolved temperature measurements of the surfaces of walls or liquids during evaporation processes have been possible. Thus, spatially resolved temperature measurements inside the fluid as and addition to the surface temperature measurements are needed. 2c/2d PLIF-Thermography is a promising measurement technique potentially capable of allowing such measurements.

2c/2d PLIF-Thermography has already been applied to evaporation processes but the fundamental question of the applicability of 2c/2d PLIF-Thermography to such processes has not been addressed in literature yet. The applicability is at least questionable because of the local concentration changes of the fluorescent dyes caused by the evaporation process. Therefore,

an investigation of the applicability of 2c/2d PLIF-Thermography to evaporation processes is needed. Achievable temporal and spatial resolution at measurement uncertainties low enough to study the temperature differences inside the fluid need to be investigated. With respect to the studies of TLC-Thermography and IR-Thermography summarized above a spatial resolution in the order of 10 µm to 30 µm per pixel and a measurement uncertainty in the order of 0.1 °C to 0.2 °C seems to be necessary.

Based on the literature available a single vapor bubble does not seem to be suitable to test the applicability of the 2c/2d PLIF-Thermography to evaporation processes. The reasons for this are the optical effects caused by the spherically shaped liquid-vapor interface, the high dynamics of the processes, and the low reproducibility. Therefore a stationary evaporating single liquid meniscus is chosen for the investigations, because it represents the simplest abstraction of the evaporation processes which includes most physical phenomena. Advantages of the stationary evaporating liquid meniscus are that there is no need for temporal resolution and that its defined constant geometry allows easy optical access. Furthermore, the stationary single extended liquid meniscus is often used in literature in order to gain a fundamental understanding of the underlying physical principles of the evaporation process.

In order to answer the question of the applicability of 2c/2d PLIF-Thermography to evaporation processes in this work first of all a spectroscopic characterization of the fluorescent dyes was performed. This was done to identify suitable dye combinations and parameter ranges with the highest likelihood of a successful application. In the next step the 2c/2d PLIF-Thermography was implemented and methods for calibration and evaluation were developed and validated. After the validation the measurement uncertainty and the repeatability were investigated. Additionally the influence of the laser fluence and the dye concentration on the measured temperature was analyzed. In the last step the implemented and validated 2c/2d PLIF-Thermography was applied to a stationary evaporating single liquid meniscus in order to analyze its applicability to evaporation processes.

3 Materials and Methods

In this chapter the experimental setups and the used materials are described along with the experimental procedures and the evaluation methods for the measurement data. The experimental setups consisted of a test cell, the laser system, and a detector setup. For the experiments two different test cells and two different detector setups were used. Two experimental setups were realized using these components. The first was used for the characterization of the single fluorescent dyes and their combinations to be used for the 2c/2d PLIF-Thermography. The second setup was used for the investigations regarding the 2c/2d PLIF-Thermography itself and its applicability to stationary evaporating meniscus. In the following sections the components of the experimental setup, the materials used, and the procedures for the experiments and the data evaluation are described.

3.1 Experimental Test Cell Setups

For the experiments two different experimental setups were used. The first setup was used for the characterization of single fluorescent dyes and dye combinations regarding their applicability for the 2c/2d PLIF-Thermography. The second setup was used for the investigations with the 2c/2d PLIF-Thermography at a stationary evaporating meniscus.

Test Cell for the Investigation of Fluorescent Dye Combination

The test cell described in this section was used for the characterization of single fluorescent dyes and dye combinations regarding their usability for 2c/2d PLIF-Thermography. A schematic of the test cell is shown in Fig. 3.1. A cross section view in the light sheet plane of the front side, a cross section view in the symmetry plane of the side view, and a cross section view in a plane halfway down from the top is shown. The front view was the observation direction of the detector setup used for the detection of the fluorescence signal.

For the measurements the dye solution under investigation was located in a cavity formed by a stainless steel framework (EN 10088-3, 1.4301) with four optical accesses. The cavity had a rectangular cross section with a width of 5 mm, a depth of 31 mm and a height of 18 mm. The temperature of the dye solution in the cavity was measured by two thermocouples, one located at the top and the other one at the bottom of the cavity. Also at the top and at the bottom of

the cavity, connections for the filling of the cavity with the dye solution were located. The liquid in the cavity could be heated to defined temperature levels by a temperature-controlled water loop. The cavity was sealed with O-rings (Eriks, EPDM 70 Compound 55985), which have an excellent resistance to ethanol. For the experiments where the pressure inside the cavity was varied a vacuum pump (vacuubrand, ME16) with a pressure controller was used. For these experiments the vacuum pump was connected to the fluid connection at the top of the cavity.

The optical accesses were made of sapphire (Thorlabs, WG31050) because of its comparatively high thermal conductivity for a transparent material of approximately 31 $\mathrm{Wm^{-1}K^{-1}}$ [45]. Two opposed optical accesses were used as entrance and exit for the laser light sheet. The laser light sheet was positioned in the middle of the depth of the cavity. One of the other two opposed optical accesses was used as access for the light collection optic of the detector setup. Fluorescence directed away from the detector's collection optic left through the opposed optical access. This prevented reflections that could lead to erroneous measurements.

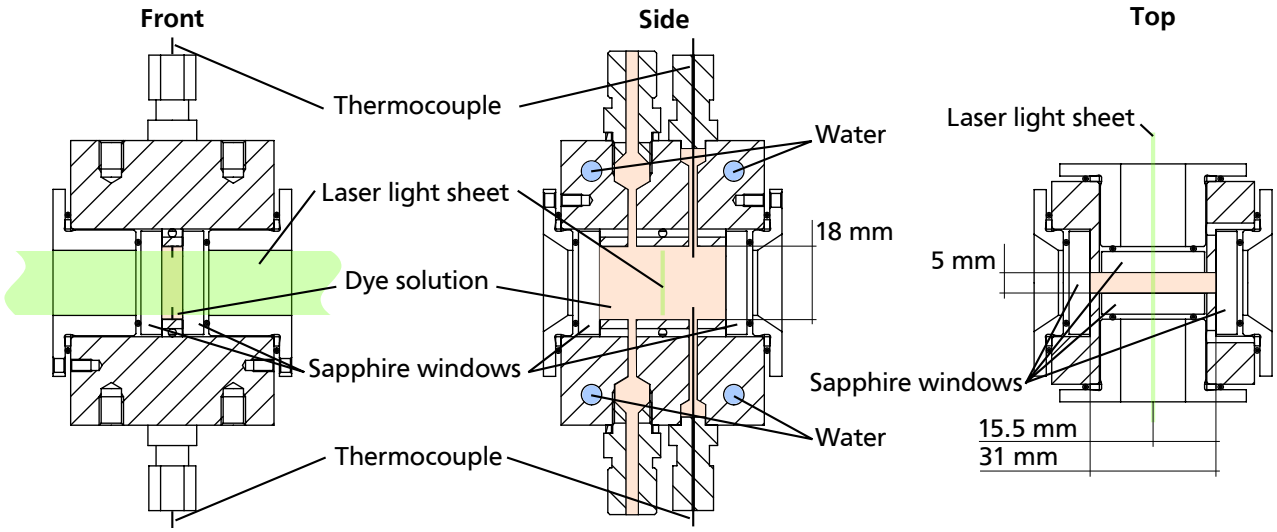

Figure 3.1: Schematic of the test cell used for the study of fluorescent dyes.

Test Cell for the Investigations at the Evaporating Liquid Meniscus

The test cell described in this section was used for the 2c/2d PLIF-Thermography measurements at a stationary evaporating meniscus. Fig. 3.2 shows a schematic of the evaporator section of the test cell used for the experiments. A cross section view in the light sheet plane of the front side, a cross section view in the symmetry plane of the side view, and a cross section view in a plane halfway down from the top view is shown. The front view is the observation direction of the detector setup used to detect the fluorescence signal. The main design aspect was the optical accessibility of the evaporation process for the laser light sheet and the detector setup used for the 2c/2d PLIF-Thermography.

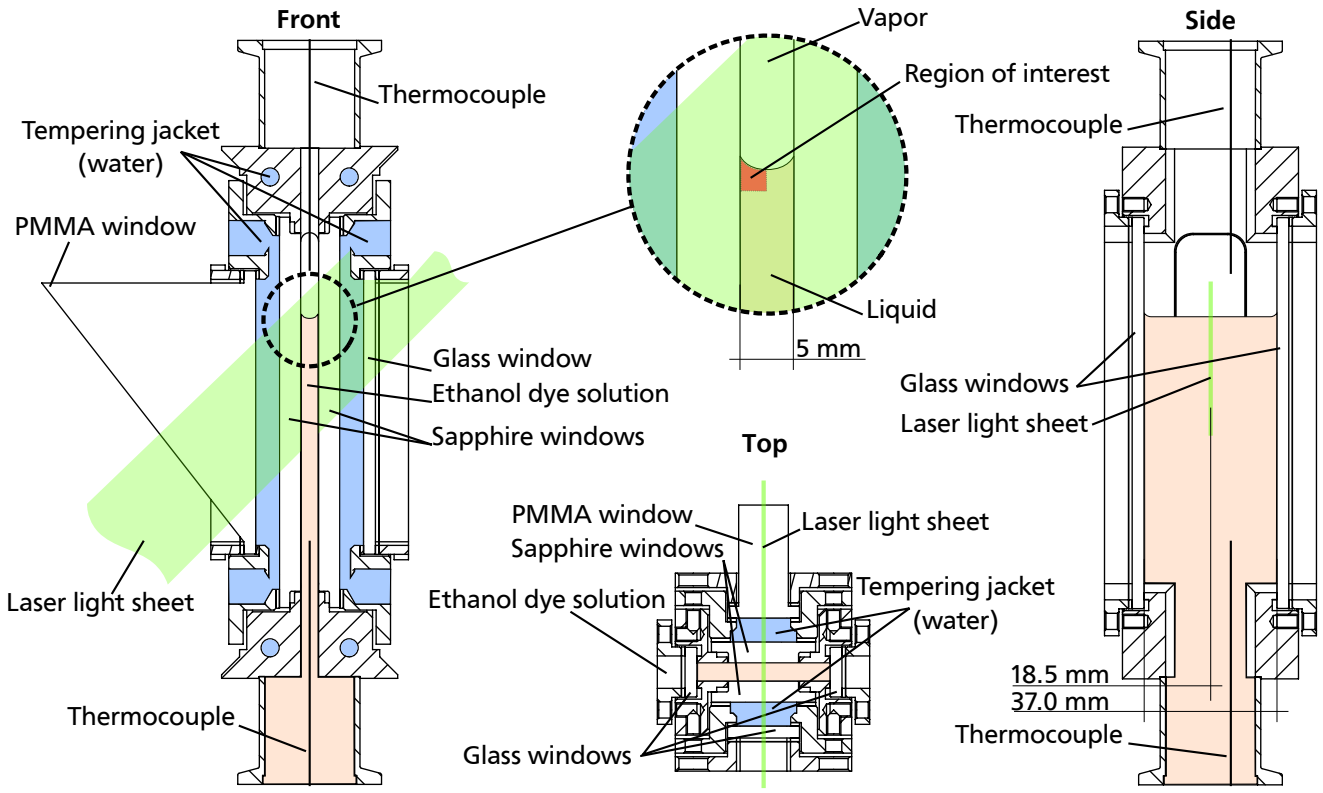

Figure 3.2: Schematic of the evaporator section of the test cell used for the experiments at the evaporating liquid meniscus.

In the middle of the evaporator a slit was formed by the stainless steel framework (EN 10088-3, 1.4301), two sapphire windows, and two glass windows. Sapphire was used because of its comparatively high thermal conductivity for a transparent material of approximately 31 $\mathrm{Wm^{-1}K^{-1}}$ [45]. The slit had a rectangular cross section with a width of 5 mm, a depth of 37 mm and a height of 100 mm. This aspect ratio was chosen to achieve a temperature distribution that is approximately two-dimensional. This was necessary because with the 2c/2d PLIF-Thermography only two dimensional temperature distributions can be measured. The slit was sealed with O-rings (Eriks, EPDM 70 Compound 55985), which have an excellent resistance to ethanol. The evaporating meniscus was located inside this slit. The slit was only partly filled with liquid so that the liquid-vapor interface, i.e. the meniscus, was located in the field of view of the detector setup used for the 2c/2d PLIF-Thermography. The temperature inside the slit was measured by two thermocouples, one located at the top and one located at the bottom of the slit. These temperature measurements were used to determine the temperature for the calibration and validation of the 2c/2d PLIF-Thermography.

The slit, the meniscus was located in, was heated by a tempering jacket. The tempering jacket was realized by two slits formed by the sapphire window and the PMMA window on the one side and the sapphire window and a glass window on the other side which was flown through by water. The water could be heated to defined temperature levels by a bath thermostat. The tem-

perature of the water was measured directly at the inlet and the outlet of the tempering jacket with thermocouples placed inside the water flow. This way of heating was chosen to achieve optical accessibility of the evaporating meniscus for the laser light sheet. Another advantage of this heating method was that the evaporation process was temperature-controlled and no higher temperatures than the temperature of the water could occur inside the ethanol.

The PMMA window and the glass windows opposite together with the sapphire windows were used as lead-through for the laser light sheet. The laser light sheet was angled with respect to horizontal. This was done in order to move the point on the curved liquid-vapor interface at which total internal reflection of the laser light occurred first out of the region of interest. The internal reflections were undesired because they lead to a large inhomogeneity of the laser light sheet fluence distribution. In order to achieve the necessary angle of incidence at the liquid-vapor interface the PMMA window was designed as a wedge. The angle of the wedge was chosen in a way that the laser light entered the PMMA windows under an angle of incidence of 90°. This was done to avoid the reduction of the angle of the laser light sheet by the refraction at the air–PMMA interface. In this configuration the angle between the laser light sheet and the horizontal had to be 39° to move the internal reflection out of the region of interest. Without the wedged PMMA windows the necessary angle of incidence at the liquid-vapor interface could not be achieved because of geometrical constraints of the setup.

The evaporator was supplemented with a condenser and a reservoir to achieve a closed loop. Fig. 3.3 shows a schematic of the complete system. The system was designed on the basis of Klein Flange DN16 with O-rings (Eriks, EPDM 70 Compound 55985) as connecting pieces. The closed loop was used to facilitate a stationary evaporation process. The reservoir could be moved up and down to allow a positioning of the liquid-vapor interface inside of the field of view of the detector setup. The topmost valve was connected to a vacuum pump to evacuate the system before the filling with ethanol and to periodically remove non-condensable gases. A pressure sensor (Wika, P-30) was inserted in the vapor section of the loop to measure the saturation pressure. From the measured pressure the saturation temperature was calculated by the ancillary equation given by Dillon and Penoncello [17].

The evaporator section could be isolated by two valves from the rest of the system. For the calibration of the 2c/2d PLIF-Thermography this section was completely filled with ethanol and separated by closing the valves below and above the evaporator section. During calibration this section was heated additionally to the tempering jacket of the evaporator by trace heating. In order to reduce the influence of the temperature of the environment the system was thermally insulated. This facilitated the homogeneous temperature distribution inside the ethanol in the evaporator needed for the calibration of the 2c/2d PLIF-Thermography. The closed loop had a leakage rate of 3.1×10^{-5} mbarLs^{-1}, which was sufficient for experiments concerning evapora-

tion of a pure fluid because non-condensable gases were removed with the vacuum pump prior to the experiments once a day.

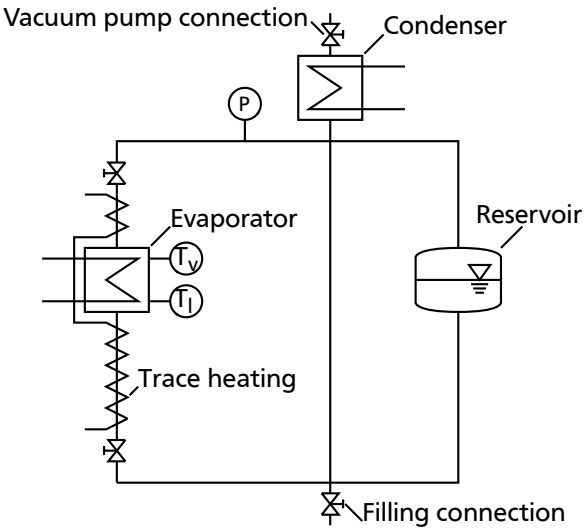

Figure 3.3: Schematic of the test cell used for experiments at the evaporating liquid meniscus.

3.2 Laser Setup

To evoke the fluorescence to be observed during the experiments the fluorescent dyes had to be excited. The dyes were excited by laser light formed into a light sheet. A light sheet was used because the 2c/2d PLIF-Thermography is a two-dimensional measurement technique and therefore requires the excitation of the fluorescent dyes only in the measurement plane. In this section the laser setup used to generate the light sheet for the excitation of the fluorescent dyes necessary for the 2c/2d PLIF-Thermography is described.

Laser System

The laser light which was used to excite the dye molecules was generated by a pulsed frequency-doubled Nd:YAG laser (Lee Laser, 800-PIV/40G) with a wavelength of 532 nm. The key properties of the laser are listed in Tab. 3.1. The pulse stability of the laser was 1.5 % and the pulse length (FWHM) was 261 ns. For this work the rather long laser pulses were not a limitation because only stationary processes were investigated. The high repetition rate of the laser was used to achieve a good signal-to-noise ratio even at low pulse energies by accumulation of the fluorescence signal generated by several laser pulses over the exposure time of one image.

Fig. 3.4a shows the development of the laser pulse energy with an increasing repetition rate. With an increasing repetition rate the maximal achievable pulse energy decreases. Fig. 3.4b

shows the normalized radiant power over time of an average laser pulse. The normalized radiant power in s^{-1} results in the radiant power if multiplied by the total pulse energy. The rather long laser pulses resulted in a comparatively low peak radiant power.

Table 3.1: Key properties of the laser system used.

Property	Value
Wavelength	532 nm
Pulse repetition rate	0–50 kHz
Pulse duration	261 ns
Pulse stability	1.5 %

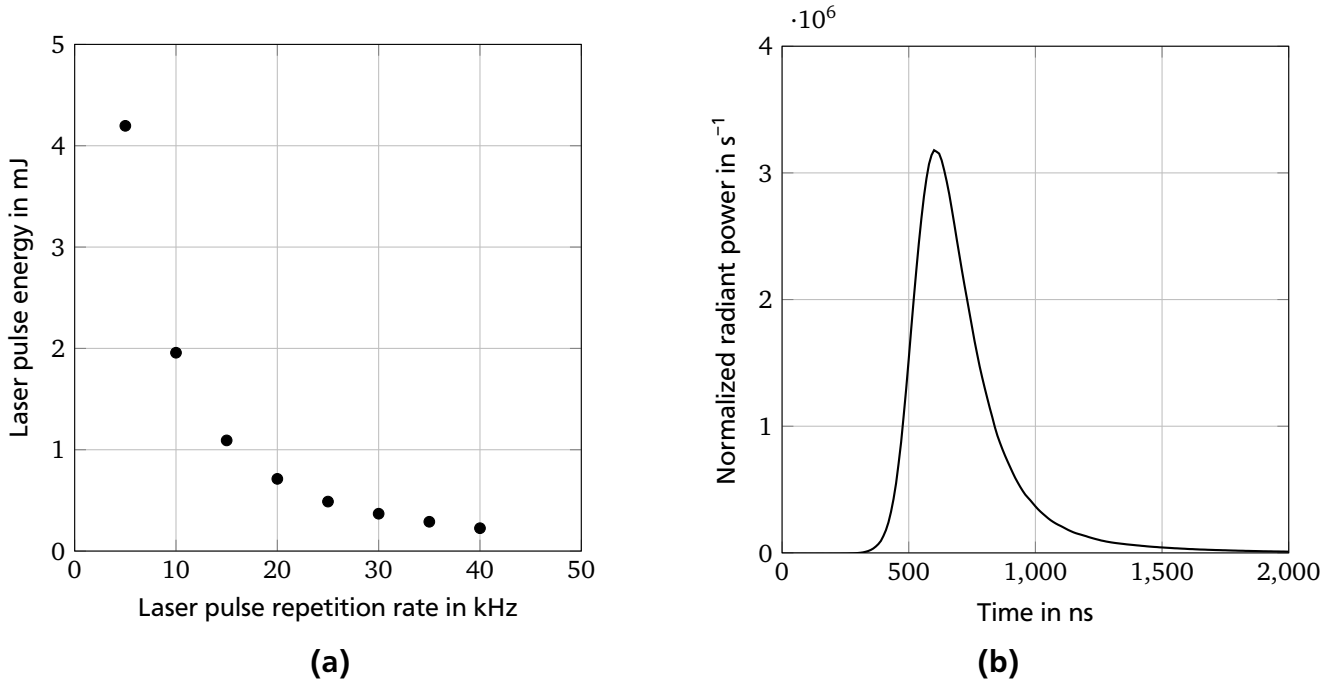

Figure 3.4: Laser pulse energy versus laser pulse repetition rate (a) and normalized radiant power of an average laser pulse versus time (b).

Optical Setup

For the experiments the laser light was formed into a laser light sheet. Fig. 3.5 shows a schematic of the optical setup used to generate the laser light sheet. The adjustability of the pulse energy was realized by a waveplate and a polarizing beam splitter (Thorlabs, VA5-532/M). The laser power was measured by a thermal laser power meter (Ophir, BeamTrack, 50(150)A-BB-26-QUAD). The laser light was directed to the lenses for the light sheet generation by two adjustable laser line mirrors (Thorlabs, NB1-K12). The light sheet was formed from a laser beam with a round cross section by a plano-concave cylindrical lens (Thorlabs, LK1743-L1-A, f=−100 mm) and a plano-convex spherical lens (Thorlabs, LA1725-A, f=400 mm), which

formed a Galilean telescope. The lenses were placed at a distance so that a light sheet with constant height was formed. This was achieved by adjusting the distance between the lenses, so that the focal points lie on top of each other. Thus, a collimation of the light along the height of the light sheet was realized. Behind the lenses the light sheet was directed to the test cell by a protected silver mirror (Thorlabs, PF20-03-P01). The last mirror and the lenses could be rotated around the optical axis to adjust the angle of incidence of the laser light sheet onto the test cell. The detector setup was located in front of the test cell under investigation.

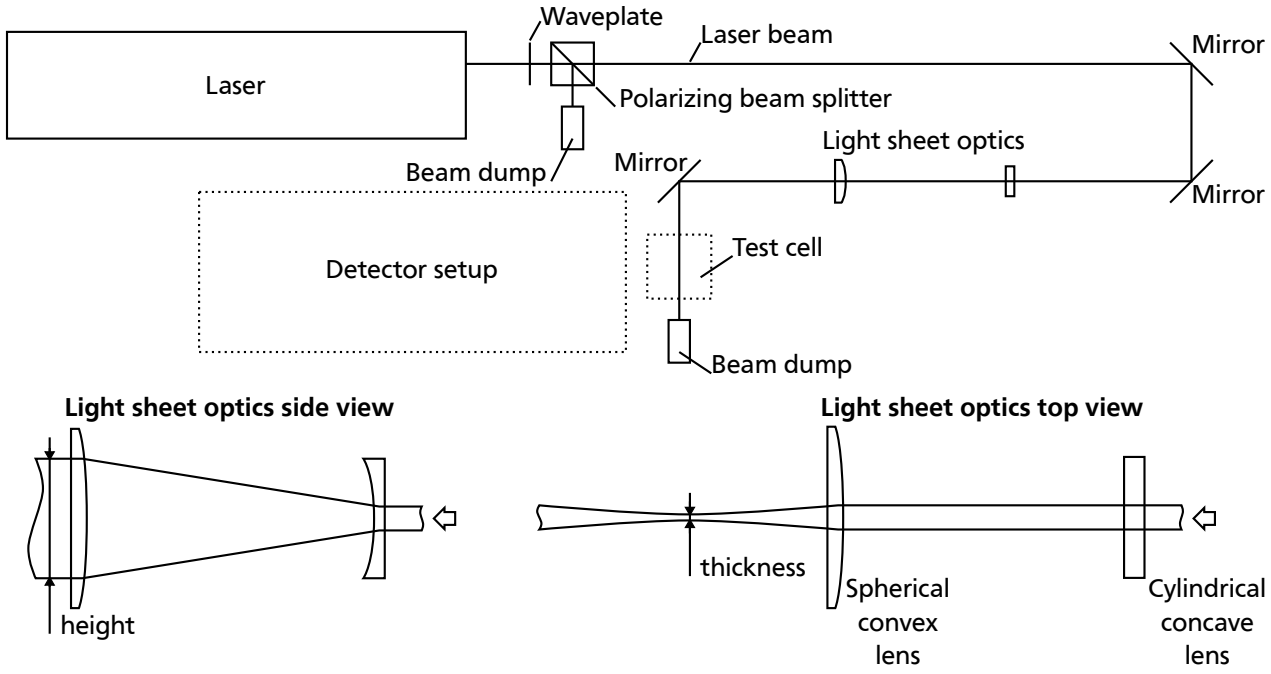

Figure 3.5: Schematic of the laser setup and the light sheet optics.

Light Sheet

In order to ensure an almost homogeneous fluence distribution along the height of the light sheet a beam profile measurement was performed. Fig. 3.6 shows the result of the beam profile measurement (DataRay Inc., WinCamD-LCM) at the thinnest position of the light sheet. The diagram shows the normalized fluence in m^{-2} that results in the fluence distribution if multiplied with the total pulse energy or in the radiant power density distribution if multiplied with the radiant power. For a threshold e^{-2} of the maximal fluence the height of the laser light sheet was 38 mm and the thickness was 642 µm. In order to have an approximately flat fluence distribution along the height only ±5 mm around the maximal fluence were used for the measurements.

In order to examine the development of the light sheet thickness along the propagation detection of the light, the thickness was measured at different locations around the thinnest position.

Fig. 3.7 shows the development of the light sheet thickness. There was no significant change of the light sheet thickness in the region ±3 mm around the thinnest position which was used for the measurements.

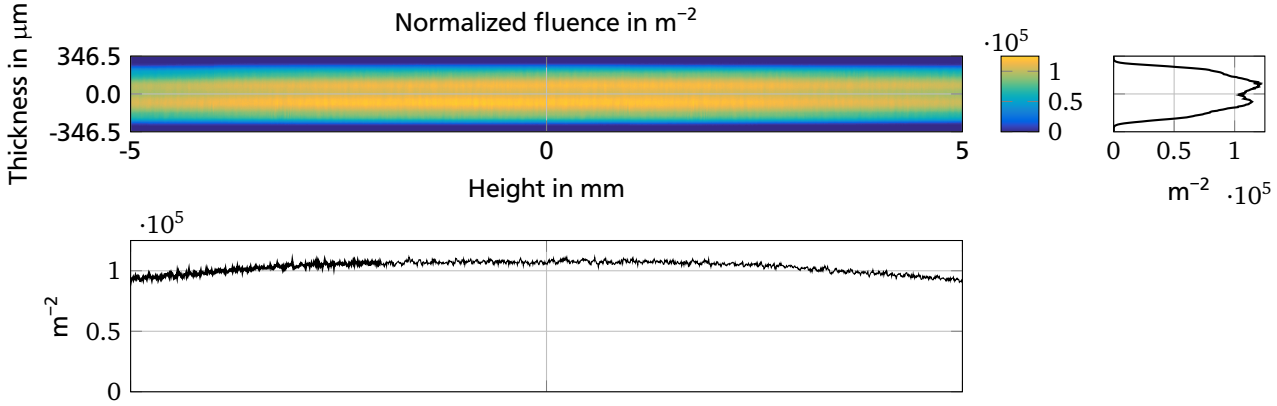

Figure 3.6: Normalized fluence distribution at the thinnest position of the light sheet.

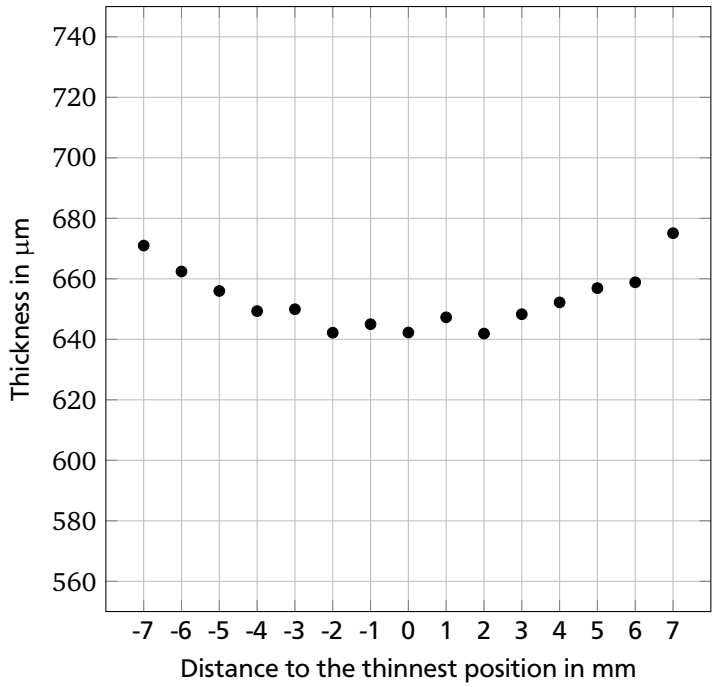

Figure 3.7: Development of the light sheet thickness along the propagation direction.

3.3 Detector Setups

In this section the detector setups used to detect the fluorescence signal are described. For the experimental investigations two different setups were used. The first setup was a spectrometer which was used for the characterization of single fluorescent dyes and possible dye combinations for the 2c/2d PLIF-Thermography. For the 2c/2d PLIF-Thermography itself the second setup, a channel-based imaging spectrometer, was used which is able to spatially resolve two spectral channels.

Spectrometer

Fig. 3.8 shows a schematic of the spectrometer setup used for dye characterization. The spectrometer was protected from the stray light of the laser by a long-pass (Semrock, 532 nm Edge-Basic, BLP01-532R-25, edge wavelength 542 nm). The transmission curve of the long-pass is shown in Fig. 3.9. The fluorescent light was collected with a collimator (Stellar Net Inc, LENS-QCOL, 3° field of view) and was fed into an optical waveguide (Stellar Net Inc, F600-UVVis-SR, 600 µm core diameter) which was connected to the spectrometer.

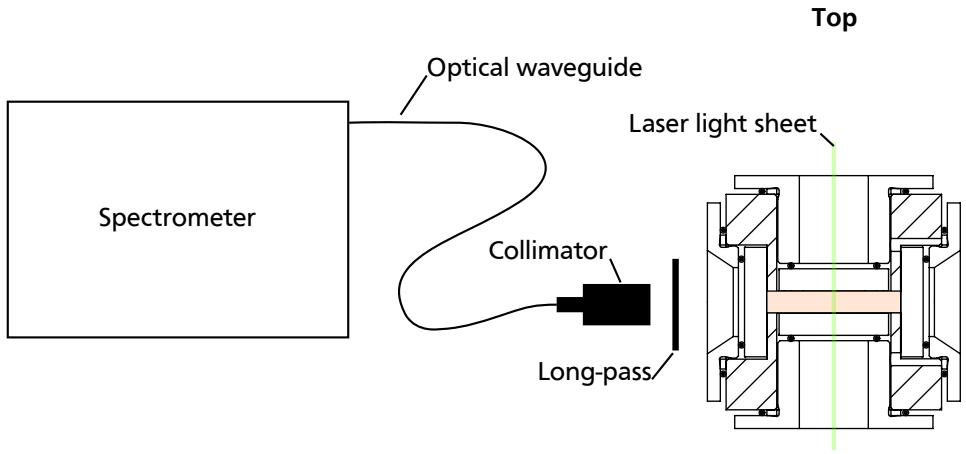

Figure 3.8: Schematic of the detector setup used for dye characterization.

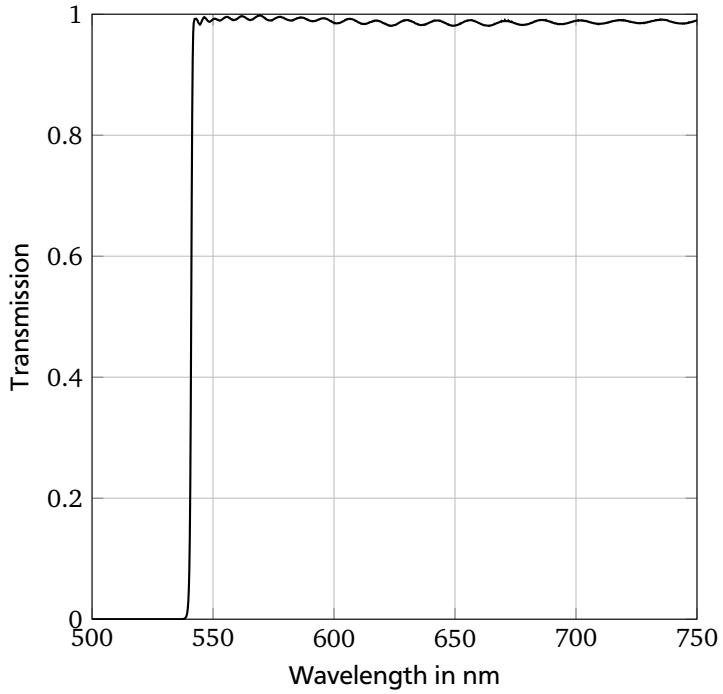

Figure 3.9: Transmission curves of the long-pass.

Fig. 3.10 shows a schematic of the channel-based imaging spectrometer used for the 2c/2d PLIF-Thermography. The channel-based spectrometer consisted of a telecentric lens, a relay lens group, a filter cube, and two detectors. The idea for the design was inspired by the setup used by Bork [5] for imaging raman spectroscopy.

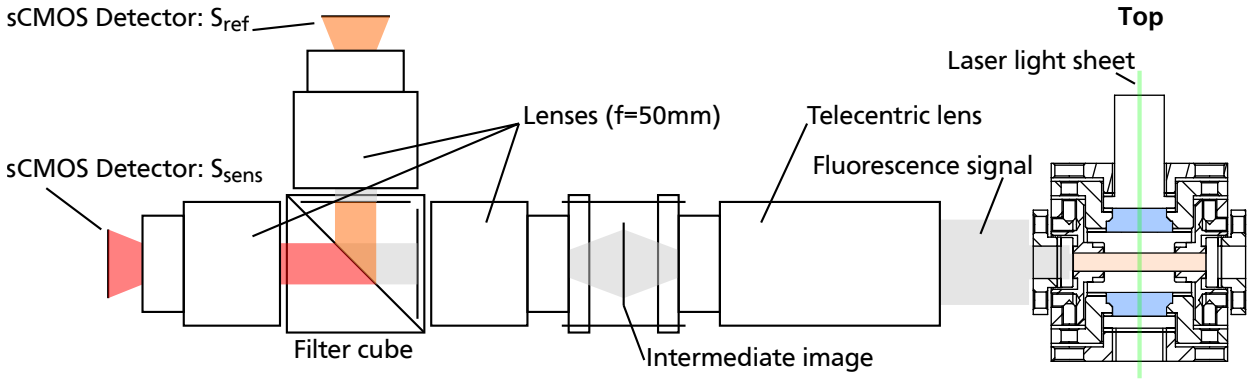

Figure 3.10: Schematic of the detector setup used for 2c/2d PLIF-Thermography.

The telecentric lens (TECHSPEC, 0.9X PlatinumTL) imaged the collected fluorescence light into an intermediate image. A telecentric lens with a magnification of 0.9 was chosen because it produces an orthographic image with little perspective distortion. This was necessary for 2c/2d PLIF-Thermography experiments at a stationary evaporating meniscus to enable an easy identification of the evaporator wall. Furthermore, this ensured that the part of the meniscus that should be observed is not hidden by the part of the meniscus that is closer to the lens and therefore would appear larger with an entocentric lens. The intermediate image was transferred through the filter cube (Thorlabs, DFM/1) to the detectors by a relay lens group. The relay lens group consisted of three lenses (Nikon, Nikkor 50 mm 1:1.4 Ai-S) with a focal length of f=50 mm and had a magnification of one. The first lens of the relay lens group imaged the intermediate image to infinity and thus parallelized the light. The other two lenses of the relay lens group imaged the parallelized light onto the two detectors.

The filter cube was located between the lenses of the relay lens group. Inside the filter cube the fluorescence light was separated spectrally by a combination of an imaging-flat dichroic mirror (Semrock, FF640-FDi01, edge wavelength 640 nm), a long-pass (Semrock, BLP02-561R, edge wavelength 572 nm), and a band-pass (Semrock, FF01-578/21, center wavelength 578 nm, bandwidth 21 nm) into a temperature-sensitive part S_{sens} and a reference part S_{ref}. The transmission curves of the filter combination are shown in Fig. 3.12. This configuration was chosen because the filter characteristics depend on the angle of incidence of the light. The filters were selected from standard filters produced by Semrock in order to maximize the dependence on

temperature of the ratio of the fluorescence signals and the height of the individual fluorescence signals. The dichroic mirror was selected from the list of filters which are imaging flat to avoid a distorted image on the detector of the reference signal due to curvature of the filter substrate.

The filter cube was attached to a kinematic mount which allowed an angular adjustment of ±4°. This way the filter cube could be tilted around two axes so that a coarse mechanical alignment of the two images by two thumb screws was facilitated. A small tilting of the filter cube led to a translation of the image on the detector for the reference signal while the position of the image on the detector for the sensitive signal remained unchanged. By a rotation of the detectors the orientation of the images could be adjusted. However, this alignment is not sufficient for the 2c/2d PLIF-Thermography. Therefore the images of the two detectors were additionally aligned by a coordinate transformation during the evaluation process.

As detectors two sCMOS Andor Zyla 5.5 were used. Fig. 3.11 shows the development of the signal-to-noise ratio of the sCMOS detectors used with increasing gray value. The key properties of the sCMOS detectors were determined according to EMVA 1288 [22] at an integrating sphere and can be found in Tab. 3.2. The sCMOS detectors have a very good linearity and a low pixel response non-uniformity. Therefore a radiometric calibration of the individual sCMOS detectors was not considered. The sCMOS detectors have a high signal-to-noise ratio and a high dynamic range. Additionally, the sCMOS detectors have a high quantum efficiency. This is important for 2c/2d PLIF-Thermography because it is desired to detect as much of the fluorescence signal as possible. The sCMOS detectors were cooled down to 0 °C so that the ambient temperature had no influence on the camera characteristics.

For the experiments the cameras were operated in the global shutter mode and two-by-two hardware binning was applied to increase the quantum efficiency and to improve the signal-to-noise ratio. The spatial resolution of the total setup was determined as 14 µm per pixel with a resolution test target. The optical resolution of the setup was measured to be in the order of 25 µm with a 1951 USAF chart at 50 % contrast. The cameras were set to an exposure time of 50 ms at a frame rate of 4 Hz. The analog digital conversion was set to 16 bit. The pixel read-out rate was set to 560 MHz and triggering mode was set to external.

Table 3.2: Key properties determined according to EMVA 1288 of the sCMOS detector used.

Property	Value
Dark noise	2.55 e^-
Dark signal non-uniformity	2.15 e^-
Signal-to-noise ratio SNR_{max}	175
SNR_{max}^{-1}	0.57 %
Pixel response non-uniformity	0.93 %
Non-linearity error LE	0.20 %

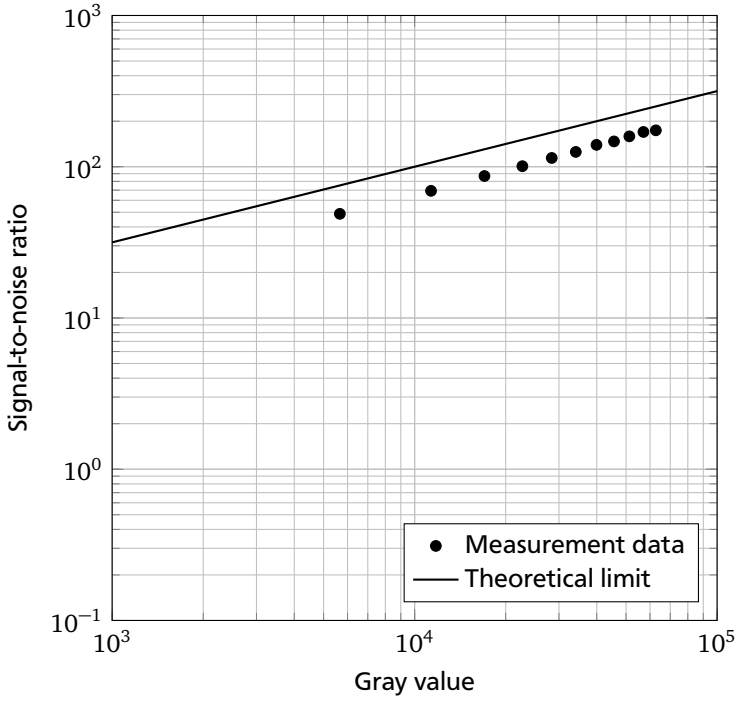

Figure 3.11: Signal-to-noise ratio versus gray value according to EMVA 1288 of the sCMOS detector used.

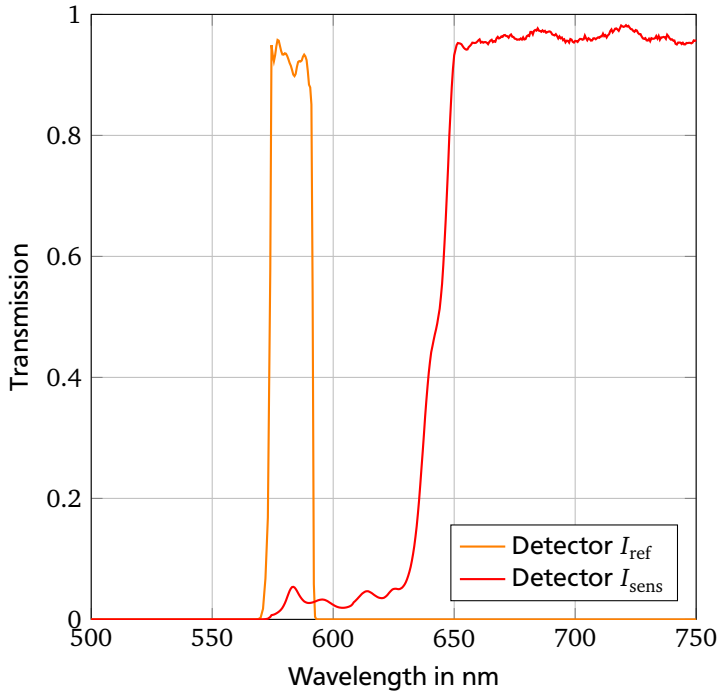

Figure 3.12: Transmission curves of the channel-based imaging spectrometer's filter setup.

3.4 Timing and Synchronization

For 2c/2d PLIF-Thermography it is necessary that the fluorescence detected by both detectors is caused by the same laser pulses, because the fluorescence signal depends on the laser fluence, which is not absolutely constant. Therefore a synchronization of the detectors' exposure time with the laser pulses has to be achieved. Fig. 3.13 shows a schematic of the timing and synchronization of the detectors and the laser pulses. The timing and synchronization was achieved by TTL signals generated by a timing hub (IDT, MotionPro Timing Hub). One TTL signal was used to trigger the exposure of the detectors and one was used to trigger the laser pulses. During each exposure a burst of several laser pulses was triggered. The exposure of the detectors was delayed by 150 µs with respect to the first laser pulse of each burst. This was necessary because the first laser pulse of each burst had a much higher pulse energy than the rest.

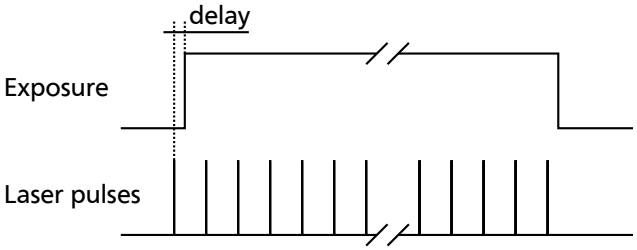

Figure 3.13: Schematic of timing and synchronization of detector exposure and laser pulses.

3.5 Chemicals Used

In Tab. 3.3 the chemicals used are listed. The fluorescent dyes were supplied by Radiant Dyes Laser & Accessories GmbH. As solvent ethanol ROTIPURAN ≥99.8 % p.a. from Carl Roth, which contains no methyl ethyl ketone (MEK), was used. This was done to avoid possible influences of the MEK, which is otherwise used to denature the ethanol. The thermodynamic properties of ethanol were calculated according to Dillon and Penoncello [17].

The dyes were dissolved separately in ethanol. The generated solutions were mixed in the desired ratios and diluted to the needed concentrations. This way the ratio of the dye concentrations was kept constant for all experiments. Two dye combinations were used: Rhodamine 6G and Pyridine 1 in a mass concentration ratio of 1:7.4 and Rhodamine 6G and DCM in a mass concentration ratio of 1:10.8. With these mass concentration ratios an almost identical signal height on both detectors could be achieved for the 2c/2d PLIF-Thermography.

These dyes were chosen with respect to the investigations of Nasarek [42], who identified them as the most promising dyes usable for 2c/2d PLIF-Thermography in ethanol among common

laser dyes which can be dissolved in ethanol. The most common dye combination for water Rhodamine B and Rhodamine 110 was not used because it has a large overlap of absorption and emission spectra in the regions used for the 2c/2d PLIF-Thermography. Therefore it was regarded as less promising for use for measurements at an evaporating liquid meniscus than the combinations described by Nasarek for ethanol. Furthermore, the combination of Rhodamine B and Rhodamine 110 is not sufficiently excitable at a wavelength of 532 nm [43].

Table 3.3: List of the chemicals used.

Name	Molecular formula	Molar mass	CAS no.
Ethanol ≥99.8 %, p.a.	C_2H_6O	46.07 $gmol^{-1}$	64-17-5
Pyridine 1	$C_{19}H_{23}N_2O_4Cl$	378.85 $gmol^{-1}$	110-86-1
DCM	$C_{19}H_{17}N_3O$	303.36 $gmol^{-1}$	51325-91-8
Rhodamine 6G	$C_{28}H_{31}N_2O_3Cl$	479.02 $gmol^{-1}$	989-38-8

3.6 Experimental Procedures

In this section the experimental procedures are described. The experimental procedures can be divided in two categories. The first category includes the procedures used for the investigation of the possible dye combinations. The second category sums up the procedures applied for the investigations of the 2c/2d PLIF-Thermography.

Experimental Procedures for Dye Characterization

Prior to the experiments the dye solution was degassed in an ultrasonic bath which was heated to approximately 60 °C for 1 h. This was done to remove dissolved air from the solution. For the experiments regarding the influence of dissolved air the degasification was omitted.

After every measured parameter set the liquid in the cavity was exchanged to avoid an influence of photobleaching. For experiments with changing dye concentrations the dye solution was removed from the test cell. Afterwards the test cell was flushed four times with ethanol. After the last flush the test cell was dried with a vacuum pump and filled with the new dye solution. This reduced the error from dye residuals in the cavity. For the investigation of the influence of photobleaching the replacement of the dye solution was omitted.

The number of laser pulses that was used to generate the fluorescence for one spectrum and the exposure time of the spectrometer was adjusted so that the highest signal of the spectrometer in the measured parameter range was at approximately 80 % of the dynamic range of the

spectrometer. This was done to avoid possible nonlinearity due to the characteristic of the spectrometer's detector close to saturation. One spectrum was the accumulated fluorescence signal generated by multiple laser pulses. The laser pulse frequency was either 10 kHz or 15 kHz. The high repetition rate of the laser was used to achieve a good signal-to-noise ratio even at low pulse energies by accumulation of the fluorescence signal generated by several laser pulses over the exposure time of the spectrometer's detector. The laser was switched on only during the exposure time of the spectrometer to avoid photobleaching of the dyes. The laser fluence was set to be in the linear regime of the dye combination. Only for the experiments regarding the influence of the laser fluence was the linear regime left.

In every experiment only one parameter was manipulated while all others were kept constant. For each parameter set 60 samples were recorded with the spectrometer. The temperature of the dye solution was kept stable within $\pm 0.05\,°C$. The temperatures at the bottom and at the top of the cavity did not differ more than 0.1 °C from each other. This was taken as an indication of a uniform temperature distribution. For the experiments where the pressure was varied the pressure was kept stable with a vacuum pump within ± 5 mbar. The measurement of the laser power was done before and after the recording of the spectra. For every laser power 100 samples were recorded with the thermal laser power meter.

Experimental Procedures for 2c/2d PLIF-Thermography

For experiments concerning the investigation of the applicability of 2c/2d PLIF-Thermography at a stationary evaporating meniscus the following procedures were used. The experimental setup for the investigation of a stationary evaporating liquid meniscus was evacuated. After the evacuation, the test cell was filled with the ethanol dye solution. In the ethanol the dyes Rhodamine 6G and Pyridine 1 were dissolved in a mass concentration ratio of 1:7.4. The concentration of Rhodamine 6G was 2.5 $\mu g L^{-1}$ and the concentration of Pyridine 1 was 18.4 $\mu g L^{-1}$. Prior to the filling process the solution had been degassed in an ultrasonic bath which was heated to approximately 60 °C for 2 h. After the filling process remaining non-condensable gases were removed by a vacuum pump through the valve at the top of the condenser. As the criterion for a successful degasification the saturation temperature calculated from the pressure measured inside the test cell and the temperature of the test cell were compared. The degasification was continued until both temperatures matched each other within the measurement uncertainty. Each day prior to the experiments non-condensable gases were removed.

A 2c/2d PLIF-Thermography measurement consisted of a series of 40 subsequent images recorded by the channel-based imaging spectrometer. For every measurement also 40 images of the background were recorded for the background subtraction. The laser was set to 30 kHz and an average power of 3.4 W measured under continuous pulsed operation.

Calibration

Prior to the actual calibration the two sCMOS detectors of the channel-based imaging spectrometer were roughly aligned mechanically with a grid target (Thorlabs, R1L3S3P). Images of the target were recorded with both detectors. These images were used for the coordinate transformation during the data evaluation. For the calibration of the 2c/2d PLIF-Thermography the whole evaporator was filled with the liquid ethanol dye solution. Therefore the reservoir was positioned in a way that the evaporator section of the test cell between the two valves was completely filled. After this the valves were closed in order to separate the evaporator from the rest of the system. This way evaporation inside the evaporator was prevented during calibration. To achieve a homogeneous temperature distribution inside the evaporator the tempering jacket and the trace heating were used. For the calibration the temperature of the dye solution was increased starting from 21.0 °C to 31.0 °C in steps of 2.0 °C. At each temperature level ten measurements were performed. As temperature reference for the calibration the two thermocouples inside the evaporator were used. The difference between the temperatures measured at the thermocouples was always below 0.05 °C under stationary conditions. This was used as indication for a homogeneous temperature distribution inside the liquid.

Validation and Repeatability

The validation of the performed calibration was conducted subsequently to the calibration with an unchanged setup. For the validation the temperature of the ethanol dye solution was raised starting from 22.0 °C to 30.0 °C in steps of 2.0 °C. At each temperature level ten 2c/2d PLIF-Thermography measurements were conducted.

For the investigation concerning the repeatability the dye solution in the evaporator was kept at 26 °C for several hours. During this time a total of 25 2c/2d PLIF-Thermography measurements were run at ten-minute intervals.

Measurements at the Stationary Evaporating Liquid Meniscus

For the measurements at the evaporating liquid meniscus the valves below and above the condenser which were closed for calibration were opened. The liquid-vapor interface was moved inside the field of view of the channel-based imaging spectrometer by lowering the reservoir. For the measurements at an evaporating meniscus only the tempering jacket of the evaporator was used as heat source and the trace heating was switched off. This ensured that the wall was only superheated inside the evaporator in order to prevent nucleate boiling below this section. The

temperature of the condenser and the temperature of the tempering jacket were first set to the same value. From this point on, the temperature of the heating jacket was increased in 1.0 °C steps until nucleate boiling started. This was done to achieve increasing levels of wall superheat and thereby increasing evaporation rates. At each temperature step 2c/2d PLIF-Thermography measurements were taken.

3.7 Data Evaluation Procedures

In this section the data evaluation procedures are described. First the data evaluation procedure for the investigation of the dye combinations for the 2c/2d PLIF-Thermography is presented. Afterwards the data evaluation procedure for the 2c/2d PLIF-Thermography itself is described.

Data Evaluation Procedure for Dye Characterization

The measurement data was evaluated spectrally resolved and integrally. For the integral evaluation two parts of the spectrum were separated by integration along two different wavelength intervals. One part (S_{ref}) was in a region of the spectrum that is only slightly affected by temperature changes (λ_1 to λ_2) and the other one (S_{sens}) covers the region of the spectrum that is most affected by temperature changes (λ_3 to λ_4). The regions were chosen with respect to the requirements for 2c/2d PLIF-Thermography given by Coppeta and Rogers [14]. The fluorescence signals are given by

$$S_{\mathrm{ref}} = \int_{\lambda_1}^{\lambda_2} S(\lambda)\,\mathrm{d}\lambda \tag{3.1}$$

$$S_{\mathrm{sens}} = \int_{\lambda_3}^{\lambda_4} S(\lambda)\,\mathrm{d}\lambda \tag{3.2}$$

where S_{ref} is the fluorescence signal in the region with almost no temperature influence; S_{sens}, the fluorescence signal in the region with high temperature influence; $S(\lambda)$, the fluorescence signal as a function of the wavelength λ. The ratio R of the fluorescence signals in the two regions of the spectrum is given by

$$R = \frac{S_{\mathrm{sens}}}{S_{\mathrm{ref}}} \tag{3.3}$$

All wavelengths were selected on the basis of standard filters from Semrock Inc. that could be used in the 2c/2d PLIF-Thermography application. The wavelength λ_1 was selected in a way that it is above the laser wavelength and the overlap of emission and absorption spectra is low. The wavelengths λ_2 to λ_4 were selected in a way that the temperature dependency of the ratio and the fluorescence signal were optimized. The integral results presented are therefore only valid for the wavelengths given in Tab. 3.4.

Table 3.4: List of the wavelengths used for the dye characterization.

Wavelengths	Rhodamine 6G and Pyridine 1	Rhodamine 6G and DCM
λ_1	565 nm	545 nm
λ_2	590 nm	570 nm
λ_3	640 nm	600 nm
λ_4	700 nm	660 nm

In Fig. 3.14 the relative emission spectra of the two dye combinations are shown. Compared to the individual dyes there was no change of the emission spectra observed. The colored areas are the regions for which the influence of laser fluence, concentration, temperature, pressure, amount of dissolved air, and photo-stability was investigated integrally.

For every measured data point 60 spectra were averaged. The measurement uncertainty of the averaged values was calculated as the root-mean-square deviation of these samples divided by the square root of the number of samples.

The results of measurements regarding the influence of the laser fluence on the fluorescence signal were fitted with a model available in literature. According to Eckbreth [20], from a rate-equation analysis of a two-level model the following relationship which describes the fluorescence-signal-collected S as a function of the laser spectral irradiance I_ν can be derived:

$$S = \frac{\Omega}{4\pi} A l \, \Delta t_\mathrm{e} \, \epsilon A_{21} \, N_1^0 \frac{B_{12}}{B_{12} + B_{21}} \frac{1}{1 + \frac{I_{\nu,\mathrm{sat}}}{I_\nu}} \tag{3.4}$$

where Ω is the collection solid angle; A, the focal area of the laser beam; l, the axial extent along the beam from which the fluorescence is observed; Δt_e, the sampling interval; ϵ, the collection efficiency; A_{21}, Einstein coefficient for spontaneous emission, N_1^0, the species population prior to excitation; B_{12}, Einstein coefficient for stimulated absorption; B_{21}, Einstein coefficient for stimulated emission; $I_{\nu,\mathrm{sat}}$, saturation spectral irradiance.

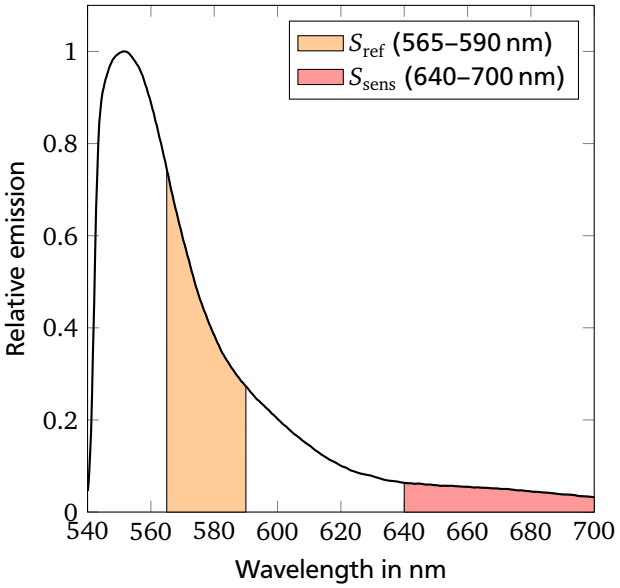

(a) Solution of 9.9 µgL^{-1} Rhodamine 6G and 73 µgL^{-1} Pyridine 1 in ethanol. Laser fluence of 2.06 mJcm^{-2}.

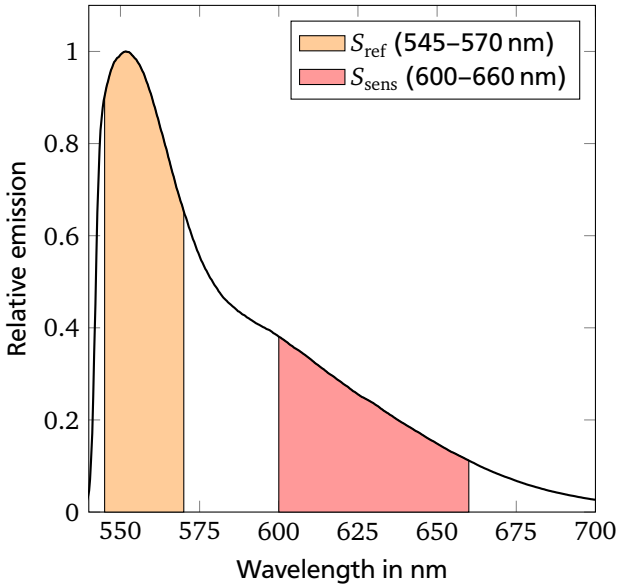

(b) Solution of 9.9 µgL^{-1} Rhodamine 6G and 106 µgL^{-1} DCM in ethanol. Laser fluence of 1.35 mJcm^{-2}.

Figure 3.14: Relative emission of the dye mixtures versus the wavelength. Solution temperature of 22.0 °C.

With the assumption of a constant pulse length Δt_p the spectral irradiance can be expressed as a function of the spectral fluence u_ν. With the assumption of a constant laser linewidth the spectral fluence can be replaced by the fluence u:

$$I = \int I_\nu \, d\nu = \frac{1}{\Delta t_p} \int u_\nu \, d\nu = \frac{u}{\Delta t} \tag{3.5}$$

With a reference laser fluence u_{ref} the relative fluorescence signal S_{rel} can be expressed as a function of the fluence with the parameter u_{sat}.

$$S_{rel}(u) = \frac{S(u)}{S(u_{ref})} = \frac{1 + u_{sat}/u_{ref}}{1 + \frac{u_{sat}/u_{ref}}{u/u_{ref}}} \tag{3.6}$$

The parameter u_{sat} was calculated spectrally resolved and integrally for the two spectral parts of the two dye combinations by a least-squares fit with experimental data.

The results of measurements regarding the influence of the dye concentration on the fluorescence signal were fitted with a model available in literature. According to Lemoine, Wolff, and

Lebouche [38] the relative fluorescence signal versus the molar dye concentration C with the molar concentration reference C_{ref} can be described by

$$S_{\mathrm{rel}}(C) = \frac{S(C)}{S(C_{\mathrm{ref}})} = \frac{C}{C_{\mathrm{ref}}}\, 10^{-\varepsilon\, l\, C_{\mathrm{ref}}\left(\frac{C}{C_{\mathrm{ref}}}-1\right)} \tag{3.7}$$

where ε is the decadic absorption coefficient and l is the path length. In the experiments the path length l was 15.5 mm. The dye mixture is treated as a solution with only one species with the molar concentration C, which is the sum of the two dyes' molar concentrations. For this reason the results are only valid for the mass concentration ratio of 1:7.4 for Rhodamine 6G and Pyridine 1 and 1:10.8 for Rhodamine 6G and DCM. The effect of concentration quenching was neglected because of the low overall concentrations used, which were at least three orders of magnitude lower than the common concentrations used for dye lasers. The absorption coefficient was calculated spectrally resolved and integrally for the two spectral parts of the two dye combinations by a least-squares fit with experimental data.

The results of measurements regarding the influence of the temperature of the dye solution on the fluorescence signal were fitted with a model available in literature. According to Lemoine et al. [39] the relative fluorescence signal versus the temperature T of the dye solution and a reference temperature T_{ref} in Kelvin can be described by

$$S_{\mathrm{rel}}(T) = \frac{S(T)}{S(T_{\mathrm{ref}})} = e^{\beta\left(\frac{1}{T}-\frac{1}{T_{\mathrm{ref}}}\right)} \tag{3.8}$$

with the temperature coefficient β. The temperature coefficient was calculated spectrally resolved and integrally for the two dye combinations by a least-squares fit with experimental data.

For the ratio $R(T)$ of the fluorescence signal from the two parts of the spectrum a similar equation can be formulated. With a ratio at a reference temperature the relative ratio $R_{\mathrm{rel}}(T)$ can be written as a function of the temperature.

$$R_{\mathrm{rel}}(T) = \frac{S_{\mathrm{sens}}(T)}{S_{\mathrm{ref}}(T)}\,\frac{S_{\mathrm{ref}}(T_{\mathrm{ref}})}{S_{\mathrm{sens}}(T_{\mathrm{ref}})} = e^{\beta_{\mathrm{R}}\left(\frac{1}{T}-\frac{1}{T_{\mathrm{ref}}}\right)} \tag{3.9}$$

with

$$\beta_{\mathrm{R}} = \beta_{\mathrm{sens}} - \beta_{\mathrm{ref}} \tag{3.10}$$

The temperature coefficients β_R of the ratio were calculated for the two spectral parts of the two dye combinations by a least-squares fit with experimental data.

Data Evaluation Procedures for 2c/2d PLIF-Thermography

The data evaluation of the 2c/2d PLIF-Thermography consisted of two parts. The first part was the calibration of the 2c/2d PLIF-Thermography and the second part was the evaluation of the measurement data of the 2c/2d PLIF-Thermography with the previously calculated calibration. For both parts of the data evaluation a coordinate transformation of the images from both detectors of the channel-based imaging spectrometer is needed, which ensures a registration in the world coordinate system and an alignment of the images from both detectors.

Coordinate Transformation

Based on the images of the grid target taken prior to each calibration a coordinate transformation to world coordinates was calculated for each detector. Fig. 3.15 shows a schematic of the calculation of the coordinate transformations. The axis of the world coordinate system were referenced to the walls of the evaporator. This way an alignment of the pixels of the two detectors was possible and potential distortion of the images was removed. Furthermore, after the transformation the orientation of the images matched the orientation of the world coordinate system and thus had the same orientation as the walls of the evaporator.

In order to calculate the transformations to the world coordinates first the nodes of the grid target images were detected. Therefore the grid images were transformed into binary images by a global threshold. On the generated binary images a morphological thinning was applied. The lines of the grid were extracted from the Hough transformation of the binary grid images. From the lines the nodes are approximated by calculation of the intersections of the lines. The approximated nodes were fine-tuned by a local cross-correlation in the neighborhood of the approximated node location of the grid images from both detectors. From the detected nodes and a digital representation of the nodes in the world coordinate system an affine transformation which included translation, scale, and rotation was calculated for each detector. From the known spacing of the grid nodes in the world coordinate system the spatial resolution was calculated.

Calibration

The data set for the calibration consisted of the N images recorded at M temperature levels from each detector $S_{\mathrm{ref},n,m}$ and $S_{\mathrm{sens},n,m}$ together with the associated background, the M temperatures

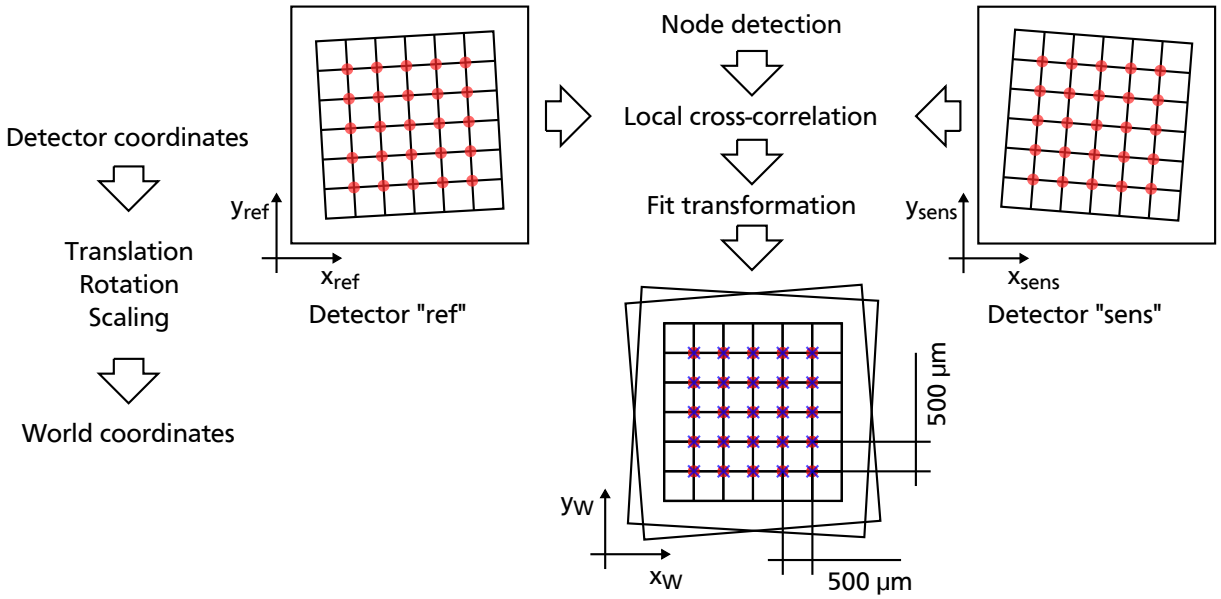

Figure 3.15: Coordinate transformation for the channel-based imaging spectrometer.

of the thermocouples T_m inside the cavity, and the coordinate transformations for each detector. The elements of $S_{\mathrm{ref},n,m}$ and $S_{\mathrm{sens},n,m}$ are given by $s_{\mathrm{sens},i,j,n,m}$ and $s_{\mathrm{ref},i,j,n,m}$ respectively, where n is the index of the image; i, j the indices of the pixel, and m the index of the temperature.

Fig. 3.16 shows a schematic of the calibration procedure. The first step of the calibration process was the background subtraction which was performed for each image. After the background subtraction the coordinate transformation was applied to each image. In this order there is no need for a coordinate transformation of the background images and so computation time is reduced.

By a pixel-wise division of the images $S_{\mathrm{ref},n,m}$ and $S_{\mathrm{sens},n,m}$ recorded at the same time by both detectors, N ratio matrices at M temperature levels $R_{n,m}$ with the elements $r_{i,j,n,m}$ were created.

$$r_{i,j,n,m} = \frac{s_{\mathrm{sens},i,j,n,m}}{s_{\mathrm{ref},i,j,n,m}} \tag{3.11}$$

The resulting N images at each temperature level were temporally averaged so that M ratio matrices R_m – one for each temperature step – were generated. Additionally the temporal standard deviation $\sigma_{i,j,m}$ for each element $r_{i,j,m}$ along the N images was calculated.

$$r_{i,j,m} = \frac{1}{N} \sum_{n=1}^{N} r_{i,j,n,m} \tag{3.12}$$

$$\sigma_{i,j,m} = \sqrt{\frac{1}{N-1}\sum_{n=1}^{N}\left(r_{i,j,n,m} - r_{i,j,m}\right)^2} \tag{3.13}$$

For each element $r_{i,j,m}$ of the ratio matrices R_m a calibration curve $r_{i,j} = f_{i,j}(T_m)$ was fitted by a least-squares analysis. Two different functions were considered for the 2c/2d PLIF-Thermography calibration. The first approach was the exponential function introduced by Lemoine et al. [39]. The function has two degrees of freedom in the form of the fitting parameters k and β.

$$r_{i,j} = k_{i,j}\, e^{\frac{\beta_{i,j}}{T}} \tag{3.14}$$

The second approach was a second-order polynomial function. The function has three degrees of freedom in the form of the fitting parameters a, b, and c.

$$r_{i,j} = a_{i,j}\, T^2 + b_{i,j}\, T + c_{i,j} \tag{3.15}$$

The fitting parameters were determined as the values that minimize $\chi^2_{i,j}$. In this approach the standard deviation of the measured data points is used as weight for the squared deviations of the fit and the measured data. This was done to account for the rise of the standard deviation with temperature caused by the decrease of the fluorescence signal at higher temperatures.

$$\chi^2_{i,j} = \sum_{m=1}^{M} \frac{\left(r_{i,j,m} - f_{i,j}(T_m)\right)^2}{\sigma^2_{i,j,m}} \tag{3.16}$$

The minimum value of $\chi^2_{i,j}$ was used to judge the quality of the fit and to compare the performance of different calibration functions by an χ^2 analysis. The χ^2 analysis offers a measure to judge the likelihood of the fit based on the random fluctuations of the measured values described by the standard deviation. A detailed description of the χ^2 analysis can be found in Berendsen (2011) – *A Student's Guide to Data and Error Analysis* [4], chapter 7.4. The other criteria to access the quality of the fit was to analyze the dependence of the residuals $r_{i,j,m} - f_{i,j}(T_m)$ on T. A reasonable fit yields residuals that are a sample from a random distribution and are therefore uncorrelated.

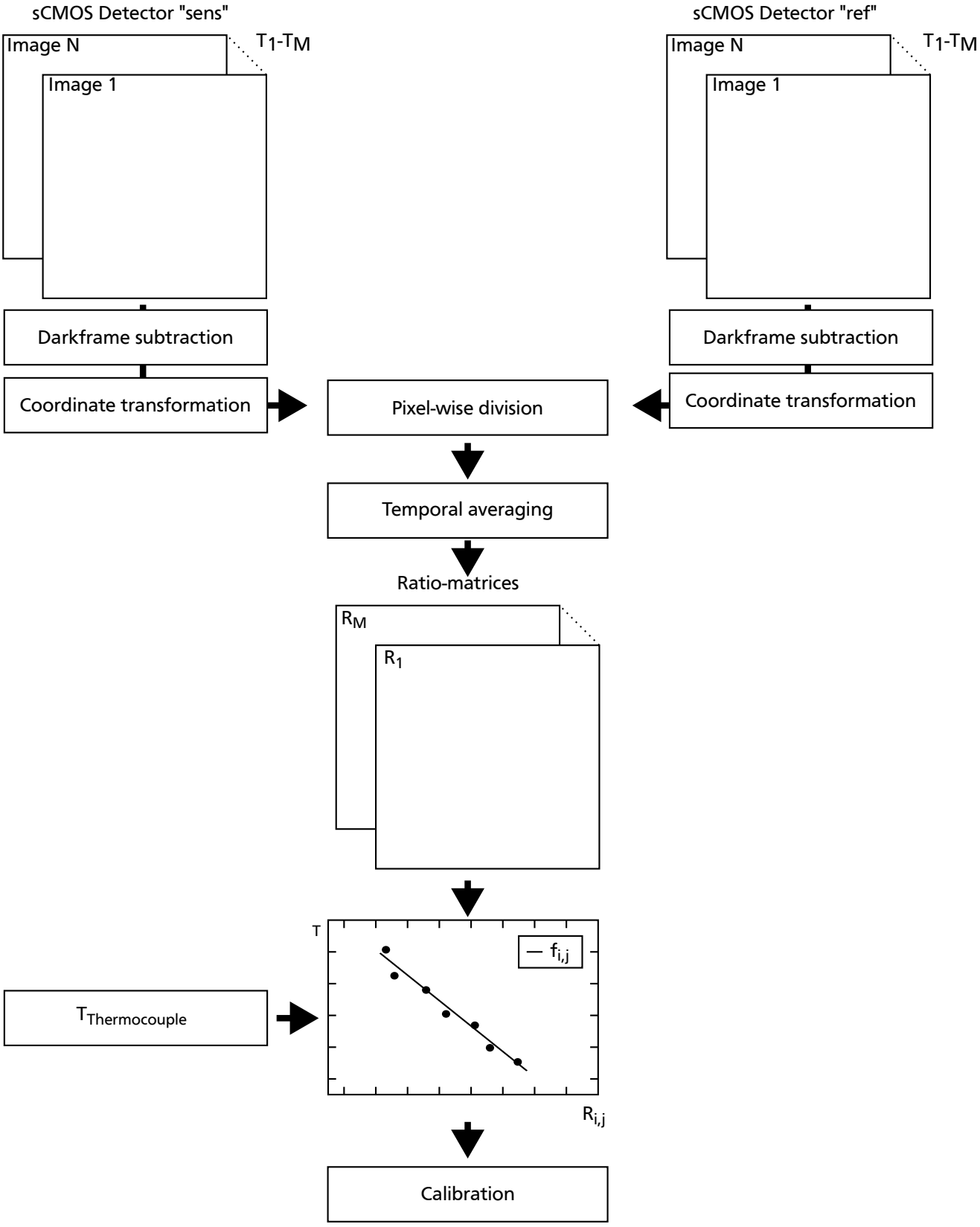

Figure 3.16: Schematic of the calibration procedure for 2c/2d PLIF-Thermography.

Evaluation

The data set of a 2c/2d PLIF-Thermography measurement consisted of N images recorded by each detector $S_{\mathrm{ref},n}$ and $S_{\mathrm{sens},n}$ together with the associated background, the coordinate transformation for each detector, and the calibration parameters for each pixel. The elements of $S_{\mathrm{ref},n}$ and $S_{\mathrm{sens},n}$ are given by $s_{\mathrm{sens},i,j,n}$ and $s_{\mathrm{ref},i,j,n}$ respectively.

Fig. 3.17 shows a schematic of the calibration procedure. The first step of the evaluation of a 2c/2d PLIF-Thermography measurement was the background subtraction which was performed for each image. After the background subtraction the coordinate transformation was applied to each image. By a pixel-wise division of the frames S_{ref} and S_{sens} recorded at the same time dy both detectors, N ratio matrices R_n with the elements $r_{i,j,n}$ were created.

$$r_{i,j,n} = \frac{s_{\mathrm{sens},i,j,n}}{s_{\mathrm{ref},i,j,n}} \tag{3.17}$$

From these ratio matrices R_n the temperature matrices T_n with the elements $t_{i,j,n}$ were retrieved by the inverse calibration function $f_{i,j}^{-1}$ with the calibration parameters for each pixel.

$$t_{i,j,n} = f_{i,j}^{-1}\left(r_{i,j,n}\right) \tag{3.18}$$

The resulting temperature matrices T_n were averaged temporally over the N images. Additionally the temporal standard deviation $\sigma_{i,j,n}^{T}$ was calculated for each element.

$$t_{i,j} = \frac{1}{N}\sum_{n=1}^{N} t_{i,j,n} \tag{3.19}$$

$$\sigma_{i,j,m}^{T} = \sqrt{\frac{1}{N-1}\sum_{n=1}^{N}\left(T_{i,j,n} - T_{i,j}\right)^2} \tag{3.20}$$

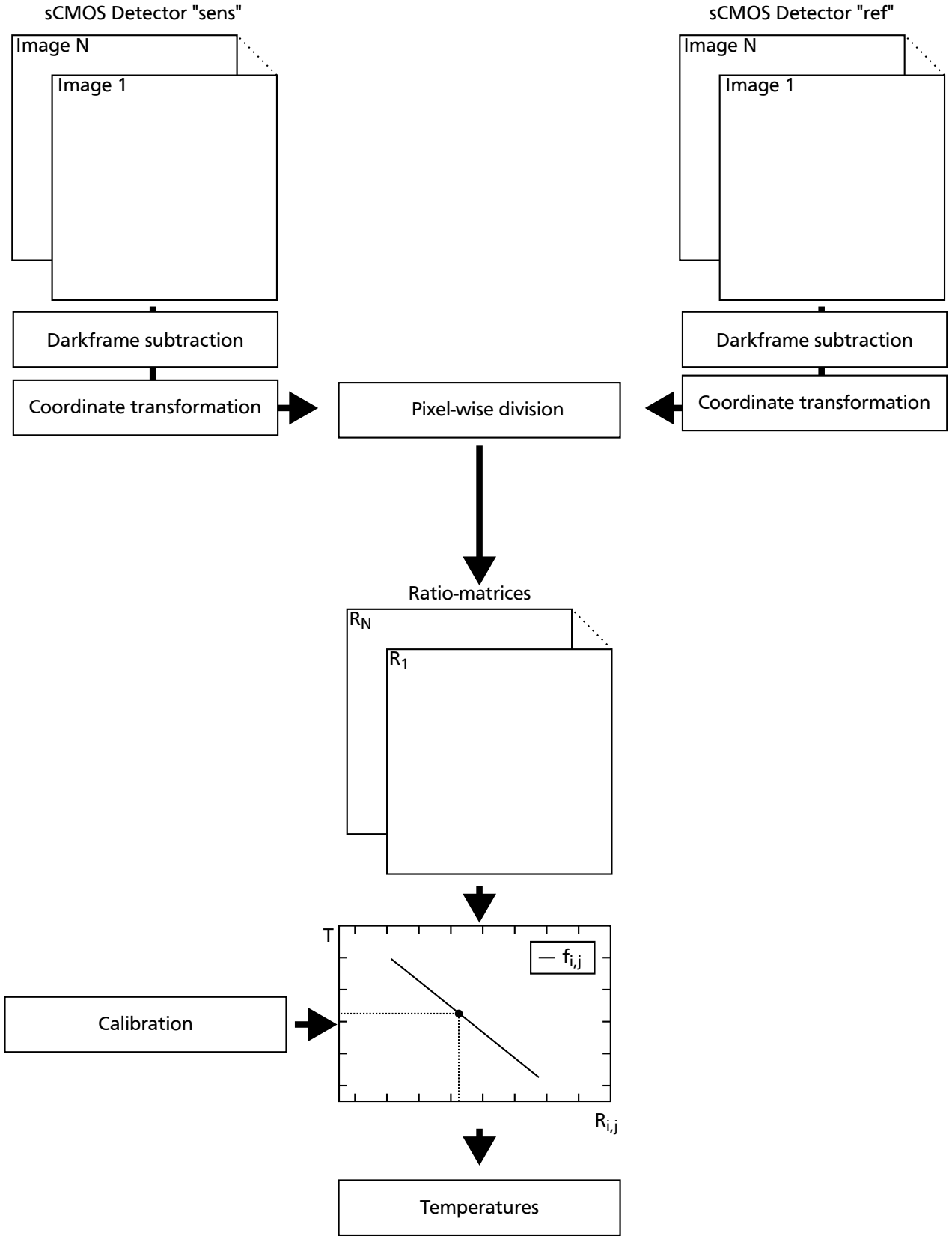

Figure 3.17: Schematic of the evaluation procedure for 2c/2d PLIF-Thermography.

3.8 General Measurement Uncertainties

If not indicated otherwise the measurement uncertainties given in Tab. 3.5 are applicable. The uncertainties are calculated as one standard deviation of the measurement data. For the calculation of the saturation temperature from the system pressure the assumption has to be made that no non-condensable gases are present. The measurement uncertainty of the saturation temperature is derived by the error propagation of the pressure uncertainty and the uncertainty of the ancillary equation given by Dillon and Penoncello [17] used for its calculation.

Table 3.5: List of general measurement uncertainties.

Measured quantity	Measurement uncertainty
Temperature	±0.05 °C
Pressure	±5 mbar
Saturation temperature	±0.2 °C
Concentration	±2 %
Decadic absorption coefficient	±4 %
Wavelength	±1.5 nm
Laser fluence	±1.5 %

4 Dye Characterization

In this chapter the results of the spectral characterization of the fluorescent dyes regarding an application for 2c/2d PLIF-Thermography are presented and discussed. First of all the absorption and emission spectra of the individual dyes (Rhodamine 6G, Pyridine 1, and DCM) dissolved in ethanol are presented. Based on the results of the investigation of the temperature dependence of the individual dyes' emission spectra, two combinations potentially suitable for 2c/2d PLIF-Thermography are selected.

For these dye combinations the investigation results of the fluorescence signals' dependence on temperature, laser fluence, and dye concentration are shown and discussed. Furthermore, the investigation results of the influence of pressure, dissolved air/oxygen, and photobleaching are presented. The results presented in this chapter have already been published by Fenner and Stephan (2017) in [23]. Based on these results the combination most suitable for the 2c/2d PLIF-Thermography is selected for the further investigations at the end of this chapter.

4.1 Absorption and Emission Spectra of the Individual Dyes

In Fig. 4.1a the measured relative absorption spectra of the dyes dissolved in ethanol are shown. The temperature of the dye solutions was 25.0 °C. The peak decadic absorption coefficient was $6.3 \times 10^4\,\mathrm{Lmol^{-1}cm^{-1}}$ at 528 nm for Rhodamine 6G, $2.8 \times 10^4\,\mathrm{Lmol^{-1}cm^{-1}}$ at 493 nm for Pyridine 1, and $2.7 \times 10^4\,\mathrm{Lmol^{-1}cm^{-1}}$ at 472 nm for DCM. At the laser wavelength of 532 nm the decadic absorption coefficient was $6.2 \times 10^4\,\mathrm{Lmol^{-1}cm^{-1}}$ for Rhodamine 6G, $1.9 \times 10^4\,\mathrm{Lmol^{-1}cm^{-1}}$ for Pyridine 1, and $6.4 \times 10^3\,\mathrm{Lmol^{-1}cm^{-1}}$ for DCM. Thus, a sufficient excitation of the dyes is possible with the laser used.

In Fig. 4.1b the emission spectra of the individual dyes dissolved in ethanol are shown. The fluorescence emission of Rhodamine 6G showed a small Stokes shift of only 22 nm. The peak emission of Rhodamine 6G was located at 550 nm. The absorption and emission spectra of Rhodamine 6G partly overlapped in the region from 540 nm to 565 nm.

In the case of DCM the Stokes shift was 138 nm. The peak emission was located at 610 nm. The absorption and emission spectra of DCM partly overlapped in the region from 540 nm to 565 nm.

Pyridine 1 showed the largest Stokes shift of the three dyes of 177 nm. The peak emission was located at 670 nm. The absorption and emission spectra of Pyridine 1 partly overlapped in the region from 540 nm to 650 nm.

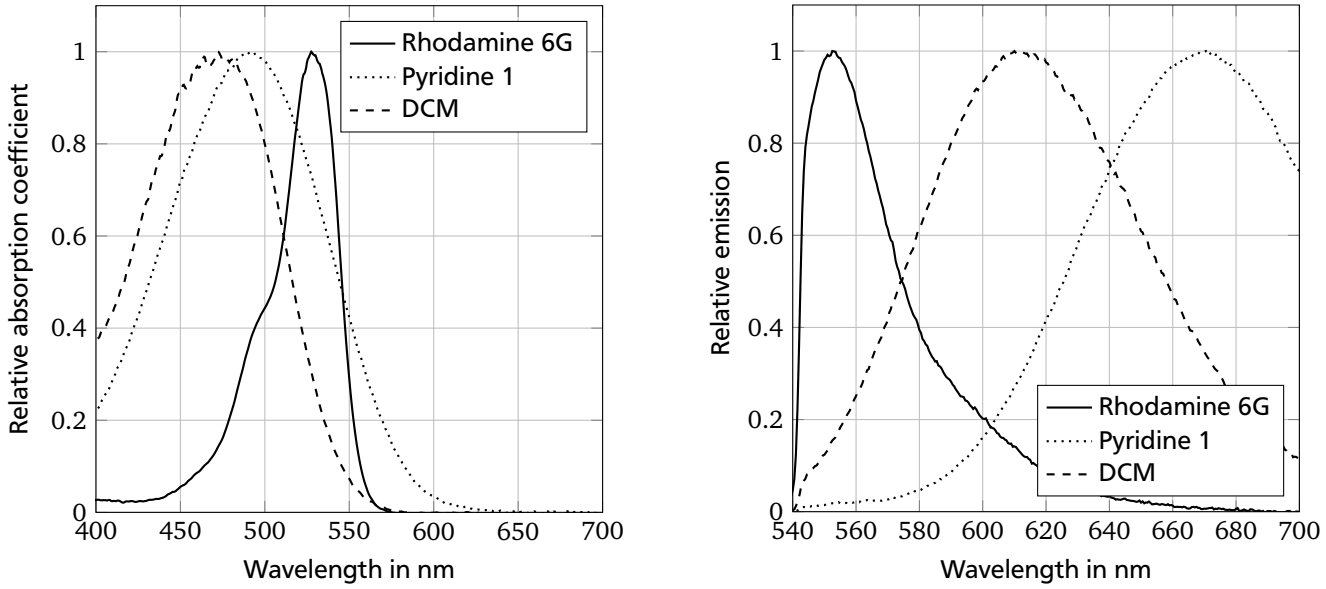

(a) Absorption spectra **(b)** Emission spectra

Figure 4.1: Absorption and emission spectra of Rhodamine 6G, Pyridine 1, and DCM in ethanol at 25.0 °C.

4.2 Influence of Temperature on the Fluorescence Signal

The temperature influence on the fluorescence signal was first investigated for the individual dyes dissolved in ethanol in order to identify dye combinations suitable for the 2c/2d PLIF-Thermography. After the identification of suitable dye combinations the influence of the temperatures on the fluorescence signal was also studied for these dye combinations.

Single Dyes

Fig. 4.2 shows the emission spectra of the single dyes dissolved in ethanol at three different temperatures. The dependence on temperature was evaluated spectrally by the sensitivity which represents the percentage change per Kelvin of the fluorescence signal. A high absolute sensitivity stands for a high dependence on temperature of the fluorescence signal and vice versa.

The emission spectra of Rhodamine 6G showed no significant change at the different temperatures. The temperature sensitivity of the emission was around $-0.3\,\%\mathrm{K}^{-1}$ in the range from

540 nm to 650 nm. This small change could be caused by the change of the dye concentration due to the expansion of the liquid with an increasing temperature. For higher wavelengths the emission of Rhodamine 6G was low and therefore the signal-to-noise ratio was also low. Therefore a meaningful evaluation of the temperature sensitivity in this region was not possible.

The emission of Pyridine 1 showed a significant change at the three temperature levels. In the range from 600 nm to 750 nm the emission decreased almost homogeneously with a temperature sensitivity of $-2.4\,\%\mathrm{K}^{-1}$. Outside of this wavelength range the emission of Pyridine 1 was low and therefore the signal-to-noise ratio was also low. Therefore a meaningful evaluation of the temperature sensitivity in this region was not possible.

Also the emission of DCM showed a significant dependence on temperature. In the range from 540 nm to 700 nm the sensitivity on temperature increased from $-0.1\,\%\mathrm{K}^{-1}$ to $-2\,\%\mathrm{K}^{-1}$. Outside of this wavelength range the emission of DCM was low and therefore the signal-to-noise ratio was also low. Therefore a meaningful evaluation of the temperature sensitivity in this region was not possible.

Dye Combinations

Based on the dependence on temperature of the three dyes, two combinations were possible for an application in 2c/2d PLIF-Thermography. Rhodamine 6G, which showed almost no dependence on temperature, was combined with one of the other two dyes which showed a significant dependence on temperature. The first combination examined was Rhodamine 6G and Pyridine 1 and the second one was a combination of Rhodamine 6G and DCM. For these two combinations the dependence on temperatures was investigated. For these combinations the emission spectra were measured at different temperatures of the dye solution.

For the combination of Rhodamine 6G and Pyridine 1 in ethanol the integral values of the relative fluorescence signal with respect to the temperature are shown in Fig. 4.3b. For the measurements a solution of $9.9\,\mu\mathrm{gL}^{-1}$ Rhodamine 6G and $73\,\mu\mathrm{gL}^{-1}$ Pyridine 1 in ethanol was used. The laser fluence was $2.03\,\mathrm{mJcm}^{-2}$ and the laser pulse frequency was 10 kHz.

For the combination of Rhodamine 6G and DCM in ethanol the integral values of the relative fluorescence signal with respect to the temperature is shown in Fig. 4.4b. For the measurements a solution of $9.9\,\mu\mathrm{gL}^{-1}$ Rhodamine 6G and $106\,\mu\mathrm{gL}^{-1}$ DCM in ethanol was used. The laser fluence was $1.35\,\mathrm{mJcm}^{-2}$ and the laser pulse frequency was 15 kHz.

The temperature coefficient β was calculated spectrally resolved and integrally for the two dye combinations by a least-squares fit with the experimental data. The results are shown in Fig. 4.3 and Fig. 4.4. For the dye combination of Rhodamine 6G and Pyridine 1 an almost constant level

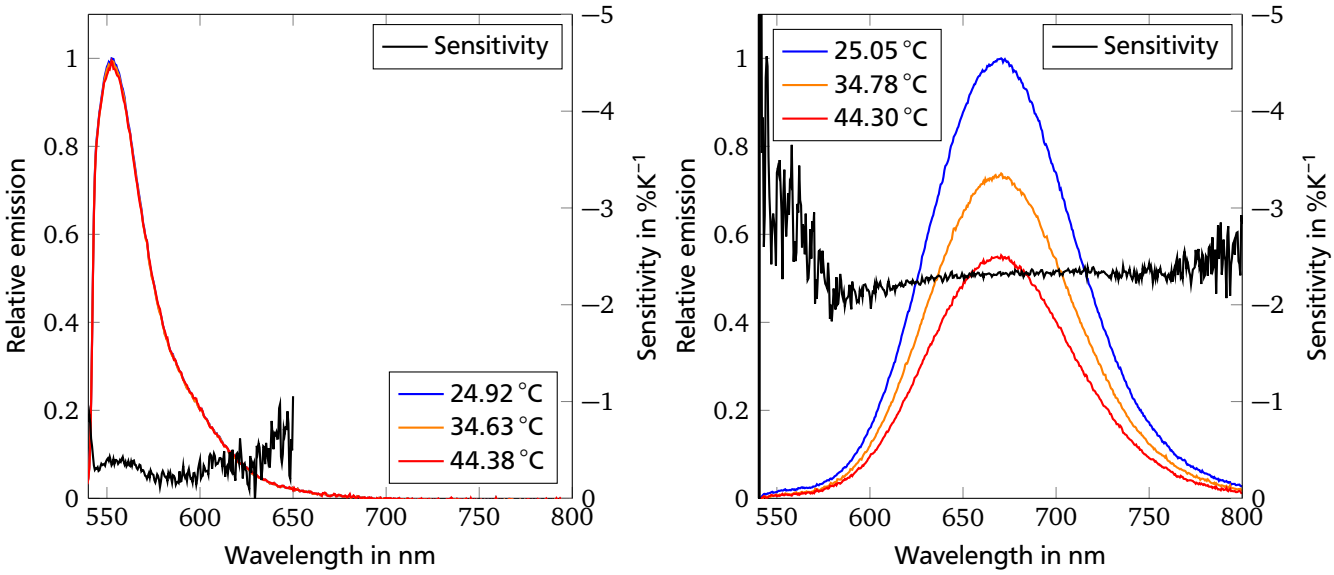

(a) Rhodamine 6G

(b) Pyridine 1

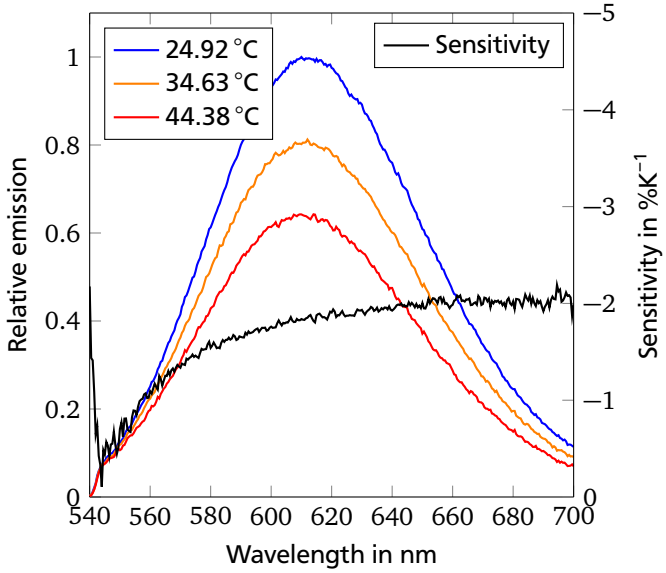

(c) DCM

Figure 4.2: Emission spectra of Rhodamine 6G, Pyridine 1 and DCM in ethanol at different temperatures.

of low temperature dependence was observed in the region from 540 nm to 600 nm, where the fluorescence signal mainly came from the Rhodamine 6G. In the region between 670 nm and 700 nm, where the fluorescence signal is dominated by the emission of the Pyridine 1, an almost constant level of high temperature dependence was observed. Between the two regions the dependence on temperature becomes continuously greater. This behavior resulted integrally in a low temperature coefficient of the reference fluorescence signal and a high temperature coefficient of the sensitive fluorescence signal.

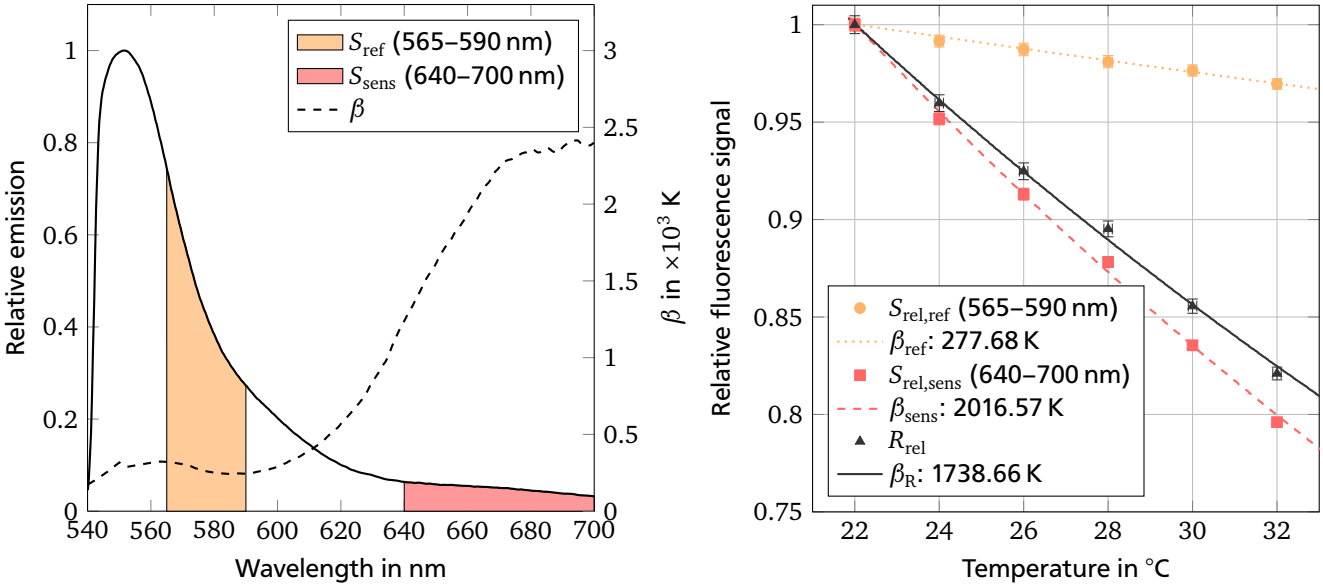

(a) Spectral **(b)** Integral

Figure 4.3: Temperature influence on the fluorescence signal of a mixture of Rhodamine 6G and Pyridine 1 in ethanol. Solution of 9.9 μgL^{-1} Rhodamine 6G and 73 μgL^{-1} Pyridine 1 in ethanol. Laser fluence of 2.03 $mJcm^{-2}$.

For the dye combination of Rhodamine 6G and DCM from 540 nm to 570 nm, where the fluorescence signal was mainly caused by the Rhodamine 6G, an almost constant level of low temperature dependence was observed as well. In the region 640 nm to 700 nm where the fluorescence signal is dominated by the emission of the DCM, an almost constant level of high temperature dependence was observed.

The level of high temperature dependence of the combination of Rhodamine 6G and DCM is lower than the level of the other combination. Between the two regions the dependence on temperature becomes continuously greater. This behavior resulted integrally in a low temperature coefficient of the reference fluorescence signal and a high temperature coefficient of the sensitive fluorescence signal. The integral temperature coefficient of the sensitive fluorescence signal of this combination is significantly lower than the one of the combination of Rhodamine 6G and Pyridine 1. This is most likely caused by the lower dependence on temperature of the fluorescence signal of DCM.

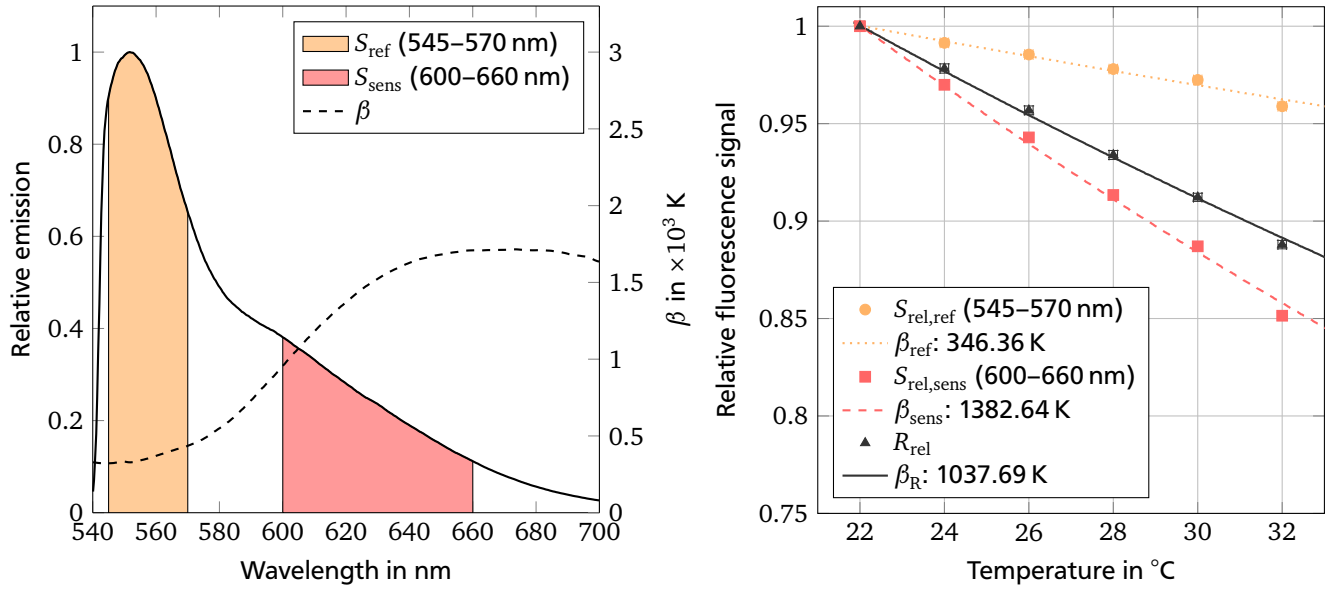

(a) Spectral **(b)** Integral

Figure 4.4: Temperature influence on the fluorescence signal of a mixture of Rhodamine 6G and DCM in ethanol. Solution of 9.9 μgL^{-1} Rhodamine 6G and 106 μgL^{-1} DCM in ethanol. Laser fluence of 1.35 $mJcm^{-2}$.

Also the temperature coefficient β_R of the ratio was calculated for the two dye combinations by a least-squares fit with the experimental data. The results are shown in Fig. 4.3b and Fig. 4.4b. In both cases the residuals were well below 0.01. This is an indication that the model proposed by Lemoine et al. [39] is suitable to describe the measurement data. The temperature coefficient of the ratio was higher for the combination of Rhodamine 6G and Pyridine 1.

4.3 Influence of Laser Fluence on the Fluorescence Signal

The influence of the laser fluence on the fluorescence signal was investigated to identify the region where the assumption of a linear relationship between laser fluence and the fluorescence signal necessary for 2c/2d PLIF-Thermography is justified. This was necessary because only in this region a compensation for laser fluence changes by the 2c/2d approach is possible. For PLIF-Thermography the deviations from linear lead to erroneous temperature measurements if laser fluence changes compared to the calibration. This contradicts the approach of 2c/2d PLIF-Thermography to eliminate the influence of the laser fluence. Within the linear regime a change of laser fluence can be compensated by the approach of 2c/2d PLIF-Thermography. Inside this regime for example the attenuation of the laser fluence along the propagation direction of the laser light due to absorption can be compensated by 2c/2d PLIF-Thermography. As there is no sharp border of the linear regime, the temperature deviations induced by laser fluence changes had to be checked for the 2c/2d PLIF-Thermography separately in situ. Additionally to this effect

Chaze et al. [13] report that outside of the linear regime the temperature dependency became a function of the laser fluence and decreased with increasing laser fluence. Within the linear regime the temperature dependency was not affected by the laser fluence.

For the combination of Rhodamine 6G and Pyridine 1 in ethanol the integral values of the relative fluorescence signal with respect to the relative laser fluence are shown in Fig. 4.5b. For the measurements a solution of 9.9 μgL^{-1} Rhodamine 6G and 73 μgL^{-1} Pyridine 1 in ethanol was used. The solution was heated to 25 °C. The laser pulse frequency was set to 10 kHz.

For low laser fluence up to 4.48 $mJcm^{-2}$ the fluorescence signal increased approximately linearly with the laser fluence. For higher laser pulse fluence the fluorescence signal developed increasingly underproportionally. The deviation from linear was not the same for both spectral regions. $S_{rel,ref}$ deviated more strongly from linear than $S_{rel,sens}$. In a 2c/2d PLIF-Thermography application this would lead to a deviation of the ratio of the fluorescence signals to higher values and therefore lower measured temperatures.

For the combination of Rhodamine 6G and DCM in ethanol the integral values of the relative fluorescence signal with respect to the relative laser fluence are shown in Fig. 4.6b. For the measurements a solution of 9.9 μgL^{-1} Rhodamine 6G and 106 μgL^{-1} DCM in ethanol was used. The solution was heated to 25 °C. The laser pulse frequency was set to 15 kHz.

For low laser fluence up to 3.23 $mJcm^{-2}$ the fluorescence signal increased approximately linearly with the laser fluence. For higher laser fluence the fluorescence signal developed increasingly underproportionally. The deviation from linear was not the same for both spectral regions. $S_{rel,ref}$ deviated more strongly from linear than $S_{rel,sens}$. In a 2c/2d PLIF-Thermography application this would lead to a deviation of the ratio of the fluorescence signals to higher values and therefore lower measured temperatures.

The saturation laser fluence u_{sat} was calculated spectrally resolved and integrally for the two spectral parts of the two dye combinations by a least-squares fit with experimental data. The results are shown in Fig. 4.5a and Fig. 4.6a. The absolute value of the residuals are below 0.1 for Rhodamine 6G and Pyridine 1 and below 0.15 for Rhodamine 6G and DCM. This is an indication that the model and the measured data are in good agreement. Qualitatively the results are in good agreement with Sutton, Fisher, and Fleming [55] for Fluorescein 27 ($C_{20}H_{10}O_5Cl_2$) in water and with the results of Chaze et al. [13] for various dyes in water.

For the dye combination of Rhodamine 6G and Pyridine 1 the spectral analysis of the saturation laser fluence showed an almost constant value in the region from 540 nm up to 640 nm. In this region the fluorescence signal is mostly caused by the emission of Rhodamine 6G. For higher wavelengths up to 700 nm the saturation laser fluence is rising with an almost constant slope. In this region the fluorescence signal is dominated by the emission of Pyridine 1. For

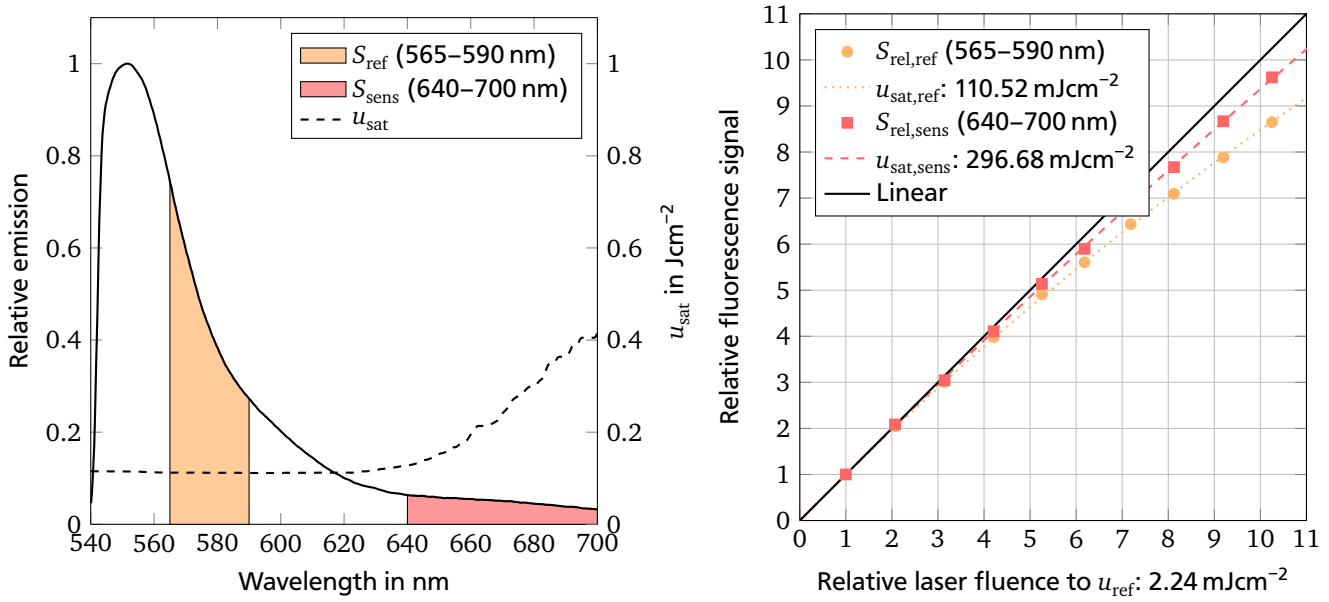

(a) Spectral **(b)** Integral

Figure 4.5: Influence of laser pulse fluence on the fluorescence signal of a mixture of Rhodamine 6G and Pyridine 1 in ethanol. Solution of 9.9 µgL^{-1} Rhodamine 6G and 73 µgL^{-1} Pyridine 1 in ethanol. Solution temperature of 25.0 °C.

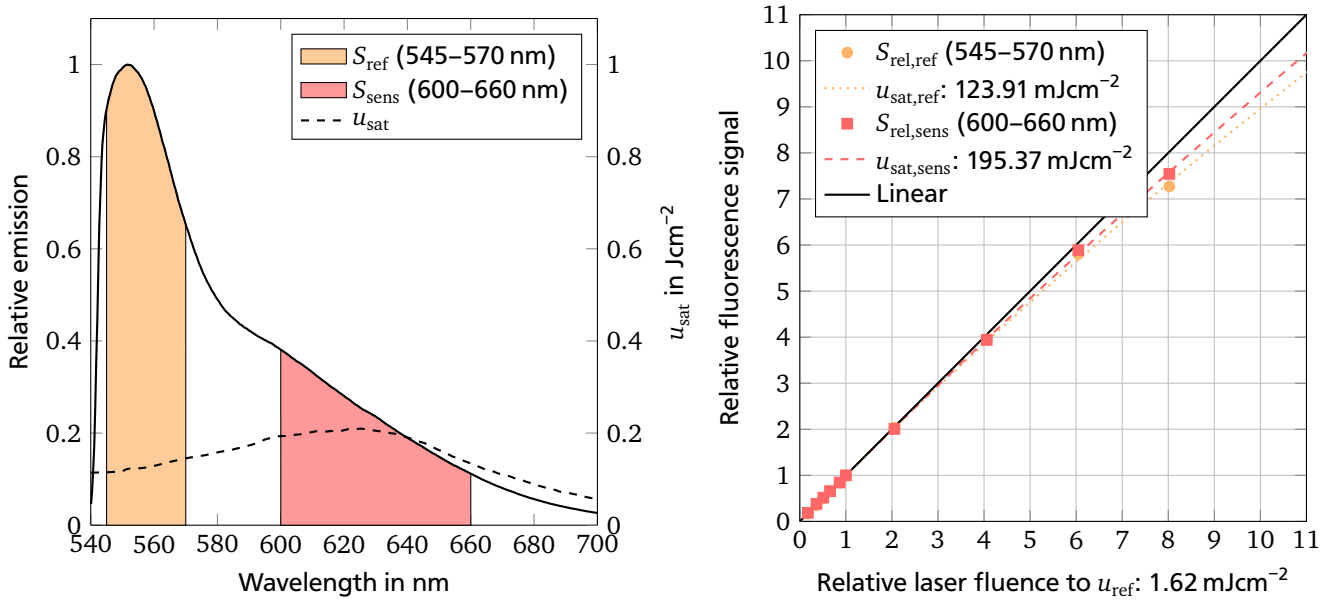

(a) Spectral **(b)** Integral

Figure 4.6: Influence of laser pulse fluence on the fluorescence signal of a mixture of Rhodamine 6G and DCM in ethanol. Solution of 9.9 µgL^{-1} Rhodamine 6G and 106 µgL^{-1} DCM in ethanol. Solution temperature of 25.0 °C.

the combination of Rhodamine 6G and DCM the spectral analysis of the saturation laser fluence revealed a maximum at 625 nm. The maximum of the saturation fluence was close to the maximum of the emission of DCM at 610 nm.

The observed behavior suggests a relationship between the dependence on temperature and the saturation laser fluence. A higher dependence seems to be connected to a higher saturation energy and vice versa. But the observation of the reduction of the saturation laser fluence after the maximum for the combination of Rhodamine 6G and DCM seems to contradict this interpretation.

4.4 Influence of Concentration on the Fluorescence Signal

The influence of the dye concentration on the fluorescence signal was investigated in order to identify the concentration range in which the assumption of a linear behavior of the fluorescence signal with a change of the dye concentration is valid. This linearity is required because in the application of 2c/2d PLIF-Thermography at a stationary evaporating meniscus the dye concentration changes locally due to the evaporation. For 2c/2d PLIF-Thermography the deviations from linear lead to erroneous temperature measurements if concentration or path length changes compared to the calibration. Within the linear regime a change of concentration and path length can be compensated by the 2c/2d approach as long as the ratio of the dye concentrations is constant. Since there is no sharp border of the linear regime, the temperature deviations induced by concentration changes had to be evaluated for the 2c/2d PLIF-Thermography experiments separately in situ.

For the combination of Rhodamine 6G and Pyridine 1 in ethanol the integral values of the relative fluorescence signal with respect to the relative concentration are shown in Fig. 4.7b. The concentration ratio was kept constant while the overall concentration was varied. The solution was heated to 25.0 °C. The laser fluence was 2.15 $\mathrm{mJcm^{-2}}$ and the laser pulse frequency was 10 kHz. For low overall concentrations up to $1.08 \times 10^{-7}\,\mathrm{molL^{-1}}$ the fluorescence signal increased approximately linearly with the concentration. For higher concentrations the fluorescence signal developed increasingly underproportionally. The part of the fluorescence signal sensitive to temperature deviated more strongly from a linear behavior than the part which is almost insensitive to temperature. In a 2c/2d PLIF-Thermography application this would lead to a deviation of the fluorescence signals' ratio to lower values and therefore to higher measured temperatures.

For the combination of Rhodamine 6G and DCM in ethanol the integral values of the relative fluorescence signal with respect to the relative concentration are shown in Fig. 4.8b. The

concentration ratio was kept constant while the overall concentration was varied. The solution was heated to 25.0 °C. The laser fluence was 1.35 mJcm^{-2} and the laser pulse frequency was 15 kHz. For low overall concentrations up to 3.76×10^{-7} molL^{-1} the fluorescence signal increased approximately linearly with the concentration. For higher concentrations the fluorescence signal developed increasingly underproportionally. In this case the part of the fluorescence signal which is almost insensitive to temperature deviated more strongly from a linear behavior than the part which is sensitive to temperature. In a 2c/2d PLIF-Thermography application this would lead to a deviation of the fluorescence signals' ratio to higher values and therefore to lower measured temperatures.

The decadic absorption coefficient ε was calculated spectrally resolved and integrally for the two spectral parts of the two dye combinations by a least-squares fit with experimental data. The results are shown in Fig. 4.7 and Fig. 4.8. The absolute value of the residuals are below 0.1 for Rhodamine 6G and Pyridine 1 and for Rhodamine 6G and DCM. This is an indication that the model and the measured data are in good agreement. The results are also qualitatively in good agreement with the results of Lemoine, Wolff, and Lebouche [38] for Rhodamine B ($C_{28}H_{31}ClN_2O_3$) in water and Melton and Lipp [40] for Rhodamine WT ($C_{29}H_{29}N_2O_5ClNa$) in water as well as the results of Sutton, Fisher, and Fleming [55] for Fluorescein 27 ($C_{20}H_{10}O_5Cl_2$) in water.

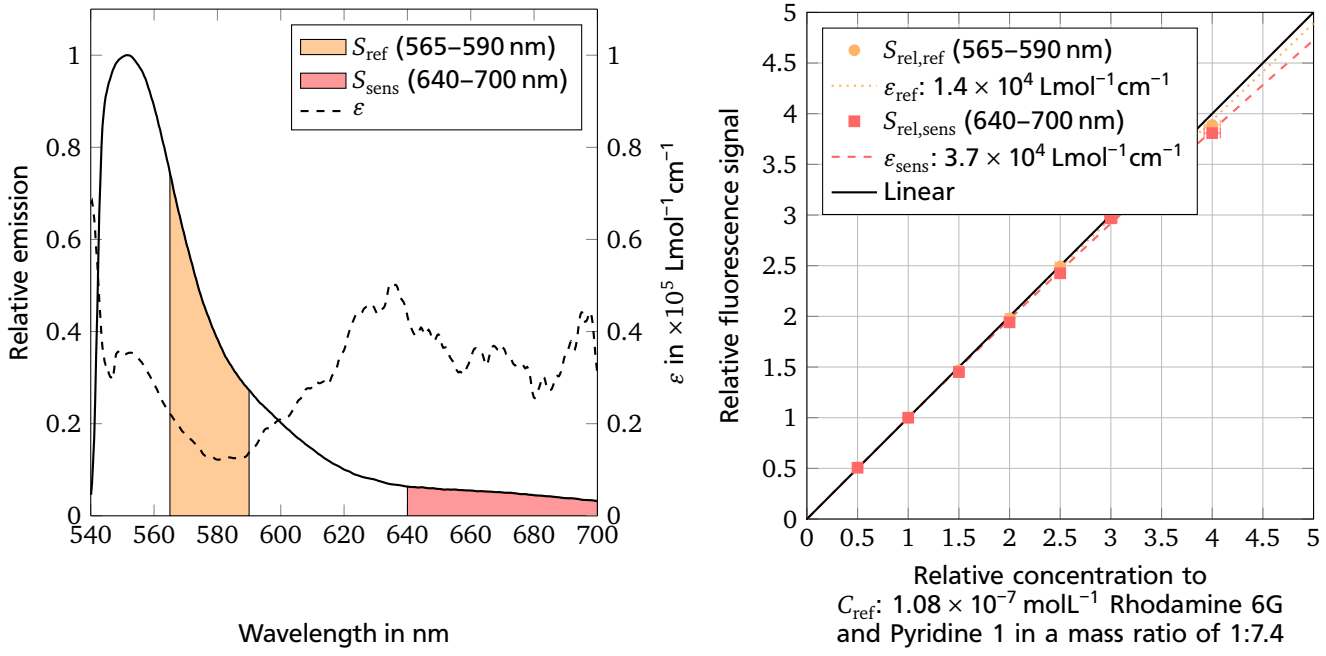

(a) Spectral **(b)** Integral

Figure 4.7: Influence of dye concentration on the fluorescence signal of a mixture of Rhodamine 6G and Pyridine 1 in ethanol. Temperature of the solution 25.0 °C. Laser pulse fluence of 2.15 mJcm^{-2}.

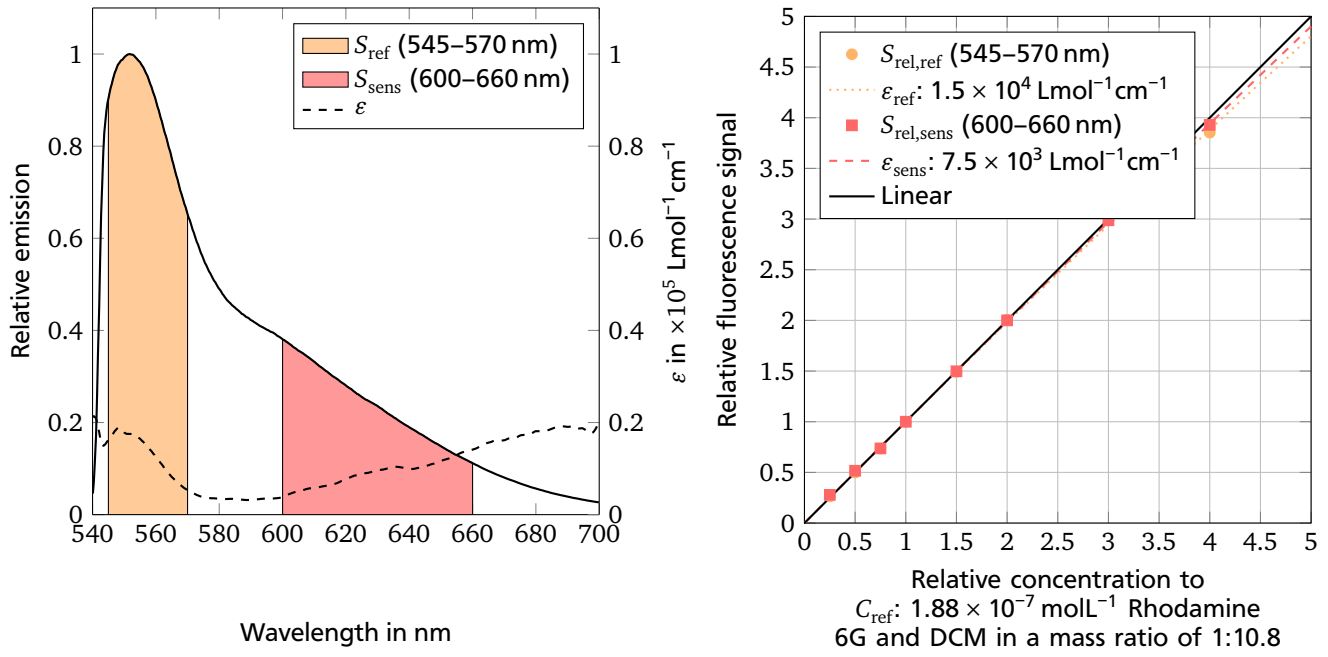

(a) Spectral **(b)** Integral

Figure 4.8: Influence of dye concentration on the fluorescence signal of a mixture of Rhodamine 6G and DCM in ethanol. Temperature of the solution 25.0 °C. Laser pulse fluence of 1.35 mJcm^{-2}.

For the combination of Rhodamine 6G and Pyridine 1 the spectral analysis of the decadic absorption coefficient showed a local minimum at 580 nm in the region which was used as reference signal for the 2c/2d PLIF-Thermography. For the combination of Rhodamine 6G and DCM the spectral analysis of the decadic absorption coefficient also showed a minimum in this region. A possible explanation for this behavior could be the overlap of the absorption and emission spectra in this region. In both cases after the minimum the decadic absorption coefficient increased again. This behavior can not be explained by the overlap of the emission and the absorption spectra since the absorption spectra do not extend into the region above 650 nm.

4.5 Influence of Pressure on the Fluorescence Signal

In the 2c/2d PLIF-Thermography application at the stationary evaporating liquid meniscus the system pressure changes between calibration and measurement. Therefore the influence of pressure on the fluorescence signal was investigated. However, since the liquid can be regarded as incompressible an influence of pressure on the fluorescence signal is not expected.

The influence of pressure was investigated in a range starting from an ambient pressure of approximately 1000 mbar down to 200 mbar. This range was chosen based on the pressure range of the experiments at the evaporating meniscus.

For the combination of Rhodamine 6G and Pyridine 1 in ethanol the relative fluorescence signal with respect to the pressure is shown in Fig. 4.9a. For the measurements a solution of 5.0 μgL^{-1} Rhodamine 6G and 36.6 μgL^{-1} Pyridine 1 in ethanol was used. The solution was heated to 23.0 °C. The laser fluence was 1.35 $mJcm^{-2}$ and the laser pulse frequency was 15 kHz.

For the combination of Rhodamine 6G and DCM in ethanol the relative fluorescence signal with respect to the pressure is shown in Fig. 4.9b. For the measurements a solution of 9.9 μgL^{-1} Rhodamine 6G and 106 μgL^{-1} DCM in ethanol was used. The solution was heated to 23.0 °C. The laser fluence was 1.35 $mJcm^{-2}$ and the laser pulse frequency was 15 kHz.

As expected in both cases no significant influence of the pressure on the fluorescence signals and their ratio in the range from ambient pressure to 200 mbar was observed. Therefore a changing pressure during the application of 2c/2d PLIF-Thermography at the stationary evaporating meniscus is not expected to have an influence on the measured temperatures.

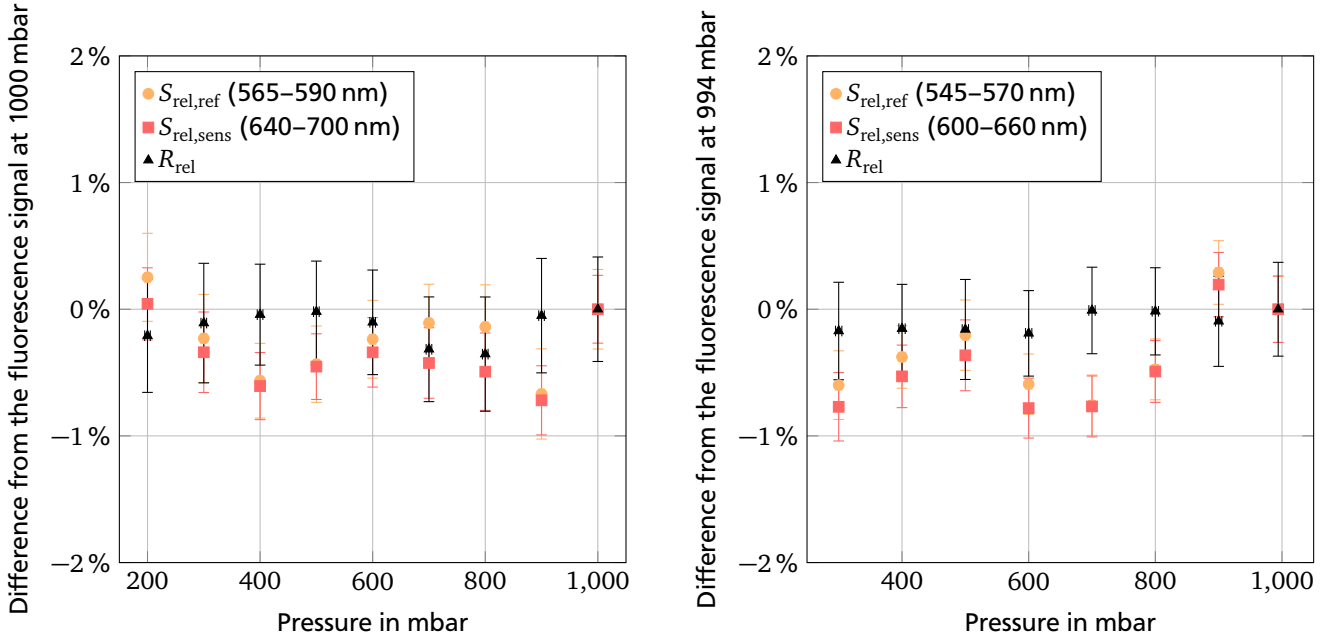

(a) Solution of 5.0 μgL^{-1} Rhodamine 6G and 36.6 μgL^{-1} Pyridine 1 in ethanol.

(b) Solution of 9.9 μgL^{-1} Rhodamine 6G and 106 μgL^{-1} DCM in ethanol.

Figure 4.9: Influence of pressure on the fluorescence signal of a mixture of Rhodamine 6G and Pyridine 1 in ethanol (a) and Rhodamine 6G and DCM in ethanol (b). Relative difference from the fluorescence signal at ambient pressure versus the fluid pressure. Solution temperature of 23 °C. Laser pulse fluence of 1.35 $mJcm^{-2}$.

4.6 Influence of Dissolved Air on the Fluorescence Signal

Since oxygen is known to be potentially a strong quencher for fluorescent dyes its influence was investigated. Knowledge about the influence of oxygen was necessary because in the ap-

plication of the 2c/2d PLIF-Thermography experiment at the stationary evaporating meniscus the amount of dissolved air and accordingly the amount of dissolved oxygen in the liquid may change between calibration and measurement. A dependence of the fluorescence signals on the amount of dissolved air would lead to erroneous temperature measurements.

For the combination of Rhodamine 6G and Pyridine 1 in ethanol the relative fluorescence signal with respect to the time that the solution was kept at 200 mbar is shown in Fig. 4.10a. For the measurements a solution of 5.0 μgL^{-1} Rhodamine 6G and 36.6 μgL^{-1} Pyridine 1 in ethanol was used. The solution was heated to 23.0 °C. The laser fluence was 1.35 $mJcm^{-2}$ and the laser pulse frequency was 15 kHz. The gas above the solution was air.

For the combination of Rhodamine 6G and DCM in ethanol the relative fluorescence signal with respect to the time that the solution was kept at 200 mbar is shown in Fig. 4.10b. For the measurements a solution of 9.9 μgL^{-1} Rhodamine 6G and 106 μgL^{-1} DCM in ethanol was used. The solution was heated to 22.0 °C. The laser fluence was 1.35 $mJcm^{-2}$ and the laser pulse frequency was 15 kHz. The gas above the solution was air.

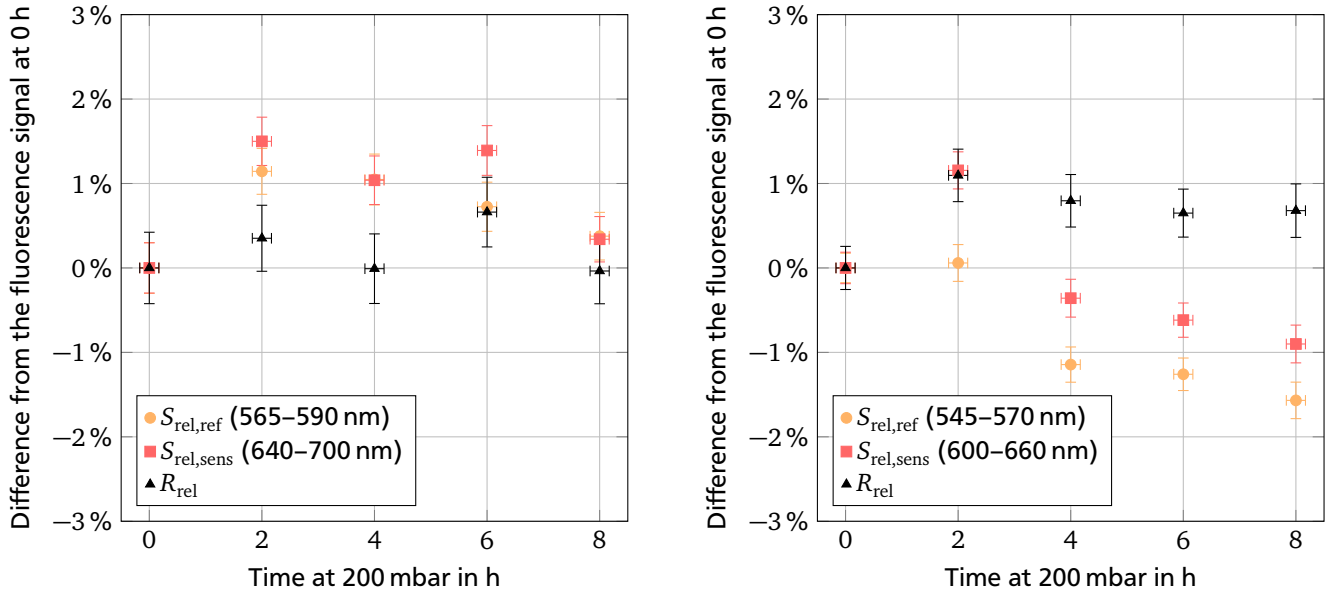

(a) Solution of 5.0 μgL^{-1} Rhodamine 6G and 36.6 μgL^{-1} Pyridine 1 in ethanol. Solution temperature of 22.0 °C.

(b) Solution of 9.9 μgL^{-1} Rhodamine 6G and 106 μgL^{-1} DCM in ethanol. Solution temperature of 23.0 °C.

Figure 4.10: Influence of dissolved air on the fluorescence signal of a mixture of Rhodamine 6G and Pyridine 1 in ethanol (a) and Rhodamine 6G and DCM in ethanol (b). Relative difference from the fluorescence signal at 0 h versus the time at 200 mbar. Laser pulse fluence of 1.35 $mJcm^{-2}$.

According to Henry's law the amount of dissolved oxygen in a liquid is proportional to the partial pressure of the oxygen in the gas phase above the liquid at equilibrium. To evaluate the oxygen influence the fluorescence signal at 1000 mbar total air pressure (≈210 mbar partial pressure

of oxygen) was compared to the fluorescence signal at 200 mbar total air pressure (≈42 mbar partial pressure of oxygen). In order to ensure that the equilibrium was reached the solution was kept at 200 mbar total air pressure for several hours. Comparison of the results showed no significant influence of oxygen on the fluorescence signal.

4.7 Influence of Photobleaching on the Fluorescence Signal

Since in the application of the 2c/2d PLIF-Thermography the dyes are exposed to numerous laser pulses it was important to investigate if there is a significant dependence of the fluorescence signals and their ratio on the number of the applied laser pulses at the needed laser fluence used for the 2c/2d PLIF-Thermography. A dependence of the fluorescence signals and their ratio would lead to a drift of the temperature measured with increasing number of laser pulses. Fig. 4.11 shows the results of the investigations for both dye combinations.

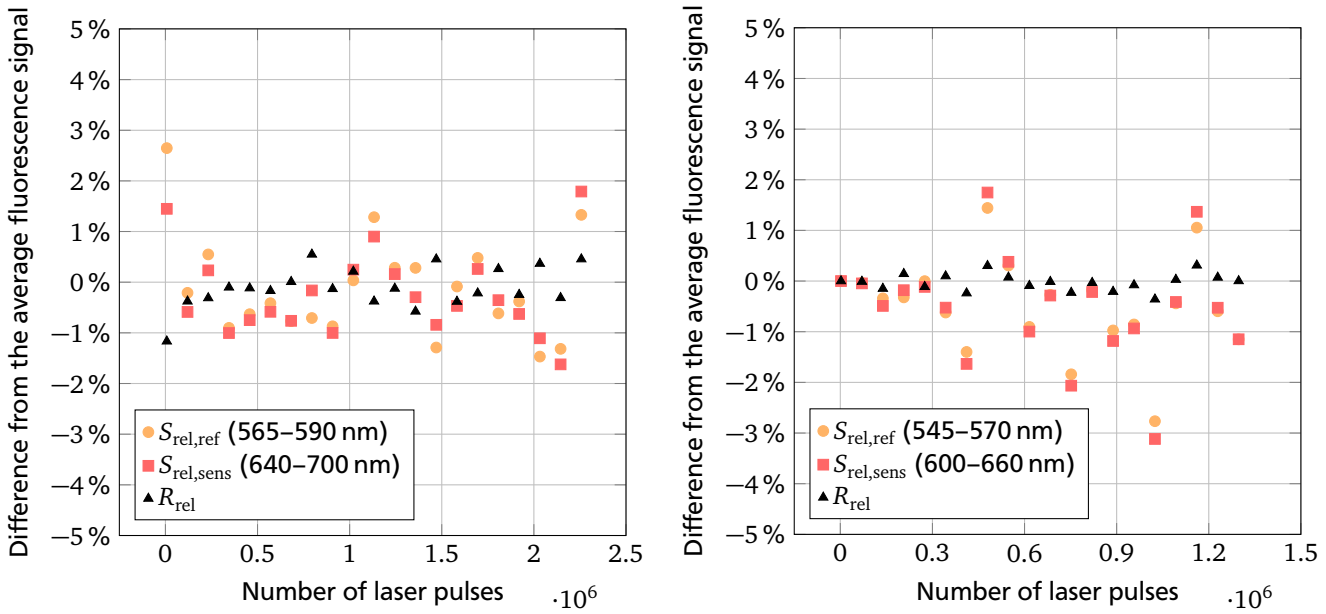

(a) Solution of 5.0 µgL^{-1} Rhodamine 6G and 36.6 µgL^{-1} Pyridine 1 in ethanol. Solution temperature of 23.0 °C.

(b) Solution of 9.9 µgL^{-1} Rhodamine 6G and 106 µgL^{-1} DCM in ethanol. Solution temperature of 25.0 °C.

Figure 4.11: Influence of photobleaching on the fluorescence signal of a mixture of Rhodamine 6G and Pyridine 1 in ethanol (a) and of Rhodamine 6G and DCM in ethanol (b). Relative difference from the average fluorescence signal versus the number of laser pulses. Laser pulse fluence of 1.35 mJcm^{-2}.

For the measurements with the first dye combination a solution of 5.0 µgL^{-1} Rhodamine 6G and 36.6 µgL^{-1} Pyridine 1 in ethanol was used. The solution was heated to 23.0 °C. The laser fluence was 1.35 mJcm^{-2} and the laser pulse frequency was 15 kHz. Over 2.25×10^6 laser pulses no significant influence of the number of laser pulses on the fluorescence signal was observed.

For the measurements with the second dye combination a solution of 9.9 μgL^{-1} Rhodamine 6G and 106 μgL^{-1} DCM in ethanol was used. The solution was heated to 25.0 °C. The laser fluence was 1.35 $mJcm^{-2}$ and the laser pulse frequency was 15 kHz. Over 1.25×10^6 laser pulses no significant influence of the number of laser pulses on the fluorescence signal was observed.

4.8 Conclusion

Based on the results of the dye characterization the combination of Rhodamine 6G and Pyridine 1 was chosen to be used for the further investigation regarding the applicability of the 2c/2d PLIF-Thermography for measurements at a stationary evaporating meniscus. The reason for this is its superior dependence on temperature. The dependence on temperature was regarded as the most important feature since the achievable measurement uncertainty of the 2c/2d PLIF-Thermography depends on this property. Since the temperature difference expected to be measured with the 2c/2d PLIF-Thermography at the stationary evaporating meniscus was in the order of 1 °C, a low measurement uncertainty was considered to be most important. The investigations regarding the influence of laser fluence, dye concentration, pressure, dissolved air, and photobleaching did not reveal a significant difference between the two dye combinations.

5 Applicability to a Stationary Evaporating Meniscus

In this chapter the investigation's results regarding the applicability of 2c/2d PLIF-Thermography to temperature measurements at a stationary evaporating meniscus are presented. In the first section of this chapter the two approaches for the calibration of the 2c/2d PLIF-Thermography are presented and compared, in order to decide which approach should be used for the following experiments. The chosen approach is investigated in detail regarding validity, measurement uncertainty, and repeatability in the following sections. Additionally, the results regarding the influence of the laser fluence and the dye concentration on the temperatures measured with the 2c/2d PLIF-Thermography are presented and an estimation of the maximum temperature error due to these influences is given. In the last sections of this chapter the results of the 2c/2d PLIF-Thermography at a stationary evaporating meniscus are presented and discussed.

5.1 Calibration

In this section the two presented calibration functions are evaluated and compared with each other in order to identify the one that represents the measurement data the best. The residuals and the weighted sum of the squared deviations are used as criteria. Additionally, the weighted sum of the squared deviations offers a possibility to judge the quality of the fit of the calibration function in an absolute way. In the first step an exemplary pixel from the middle of the sensor is examined. Because sCMOS detectors were used for the 2c/2d PLIF-Thermography the examination of single pixels is not sufficient to judge the quality of the calibration function's fit for the whole detector. Therefore in the second step every pixel was examined. This was done by evaluating the residuals' distribution and the distribution of the weighted sum of the squared deviations in the form of histograms for the whole detector.

Fig. 5.1 shows the measured ratio of an exemplary pixel from the middle of the detector at the temperature levels used for the calibration. The dashed and the solid lines are the two calibration functions. The dashed line is the result of the exponential calibration approach and the solid line is the result of the second-order polynomial calibration approach. The residuals of the exponential calibration approach were a function of temperature and therefore showed a characteristic pattern. The first and the last calibration points were underestimated and the rest

were overestimated by the exponential calibration function. The residuals were in most cases higher than the standard deviation of the ratio. These were indications that the exponential calibration approach did not sufficiently describe the calibration data. For the second-order polynomial approach the residuals were randomly distributed around zero within the standard deviation of the ratio. These are indications that the second-order polynomial approach is a reasonable description of the calibration data.

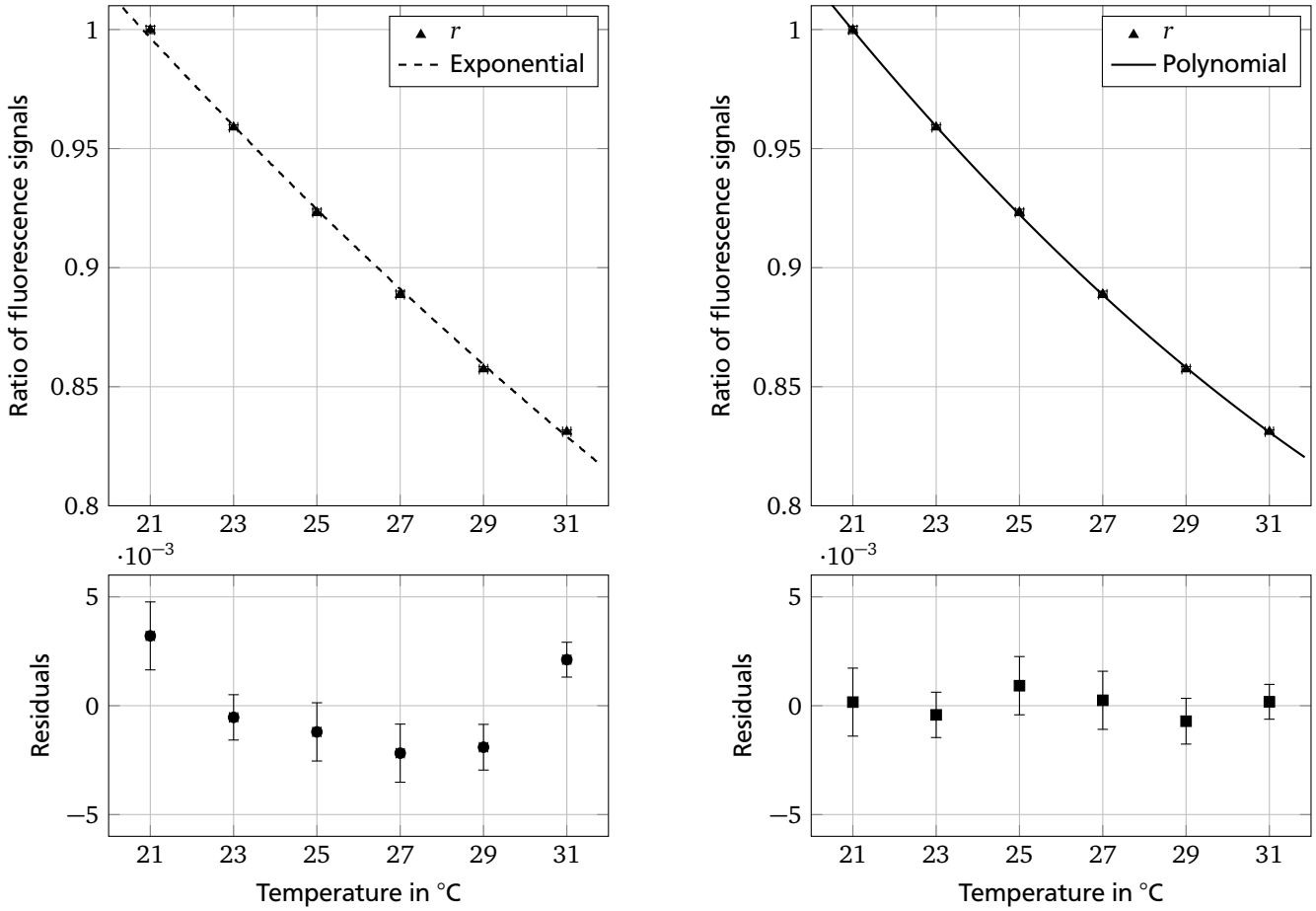

(a) Exponential **(b)** Polynomial

Figure 5.1: Calibration curves and residuals for an exemplary pixel from the middle of the detector for both calibration approaches.

In the following the two calibration approaches are evaluated statistically for the whole sensor. For comparison of the two calibration approaches the residuals and the weighted sum of the squared deviations χ^2 were used. Fig. 5.2 shows the histograms of the residuals of the ratio for all pixels of the sensor for both calibration approaches. Fig. 5.2a shows the histogram of the residuals of the exponential calibration approach. For the exponential calibration approach the histogram of the residuals shows two peaks. This is the result of the characteristic pattern of the residuals where the first and the last calibration point are underestimated and the calibration points in between are overestimated by the calibration function. This leads to a bimodal distribution with one small peak and one large peak around zero. This is an indication that

the exponential calibration approach is not a good description of the calibration data for the whole sensor. Fig. 5.2b shows the histogram of the residuals of the second-order polynomial calibration approach. For the second-order polynomial approach the histogram of the residuals shows a symmetric distribution around zero with one peak in the middle. This is the result of the random distribution of the residuals around zero. This is an indication that the second-order polynomial calibration approach is a reasonable description of the calibration data for all pixels of the sensor.

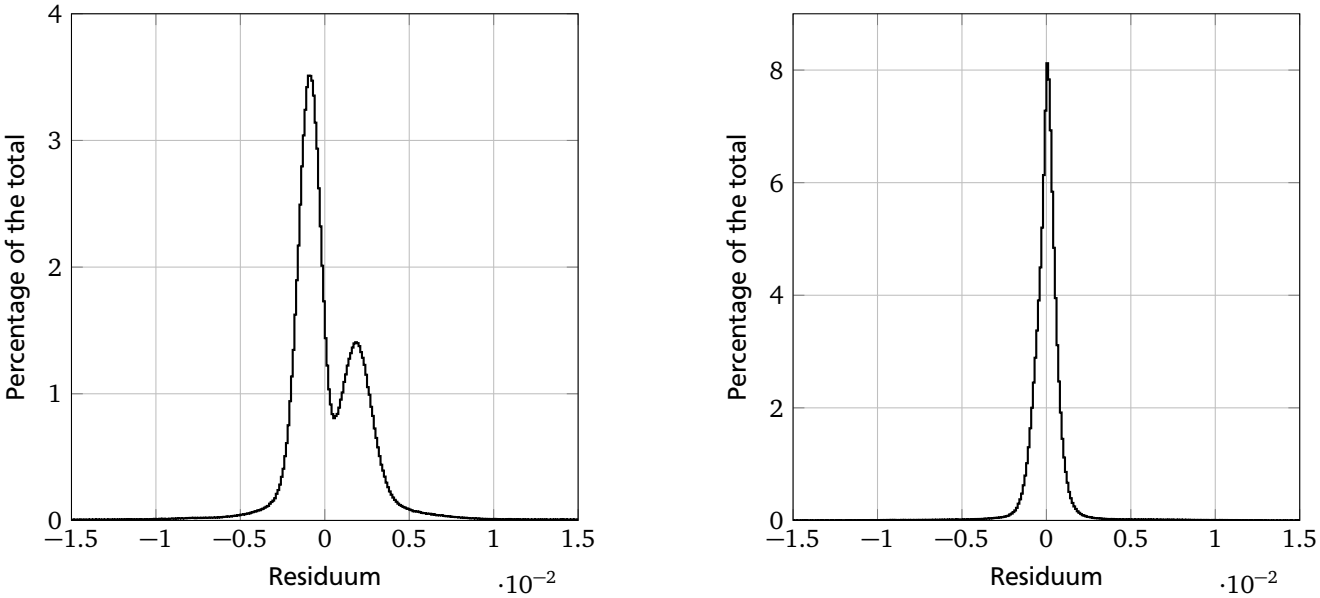

(a) Exponential **(b)** Polynomial

Figure 5.2: Histograms of the residuals of the exponential and the polynomial calibration curve and the measured ratios for the whole region of interest.

Fig. 5.3 shows the cumulative histogram of the weighted sum of the squared deviations χ^2 of both calibration approaches. χ^2 is a measure for the likelihood of the fit and therefore it can be used to judge the quality of the fit. As acceptance limit 90 % is chosen. For this limit χ^2 has to be below 7.779 for the exponential approach and below 6.251 for the second-order polynomial approach. This means that for the exponential calibration approach only for 37 % of all pixels is the fit of the calibration function reasonable. This implies that the deviations of the residuals can not be explained by the measurement uncertainties of the ratios for the majority of the pixels. In the case of the second-order polynomial calibration approach, for 97 % of all pixels the deviations from the calibration data can be explained by the measurement uncertainty of the ratios. This indicates that the second-order polynomial calibration approach seems to be a reasonable description of the calibration data for almost all pixels.

The second-order polynomial calibration approach showed superior performance to the exponential calibration approach. According to the analysis of the weighted sum of the squared

deviations it was a reasonable description of the measurement data. Therefore it was chosen to be used as calibration function for further investigations.

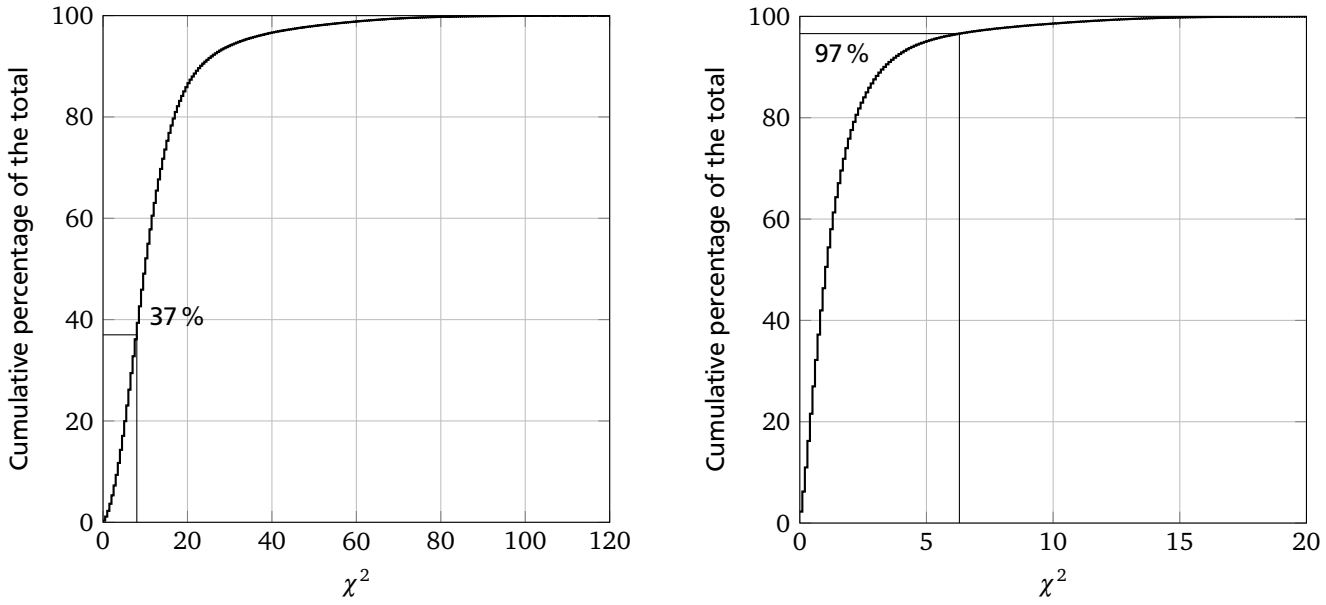

(a) Exponential **(b)** Polynomial

Figure 5.3: Histograms of the weighted sum of the squared deviations χ^2 of the exponential and the polynomial calibration approaches for the whole region of interest.

5.2 Measurement Uncertainty

In order to evaluate the single-shot temperature uncertainty of the 2c/2d PLIF-Thermography the temporal standard deviation of each pixel at the validation points was calculated. The results are displayed in Fig. 5.4. It can be seen that the standard deviations increased with increasing temperatures. This behavior can be explained by the lower fluorescence signal sensitive to temperature at higher temperatures. Therefore with increasing temperature the signal-to-noise ratio of the images for the temperature-sensitive fluorescence signal became lower. This results in higher standard deviations of the ratio and in turn higher standard deviations of the calculated temperatures.

It also can be seen that the temporal standard deviations had a distribution across the detector. This is most likely caused by the slightly inhomogeneous illumination of the region of interest by the laser light sheet. The inhomogeneity of the illumination led to an inhomogeneity of the fluorescence signal with areas of lower fluorescence signal and areas of higher fluorescence signal. The areas with a lower fluorescence signal had a lower signal-to-noise ratio, which in turn led to a higher standard deviation of the temperatures measured with the 2c/2d PLIF-Thermography and vice versa. Since the inhomogeneity of the illumination is quite low the resulting distribution of the temperature uncertainty is narrow.

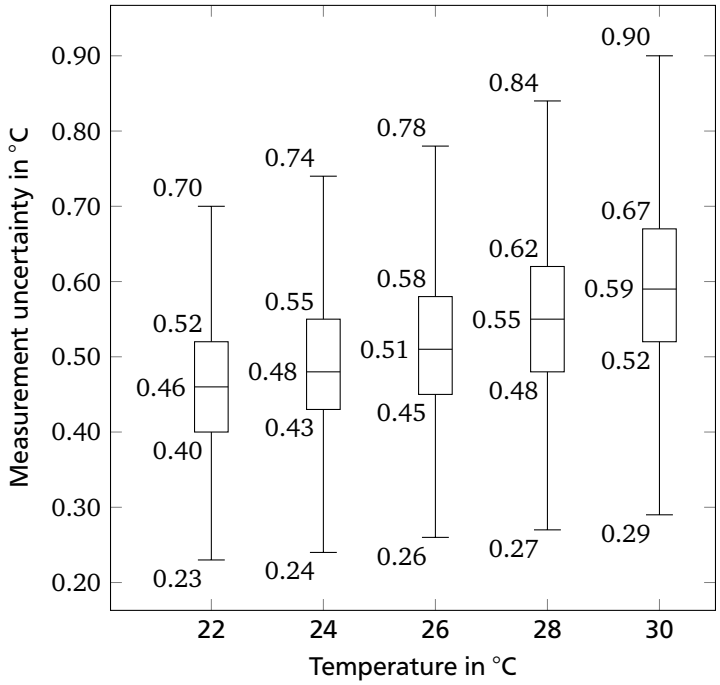

Figure 5.4: Single-shot temporal measurement uncertainty of each pixel at the validation point versus the temperature of the validation point.

The temperature uncertainty originates from different sources. One source which could be identified is the noise of the detectors used. The temperature uncertainty related to the noise of the detectors can be calculated from the signal-to-noise ratio of the detectors and the slope of the calibration function at a given temperature by

$$\sigma^T = \sigma^R \cdot \left|\frac{d\,T}{d\,R}\right| = \sqrt{\frac{1}{SNR_{\text{ref}}}^2 + \frac{1}{SNR_{\text{sens}}}^2} \cdot \frac{1}{\sqrt{N}} \cdot R \cdot \left|\frac{d\,T}{d\,R}\right| \tag{5.1}$$

where SNR_{ref} and SNR_{sens} are the signal-to-noise ratios of the two detectors; N, the number of the pixels binned; T, the temperature; R, the ratio of the fluorescence signals. For example at a temperature of 22 °C the mean gray value of each of the detectors is approximately 30 000. Therefore the signal-to-noise ratio of each of the detectors is approximately 114 and the ratio is 1, the gradient of the calibration curve is 49.16 °C, and the number of pixels binned is 4. In this case the part of the temperature uncertainty caused by the noise of the detectors is 0.3 °C. Thus, the main part of the temperature uncertainty of the 2c/2d PLIF-Thermography is caused by the noise of the detectors. Since for the 2c/2d PLIF-Thermography measurements the number of photons detected is high, the noise of the detectors is dominated by the photon noise. Therefore the noise of the detectors scales with 1 divided by the square root of the detected photons.

Also the dependence on temperatures of the used dye combination has a significant influence on the temperature uncertainty since the noise of the detectors is scaled by the slope of the calibration curve. A higher dependence on temperature of the ratio leads to a lower scaling factor and therefore results in a lower temperature uncertainty.

In order to improve the standard deviation of the 2c/2d PLIF-Thermography into the region of 0.1 °C the signal-to-noise ratio of the detectors had to be improved. An improvement of the signal-to-noise ratio of the detectors is possible by increasing the number of detected photons. This was done by averaging 40 subsequent images for the 2c/2d PLIF-Thermography measurements at the cost of temporal resolution, which is not needed in the context of this work because only stationary processes were investigated. As a result, the standard deviation of the average was reduced by the factor $\sqrt{40}$ compared to the standard deviation of a single shot.

5.3 Validation

In order to judge the validity of the 2c/2d PLIF-Thermography calibration, measurements at homogeneous temperature distributions were evaluated. The measurements were performed at the temperature levels which lay halfway between the temperature levels used for the calibration. For the judgment of the calibration's validity the remaining systematic temperature deviations are of interest. The deviations could be a global offset, which would result in a bias of the temperature distribution or the formation of a fixed deviation pattern, which in turn would lead to inhomogeneities. Therefore the random fluctuations of the temperatures measured were reduced by taking the average of all images which were recorded at each temperature level.

The validity of the calibration was judged by two criteria. The first criteria was the difference of the temperatures measured with 2c/2d PLIF-Thermography to the temperatures of the solution measured with the thermocouples. The second criteria was the spatial standard deviation which is used to judge the spatial homogeneity of the temperature distribution measured with the 2c/2d PLIF-Thermography. A valid calibration should yield values for both criteria in the order of the remaining temperature uncertainty, which is based on random temporal fluctuations.

Fig. 5.5 shows the difference of the temperatures measured with the 2c/2d PLIF-Thermography for each pixel of the detector to the temperature of the solution measured with the thermocouples. It can be seen that for all validation measurements the median of the differences was very close to zero. Therefore the calibration of the 2c/2d PLIF-Thermography did not lead to a significant bias of the measured temperatures. Fifty percent of the pixels had an absolute difference to the temperature of the solution measured with the thermocouples below 0.1 °C. Therefore

the calibration of the 2c/2d PLIF-Thermography did not exhibit a global bias of temperature distributions above its temperature uncertainty.

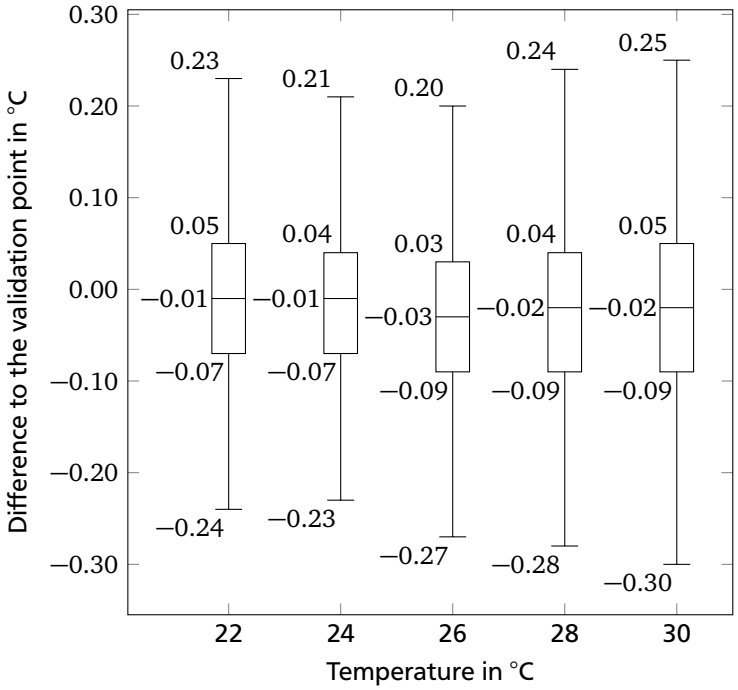

Figure 5.5: Difference of each pixel's temperature to the temperature at the validation point ($T_{\text{pixel}} - T_{\text{val}}$) versus the temperature of the validation point.

In addition the homogeneity of the temperature distributions measured with the 2c/2d PLIF-Thermography was evaluated. This was done by calculating the spatial standard deviation of each measured temperature distribution. A low value of the spatial standard deviation is an indication for a homogeneous temperature distribution without a remaining fixed deviation pattern. In Tab. 5.1 the spatial standard deviations of the temperature distributions can be found. The spatial standard deviations were within the order of the temperature uncertainty of the 2c/2d PLIF-Thermography that remained after the temporal averaging. This suggests that the remaining inhomogeneities were most likely caused by the random temporal fluctuations of the measured temperatures that could not be completely eliminated by the averaging due to the limited number of images to average. Therefore the calibration was accepted as valid for the calibrated temperature range.

Table 5.1: Spatial standard deviation of the average temperature fields at the validation points.

Validation point	Spatial standard deviation
22.00 °C	±0.08 °C
24.00 °C	±0.08 °C
26.00 °C	±0.09 °C
28.00 °C	±0.10 °C
30.00 °C	±0.10 °C

5.4 Repeatability

In order to judge the repeatability of the 2c/2d PLIF-Thermography, 25 measurements at 26 °C were evaluated. The measurements were performed within a time range of five hours. Therefore fluctuations on time scales up to several hours were included in the measurements. The 40 images of each measurement were averaged temporally.

The measured temperatures of all pixels of the detectors were combined in a cumulative histogram which is shown in Fig 5.6. The confidence intervals calculated for three confidence levels averaged temporally over 40 images can be found in Tab. 5.2.

The resulting confidence intervals are slightly larger compared to the confidence intervals calculated from the measurement uncertainty at the validation point. The calculation of a 95 % confidence level from the measurement uncertainty at the validation point with a temperature of 26 °C resulted in a confidence interval of ±0.15 °C. The reason for this is most likely that the measurements at the validation point only covered fluctuations on a time range of several minutes and therefore fluctuations on higher time scales were not covered.

In order to have a conservative approximation of the repeatability the higher value was chosen. 2c/2d PLIF-Thermography measurements averaged over 40 images were repeatable with a confidence level of 95 % within a confidence interval of ±0.20 °C.

Table 5.2: Confidence intervals for different confidence levels for an average of 40 images.

Confidence level	Confidence interval
90 %	±0.17 °C
95 %	±0.20 °C
99 %	±0.26 °C

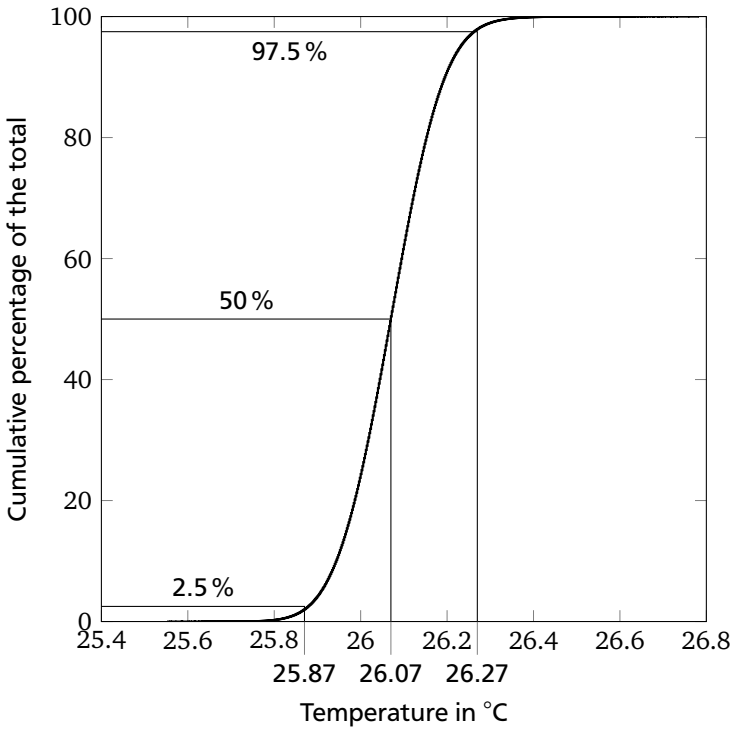

Figure 5.6: Histogram of all pixels from 25 measurements averaged over 40 images at 26 °C.

5.5 Influence of Dye Concentration on the Measured Temperature

During the experiments at the stationary evaporating meniscus the concentration of the dyes could not be kept constant. Therefore the influence of the dye concentration on the temperature measured by the 2c/2d PLIF-Thermography was evaluated. The influence was evaluated by two specific values. The first specific value was the change of the measured temperature compared to the temperature measured under the same conditions as during the calibration. This value was used to evaluate if there was a bias of the measured temperature caused by the change of the dye concentration. The second specific value was the spatial standard deviation. This value was used to analyze if there was any spatial inhomogeneity in the measured temperatures induced by the change of the dye concentration.

To evaluate the influence of the dye concentration on the temperature measured by the 2c/2d PLIF-Thermography a calibration with the standard dye concentration, which was also used for the other 2c/2d PLIF-Thermography measurements, was performed. After the calibration 2c/2d PLIF-Thermography measurements at two lower, the original, and three higher concentrations with the same mass concentration ratio were performed. The concentration levels were chosen in a way that the whole dynamic range of the detectors was covered. Thus, no higher concentration change in the dynamic range of the detectors is possible. The dye solution was heated

to 26 °C for the measurements. The 2c/2d PLIF-Thermography data were averaged temporally and spatially to achieve a single temperature value for each concentration.

In Fig. 5.7a the temperature difference from the temperature measured at the concentration used for the calibration is shown. For lower concentrations a slightly higher temperature was measured and for higher concentrations a slightly lower temperature was measured. The maximum absolute change of the temperature measured was below 0.2 °C for the concentration range measured. Therefore the maximum temperature error in the measurement range of the detectors due to a change of concentration with a constant mass concentration ratio can be estimated to be approximately 0.2 °C.

The reason for the change in temperature with increasing concentration could be explained by the different amount of re-absorption in the wavelength ranges of the two detector channels or the slightly different response curves of the two detectors. According to the investigations of the concentration influence on the fluorescence signal during dye characterization an increase in concentration would lead to a higher measured temperature. Since in this case a decrease of the measured temperatures was observed the different amount of re-absorption in the wavelength ranges of the two detector channels can not explain the change of the temperature measured. Therefore the difference of the response curves to the fluorescence signal of the two detectors seems to be dominant in the regime of low dye concentrations.

Fig. 5.7b shows the influence of the dye concentration at a constant mass concentration ratio of the spatial standard deviation. The spatial standard deviation is used as a measure for the homogeneity of the measured temperature distribution. A higher value stands for a higher level of inhomogeneity. For concentrations other than the concentration used for the calibration the spatial standard deviation slightly increased.

The reason for this is most likely the photo-response non-uniformity of the used detectors. Each pixel of the detectors has a slightly different gain. This difference is compensated for by the gray values occurring during the calibration. At other gray values the inhomogeneities are not completely compensated and become stronger with an increasing difference from the gray values occurring during calibration. With a change of dye concentration the gray values are altered compared to the calibration. Therefore inhomogeneity increases with increasing concentration change.

However, an increase of the concentration caused the spatial standard deviation to increase only slightly from 0.04 °C to 0.07 °C on an overall low level. Since a decrease of the concentration did not occur during 2c/2d PLIF-Thermography at the stationary evaporating meniscus it has no relevance for the measurements at the stationary evaporating meniscus.

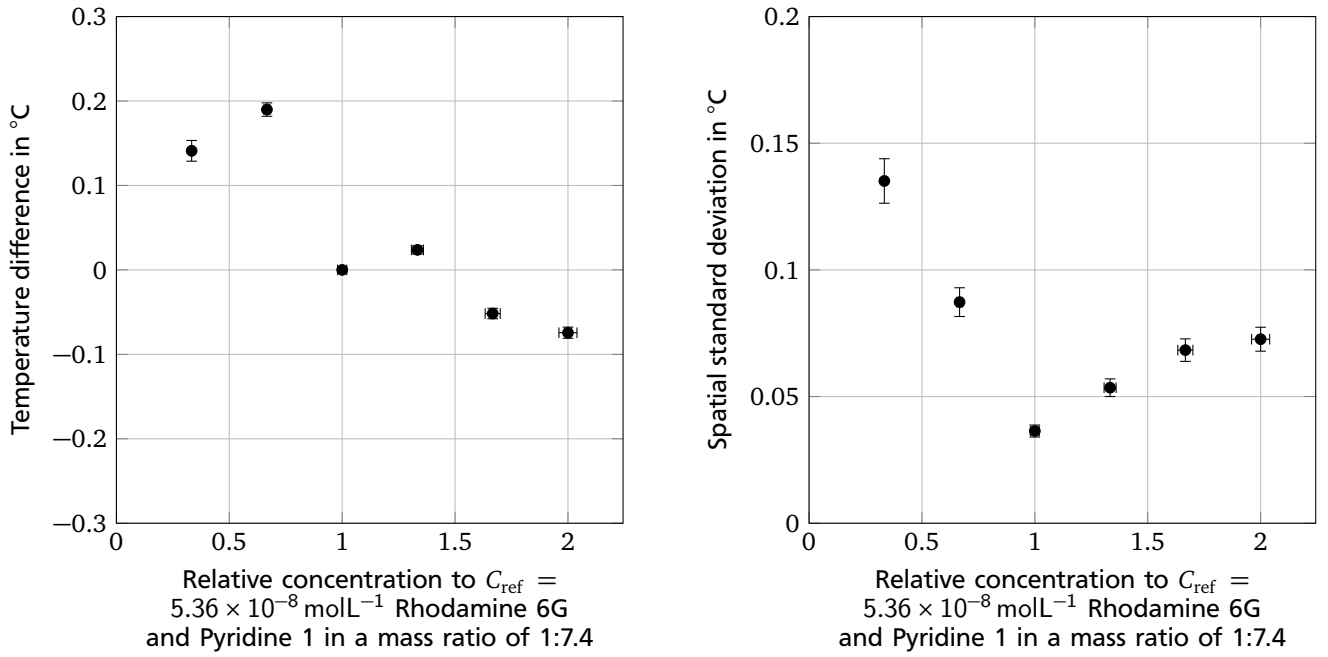

(a) Temperature difference from the measured temperature at the concentration used for calibration versus dye concentration.

(b) Spatial standard deviation versus dye concentration.

Figure 5.7: Influence of the dye concentration on the temperature measured with 2c/2d PLIF-Thermography (a) and the spatial standard deviation (b).

5.6 Influence of Laser Fluence on the Measured Temperature

The 2c/2d PLIF-Thermography approach is used to compensate the influence of the laser fluence used for the excitation of the fluorescent dyes. However, due to the different response curves of the fluorescence signals to the laser fluence the compensation did not eliminate the influence completely. Therefore the influence of the laser fluence on the temperatures measured with the 2c/2d PLIF-Thermography was evaluated. As in the case of the influence of the dye concentration also here the change of the measured temperatures and the spatial standard deviation were used as specific values to analyze the influence of the laser fluence.

To evaluate the influence of the laser fluence on the temperature measured by the 2c/2d PLIF-Thermography a calibration at the standard laser fluence which was used for the other 2c/2d PLIF-Thermography measurements was performed. After the calibration 2c/2d PLIF-Thermography measurements were conducted at various laser fluence levels. Two measurements were performed at lower laser fluence levels, one at the original laser fluence and three at higher laser fluence levels. The laser fluence range was chosen in a way that the whole dynamic range of the detectors was covered. For the measurements the dye solution was keep at 26 °C.

Fig. 5.8a shows the temperature difference from the temperature measured at the laser fluence that was used for calibration. With decreasing laser fluence compared to the laser fluence used during calibration the temperature measured slightly increased by about 0.3 °C. With increasing laser fluence compared to the laser fluence during calibration the temperature measured decreased by about 0.7 °C.

This behavior is compliant with the investigation results of the laser fluence influence on the fluorescence signal of the spectral dye characterization. Increasing laser fluence also resulted in a higher ratio of the fluorescence signals and thus in a lower measured temperature and vice versa.

However, the laser fluence was quite stable in the region of interest for the measurements at the stationary evaporating meniscus. Thus, only minor fluctuations around the laser fluence used for the calibration of approximately $\pm 1.5\,\%$ occurred due to the instability of the laser system. Therefore the influence of laser fluence on the measured temperatures was not significant for the 2c/2d PLIF-Thermography measurements presented in this work.

Fig. 5.8b shows the influence of laser fluence on the spatial standard deviation of the measured temperatures. The spatial standard deviation was used as a measure for the homogeneity of the temperature distribution measured. A higher value stands for a higher inhomogeneity. For laser fluence other than the one used for calibration the spatial standard deviation slightly increased.

The reason for this was most likely the photo response non-uniformity of the used detectors. Each pixel of the detectors has a slightly different gain. The different gain was compensated for by the gray values occurring during calibration. At other gray values the inhomogeneities are not completely compensated and become stronger with increasing difference from the gray values occurring during calibration. With a change of the laser fluence the gray values were altered compared to the calibration. Therefore the inhomogeneity increased the more the laser fluence was changed. The behavior of the spatial standard deviation was almost identical with its behavior observed for the different dye concentrations. Since the same gray value range of the detectors was used in both cases a similar behavior is an indication that it is caused by the photo-response non-uniformity rather than by the laser fluence or the dye concentration itself.

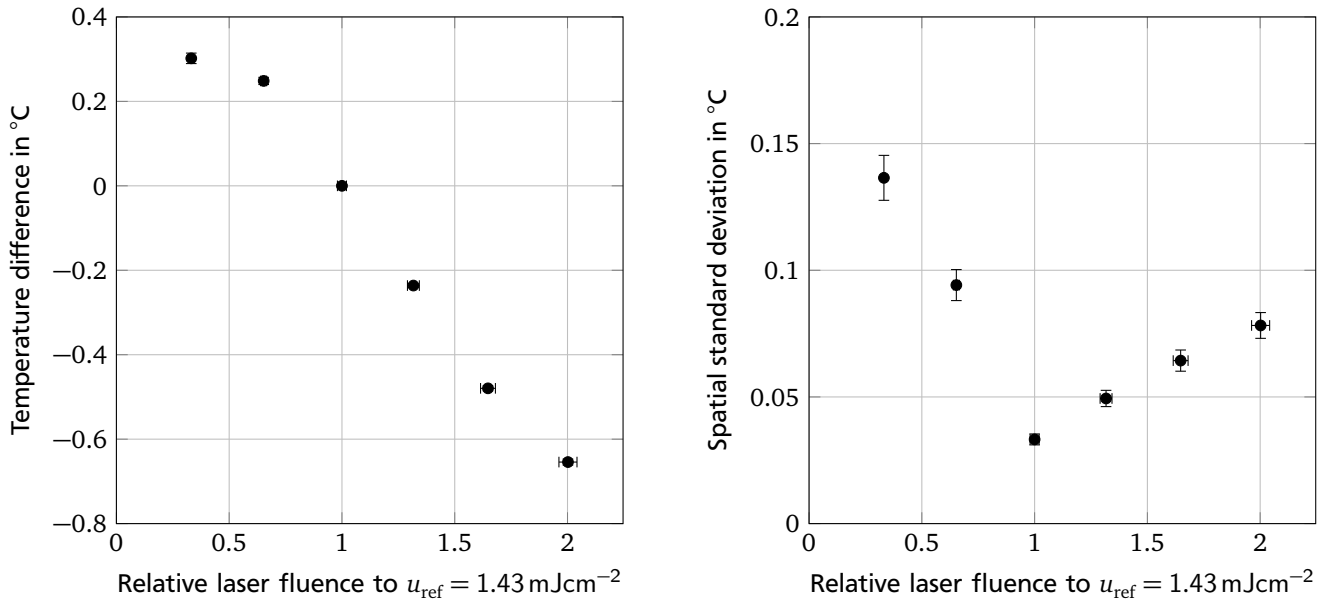

(a) Temperature difference from the temperature measured at the laser fluence used for the calibration versus laser fluence.

(b) Spatial standard deviation versus laser fluence.

Figure 5.8: Influence of the laser fluence on the temperature measured with 2c/2d PLIF-Thermography (a) and the spatial standard deviation (b).

5.7 Estimation of Energy Input and Temperature Change by the Laser Light

In this section the energy input to the ethanol dye solution by the laser light is estimated by an energy balance. Based on this the temperature change of the dye solution arising from the change of the inner energy is calculated.

With the assumptions of a homogeneous energy input throughout the illuminated volume and no heat transfer to the surrounding ethanol, the change of the inner energy ΔU and the temperature change ΔT of the illuminated ethanol are given by:

$$\Delta U = (1-\Phi)\, E_{\mathrm{P}}\, N_{\mathrm{P}}\, a\, b\, 10^5\,\mathrm{m^{-2}} \left(1 - 10^{-d\,(C_{\mathrm{Rh6G}}\,\varepsilon_{\mathrm{Rh6G}} + C_{\mathrm{Py1}}\,\varepsilon_{\mathrm{Py1}})}\right) \tag{5.2}$$

$$\Delta T = \frac{\Delta U}{a\, d\, b\, \rho_{\mathrm{EtOH}}\, c_{\mathrm{EtOH}}} \tag{5.3}$$

where Φ is the quantum yield; $E_{\mathrm{P}} = 113\,\mu\mathrm{J}$, the laser pulse energy; $N_{\mathrm{P}} = 1500$, the number of laser pulses used for one image; $a = 10\,\mathrm{mm}$, the used height of the laser light sheet; $b = 642\,\mu\mathrm{m}$, the thickness of the laser light sheet; $10^5\,\mathrm{m^{-2}}$, the normalized fluence in the used region of the light sheet; $d = 6.4\,\mathrm{mm}$, the optical path length for the absorption of

the laser light; $C_{\mathrm{Rh6G}} = 2.5\,\mu\mathrm{gL}^{-1}$ and $C_{\mathrm{Py1}} = 18.4\,\mu\mathrm{gL}^{-1}$, the fluorescent dyes' concentrations; $\varepsilon_{\mathrm{Rh6G}} = 6.2 \times 10^4\,\mathrm{Lmol}^{-1}\mathrm{cm}^{-1}$ and $\varepsilon_{\mathrm{Py1}} = 1.9 \times 10^4\,\mathrm{Lmol}^{-1}\mathrm{cm}^{-1}$, the fluorescent dyes' absorption coefficients at the laser wavelength; $\rho_{\mathrm{EtOH}} = 789\,\mathrm{kgm}^{-3}$, the ethanol's density and $c_{\mathrm{EtOH}} = 2.43\,\mathrm{kJkg}^{-1}\mathrm{K}^{-1}$, the ethanol's specific thermal capacity.

With the assumption of a quantum yield of $\Phi = 90\,\%$ the change of the inner energy during the acquisition of one image is in the order of 20 µJ and the temperature change is in the order of 0.25 mK. Therefore based on this estimation the energy input by the laser seems to have no significant influence on the measured temperature since the effect is well below the measurement uncertainty.

5.8 Temperature Measurements at the Evaporating Liquid Meniscus

Fig. 5.9 shows three representative results of the 2c/2d PLIF-Thermography measurements at the stationary evaporating meniscus with an increasing amount of wall superheat and therefore an increasing evaporation rate. The temperature of the water t_{Water} used to heat the evaporator walls was varied from 25 °C to 27 °C in steps of 1 °C. In this range the wall superheat was increasing from 0.5 °C to 1 °C. A higher amount of wall superheat was not possible because of oscillations of the liquid-vapor interface and the occurrence of nucleate boiling when the temperature of the evaporator rose above 27 °C.

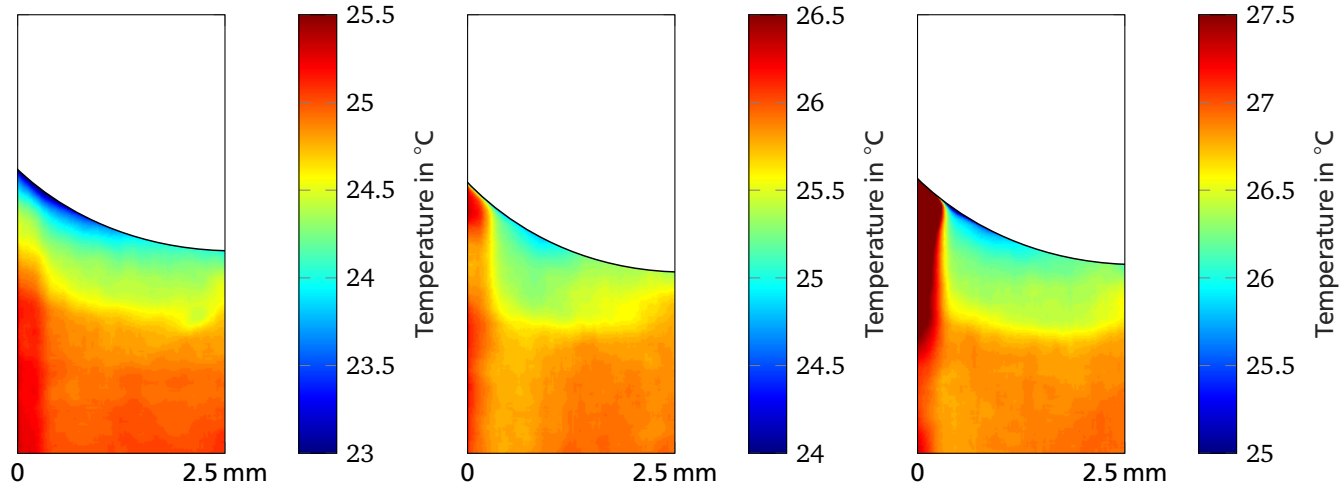

(a) $t_{\mathrm{Water}} = 25.0\,°\mathrm{C}$, $t_{\mathrm{sat}} = 24.5\,°\mathrm{C}$ **(b)** $t_{\mathrm{Water}} = 26.0\,°\mathrm{C}$, $t_{\mathrm{sat}} = 25.3\,°\mathrm{C}$ **(c)** $t_{\mathrm{Water}} = 27.0\,°\mathrm{C}$, $t_{\mathrm{sat}} = 26.0\,°\mathrm{C}$

Figure 5.9: Temperature distribution measured with 2c/2d PLIF-Thermography at a stationary evaporating meniscus with an increasing amount of wall superheat.

In all three cases the temperature distribution was quite similar. The bulk had an almost constant temperature similar to the temperature of the water used to heat the evaporator. In a region of approximately 1 mm thickness close to the liquid-vapor interface the temperature decreased

to approximately saturation temperature. The lowest temperature occurred in all three cases at the liquid-vapor interface. Directly at the liquid-vapor interface temperatures slightly lower than the saturation temperature t_{sat} calculated from the measured system pressure were measured. In the experiment with the lowest wall superheat the temperature distribution at the wall is similar to the distribution further away from the wall. In the experiment with medium wall superheat the temperatures at the wall matched the temperature of the bulk all the way up to the liquid-vapor interface. In the experiment with with the highest evaporation rate the measured temperature at the wall reached values higher than the temperature of the water used to heat the evaporator. In the region of the wall close to the liquid-vapor interface temperatures of up to 32 °C were measured. Since the water used to heat the evaporator only had a temperature of 27 °C the occurrence of higher temperatures is physically not tenable. Obviously a measurement error of the 2c/2d PLIF-Thermography was encountered in this case.

Fig. 5.10 shows the fluorescence signal detected by the detector of the channel-based imaging spectrometer, which is almost insensitive to temperature. It suggests that the fluorescence signal is mostly a function of the local dye concentration and the local laser fluence. For the first two temperature levels of the evaporator the distribution of the fluorescence signal was quite spatially homogeneous. For the last case the fluorescence signal in the corner of the meniscus where the vapor-liquid interface meets the wall of the evaporator the fluorescence signal was much higher than the rest of in the image.

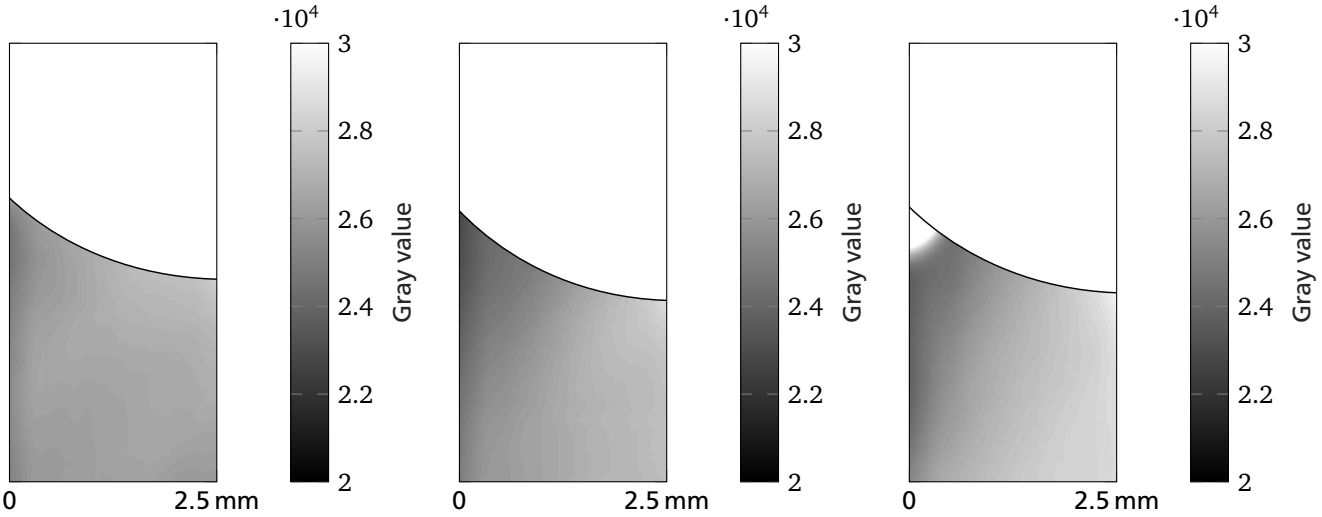

(a) $t_{Water} = 25.0\,°C$, $t_{sat} = 24.5\,°C$ **(b)** $t_{Water} = 26.0\,°C$, $t_{sat} = 25.3\,°C$ **(c)** $t_{Water} = 27.0\,°C$, $t_{sat} = 26.0\,°C$

Figure 5.10: Gray value distribution measured with the detector insensitive to temperature of the channel-based imaging spectrometer at a stationary evaporating meniscus with an increasing amount of wall superheat.

Since in the region discussed the laser fluence is quite constant, it is assumed that the magnitude of the fluorescence signal is dominated by the dye concentration. Therefore the high fluorescence signal seems to originate from an increased dye concentration in this region. This local

increase is most likely caused by the evaporation of the solvent, which seems to be strongest in this region. Since the erroneous measured temperatures occurred in the region with the increased concentration of the fluorescent dyes a causal relationship seems to be likely.

With the results of the influence of the dyes' concentrations on the measured temperature with the 2c/2d PLIF-Thermography under the assumption of a constant mass concentration ratio such a deviation can not be explained either in magnitude or in algebraic sign. Therefore it is assumed that the assumption of a constant mass concentration ratio of the two fluorescent dyes is violated locally in the case of evaporation.

The reason for this could be the different diffusion rates of the two dyes, which would lead to a shift of the mass concentration ratio if a concentration gradient is present. Since Pyridine 1 has the lower molar mass, it is assumed to have a higher diffusion coefficient compared to Rhodamine 6G. Under this assumption the mass concentration ratio would be shifted in the region of high concentration to a lower value, which would in turn lead to a lower ratio of the fluorescence signals and thus a higher measured temperature. Because the diffusion coefficients of the two dyes and their local concentrations are unknown it is not possible to calculate the shift of the concentration ratio. But a decrease of the mass concentration ratio of 17 % would lead to an increase of the measured temperature of approximately 10 °C. If the diffusion coefficients are assumed to be proportional to the molar mass of the dyes, a change of the concentration ratio of this amount would be reasonable. Since the initial concentrations are not the same for both fluorescent dyes also the concentration gradients would be different if the concentration rises locally due to evaporation. In this case the concentration gradient of Pyridine 1 would be higher because of its higher initial concentration. This would also lead to a shift of of the concentration ratio to lower values in the region of high dye concentration and thus a higher measured temperature. Apart from different diffusion rates also other effects might be involved e.g. convection or dye molecules leaving the liquid together with the evaporating ethanol.

Outside the region where the measurement error was encountered the temperature distribution close to the liquid-vapor interface is qualitatively in good agreement with results found in literature. Buffone and Sefiane [8] and Buffone, Sefiane, and Minetti [12] investigated the temperature distribution on the liquid-vapor interface of an evaporating ethanol meniscus located inside a capillary tube. They also observed the lowest temperature in the region in which the liquid-vapor interface meets the wall. Starting from this point they also observed a rising temperature towards the middle of capillary tube on the liquid-vapor interface.

Wang, Murthy, and Garimella [58] performed a numerical investigation of an evaporating methanol meniscus located inside a capillary tube. The temperature distribution inside the liquid calculated by them is qualitatively also in good agreement with the results presented here. They also observed the lowest temperature in the region where the liquid-vapor interface

meets the wall. In the middle of the capillary tube they also observed that the warmer liquid from the bulk region is pushed towards the liquid-vapor interface due to convection.

5.9 Conclusion

The investigation of the 2c/2d PLIF-Thermography showed that the calibration of the 2c/2d PLIF-Thermography is possible with high precision with the second-order polynomial approach. With the achieved temperature uncertainty of 0.2 °C the temperature differences expected during evaporation could be resolved. Also the achieved spatial resolution of 14 µm was sufficient for the investigation at the stationary evaporating meniscus. The investigations of the influence of the dye concentration and the laser fluence on the measured temperatures revealed that an additional radiometric calibration of the individual sCMOS detectors could be beneficial to reduce the influence of the signal height on the validity of the calibration caused by the photoresponse non-uniformity of the detectors used. The influence on the measured temperature due to different amounts of re-absorption of the fluorescence signal when it passes the dye solution on its way to the detector has been shown to be negligible in the dynamic range of the detectors for the path length and the low dye concentrations used.

However, based on the results of the investigation of the 2c/2d PLIF-Thermography at the stationary evaporating meniscus a reliable application of the 2c/2d PLIF-Thermography during evaporation was not possible in and close to the region where the liquid-vapor interface meets the wall. Deviations of the measured temperatures in the order of 10 °C were observed. The reason for this is most likely the violation of the assumption of a constant mass concentration ratio of the dye concentrations. Outside the region where the temperature deviations were observed valid temperature measurements seem to be possible. The obtained results are qualitatively in good agreement with results found in literature.

6 Summary and Outlook

In this chapter a brief summary of the content and the main results of this work are given. Additionally the open scientific questions arising from the findings of this work which are worthy of further investigation are described at the end of this chapter. The focus is put on questions that could be addressed with no or only minor changes to the experimental setup designed and implemented in the context of this work.

6.1 Summary

Two dye combinations suitable for 2c/2d PLIF-Thermography in ethanol were investigated in detail regarding the influence of temperature, laser fluence, dye concentration, photobleaching, pressure, and dissolved air/oxygen. The two dye combinations investigated were Rhodamine 6G combined with DCM and Rhodamine 6G combined with Pyridine 1. The investigation of the dye combinations was used to determine parameter ranges for laser fluence and dye concentration in which the linearity assumptions required for 2c/2d PLIF-Thermography are valid. Based on the investigations the dye combination Rhodamine 6G and Pyridine 1 dissolved in ethanol was chosen for the investigations regarding the applicability of 2c/2d PLIF-Thermography to evaporation processes, because of its superior dependence on temperature. A high dependence on temperature was needed in order to meet the requirement regarding a low temperature measurement uncertainty.

A channel-based imaging spectrometer with two spectral channels was designed and implemented for the 2c/2d PLIF-Thermography. sCMOS cameras were used as detectors for the fluorescence signal. The channel-based imaging spectrometer had a spatial resolution of 14 µm per pixel. For the excitation of the fluorescent dyes a laser light sheet was generated by a high-repetition-rate pulsed frequency-doubled Nd:YAG laser system which was synchronized with the detectors of the channel-based imaging spectrometer. The high repetition rate of the laser was used for a multiple excitation of the fluorescent dyes during the exposure time of the channel-based imaging spectrometer in order to increase the signal-to-noise ratio within the linear regime of low laser fluence.

Experimental and data evaluation procedures for the calibration and the evaluation of 2c/2d PLIF-Thermography measurement data were developed and implemented. An exponential

and a second-order polynomial approach for the calibration and evaluation of the 2c/2d PLIF-Thermography measurement data were implemented and compared with each other regarding the representation of the calibration data. The second-order polynomial model showed a superior performance and therefore was chosen to be used for this work. For the chosen calibration approach validation measurements were performed which showed that the second-order polynomial model is a valid description of the measurement data in the measurement range. The analysis of the temperature measurement uncertainty of the 2c/2d PLIF-Thermography showed that the measurement uncertainty was dominated by the photon noise and therefore can mainly be improved by an increase of the detected photons, e.g. by temporal averaging. With the settings used for the measurements in this work a confidence interval of 0.2 °C at a confidence level of 95 % could be reached for the 2c/2d PLIF-Thermography.

To analyze the applicability of the 2c/2d PLIF-Thermography to evaporation processes a stationary evaporating liquid meniscus was chosen as test scenario. A stationary evaporating liquid meniscus was chosen because it is considered to be the simplest representation of the evaporation process which includes most of the physical phenomena. An experimental setup was designed and implemented which allowed the investigation of the applicability of the 2c/2d PLIF-Thermography to a stationary evaporating liquid meniscus. The setup enabled the investigations at a stationary evaporating liquid meniscus in a closed, single-species system in a temperature range of 21 °C to 31 °C.

The investigations at the stationary evaporating liquid meniscus revealed that a reliable application of the 2c/2d PLIF-Thermography to evaporation processes is not possible. Only for very low evaporation rates temperature measurements seem to be possible in and close to the region where the liquid-vapor interface meets the wall. For higher evaporation rates the measured temperatures deviated significantly locally to higher temperatures which exceeded the applied evaporator temperature and can therefore be regarded as erroneous. The deviations were observed in and close to the region where the liquid-vapor interface meets the evaporator wall. In this region an increase of the fluorescence signal could be observed. This was most likely caused by the accumulation of fluorescent dyes induced by the evaporation process. Outside the region where the temperature deviations were observed valid temperature measurements seem to be possible. The obtained results are qualitatively in good agreement with results found in literature.

An analysis regarding the origin of these deviations leads to the conclusion that they are most likely caused by a local violation of the assumption of a constant concentration ratio of the two dyes. The local dye concentration ratio is assumed to be shifted by the different diffusion rates of the two fluorescent dyes. Therefore any 2c/2d PLIF-Thermography application to evaporation processes would be compromised by the drawback that it cannot be guaranteed that the

concentration ratio is locally constant in and close to the region where the liquid-vapor interface meets the wall.

6.2 Outlook

The present 2c/2d PLIF-Thermography setup and the data evaluation procedures could be used without any changes for 2c/2d PLIF-Thermography for measurements where a constant concentration ratio of the two dyes can be assured. This could be measurements regarding every kind of convection, e.g. natural convection, forced convection, and a mixture of both. It could also be applied to evaporation processes with the limitations described in this work.

Since the deviations of measured temperature by 2c/2d PLIF-Thermography most likely originate from the shifted concentration ratio of the two dyes, the applicability of two-color/one-dye (2c/1d) PLIF-Thermography to evaporation processes could be investigated. Because for 2c/1d PLIF-Thermography only one fluorescent dye is used, the drawback of the changing concentration ratio with 2c/2d PLIF-Thermography could be overcome. For the investigation of the applicability of 2c/1d PLIF-Thermography to evaporation processes only the optical filters used to separate the fluorescence signals would have to be changed. As fluorescent dye Rhodamine B in water could be used since its usage for 2c/1d PLIF-Thermography is well reported in literature together with the necessary optical filters [6]. The major question in the case of 2c/1d PLIF-Thermography would be whether a measurement uncertainty low enough to sufficiently resolve the temperature differences during evaporation could be achieved. Since Rhodamine B in water suffers from a large overlap of the emission and the absorption band in the region used for the 2c/1d PLIF-Thermography, attention has to be paid to the temperature deviations arising from this if the concentration is changing due to evaporation. All necessary investigations could be done with the present setup and data evaluation procedures following the methodology presented in this work.

This work is focused on the technical aspect of the applicability of 2c/2d PLIF-Thermography to evaporation processes. The question of whether the results that could be achieved by PLIF-Thermography are affected by the fluorescent dyes is not addressed. First preliminary investigations conducted in the context of this work regarding the influence on surface tension and contact angle of dissolved Pyridine 1 and Rhodamine 6G in ethanol did not show a significant influence. Also an influence of the dyes Pyridine 1 and Rhodamine 6G dissolved in ethanol on its saturation pressure could not be observed. Further investigation of how the evaporation process is affected by the fluorescent dyes and their accumulation close to the liquid-vapor interface is needed.

Bibliography

[1] Arden, Jutta et al. “Fluorescence and lasing properties of rhodamine dyes”. In: *Journal of Luminescence* 48-49.PART 1 (Jan. 1991), pp. 352–358. ISSN: 00222313. DOI: 10.1016/0022-2313(91)90137-K. URL: http://linkinghub.elsevier.com/retrieve/pii/002223139190137K.

[2] Atkins, Peter W. and Paulo, Julio de. *Physikalische Chemie*. Wiley-VCH-Verl, 2013, p. 1029. ISBN: 978-3-527-33247-2.

[3] Basu, Sekhar and Rohatgi-Mukherjee, K.K. “Temperature dependence of fluorescence quantum yields of some side-substituted anthracene sulphonates”. In: *Journal of Luminescence* 29.1 (Jan. 1984), pp. 39–45. ISSN: 00222313. DOI: 10.1016/0022-2313(84)90039-5. URL: http://linkinghub.elsevier.com/retrieve/pii/0022231384900395.

[4] Berendsen, Herman J. C. *A Student’s Guide to Data and Error Analysis*. Cambridge: Cambridge University Press, 2011. ISBN: 9780511921247. DOI: 10.1017/CBO9780511921247. URL: http://ebooks.cambridge.org/ref/id/CBO9780511921247.

[5] Bork, Benjamin Sebastian. “Tropfenverdampfung in transkritischer Umgebung: Untersuchung mit laserspektroskopischen Methoden”. PhD thesis. Darmstadt: Technische Universit{ä}t Darmstadt, 2017. URL: http://tuprints.ulb.tu-darmstadt.de/6015/.

[6] Bruchhausen, Matthias, Guillard, Fabrice, and Lemoine, Fabrice. “Instantaneous measurement of two-dimensional temperature distributions by means of two-color planar laser induced fluorescence (PLIF)”. In: *Experiments in Fluids* 38.1 (Dec. 2005), pp. 123–131. ISSN: 0723-4864. DOI: 10.1007/s00348-004-0911-2. URL: http://link.springer.com/10.1007/s00348-004-0911-2.

[7] Buffone, C. and Sefiane, K. “Investigation of thermocapillary convective patterns and their role in the enhancement of evaporation from pores”. In: *International Journal of Multiphase Flow* 30.9 (Sept. 2004), pp. 1071–1091. ISSN: 03019322. DOI: 10.1016/j.ijmultiphaseflow.2004.05.010. URL: http://dx.doi.org/10.1016/j.ijmultiphaseflow.2004.05.010.

[8] Buffone, C. and Sefiane, K. “IR measurements of interfacial temperature during phase change in a confined environment”. In: *Experimental Thermal and Fluid Science* 29.1 (Dec. 2004), pp. 65–74. ISSN: 08941777. DOI: 10.1016/j.expthermflusci.2004.02.004. URL: http://dx.doi.org/10.1016/j.expthermflusci.2004.02.004.

[9] Buffone, C. and Sefiane, K. “Temperature measurement near the triple line during phase change using thermochromic liquid crystal thermography”. In: *Experiments in Fluids* 39.1 (May 2005), pp. 99–110. ISSN: 0723-4864. DOI: 10.1007/s00348-005-0986-4. URL: http://link.springer.com/10.1007/s00348-005-0986-4.

[10] Buffone, C. and Sefiane, K. “Controlling evaporative thermocapillary convection using external heating: An experimental investigation”. In: *Experimental Thermal and Fluid Science* 32.6 (May 2008), pp. 1287–1300. ISSN: 08941777. DOI: 10.1016/j.expthermflusci.2008.02.009. URL: http://dx.doi.org/10.1016/j.expthermflusci.2008.02.009.

[11] Buffone, C., Sefiane, K., and Christy, J.R.E. “Experimental investigation of the hydrodynamics and stability of an evaporating wetting film placed in a temperature gradient”. In: *Applied Thermal Engineering* 24.8-9 (June 2004), pp. 1157–1170. ISSN: 13594311. DOI: 10.1016/j.applthermaleng.2003.10.038. URL: http://www.sciencedirect.com/science/article/pii/S1359431104000304.

[12] Buffone, Cosimo, Sefiane, Khellil, and Minetti, Christophe. “The effect of wall thickness and material on Marangoni driven convection in capillaries”. In: *Colloids and Surfaces A: Physicochemical and Engineering Aspects* 481 (Sept. 2015), pp. 384–392. ISSN: 09277757. DOI: 10.1016/j.colsurfa.2015.05.050. URL: http://dx.doi.org/10.1016/j.colsurfa.2015.05.050%20http://linkinghub.elsevier.com/retrieve/pii/S0927775715004458.

[13] Chaze, William et al. “The saturation of the fluorescence and its consequences for laser-induced fluorescence thermometry in liquid flows”. In: *Experiments in Fluids* 57.4 (Apr. 2016), p. 58. ISSN: 0723-4864. DOI: 10.1007/s00348-016-2142-8.

[14] Coppeta, J. and Rogers, C. “Dual emission laser induced fluorescence for direct planar scalar behavior measurements”. In: *Experiments in Fluids* 25.1 (1998), pp. 1–15. ISSN: 07234864. DOI: 10.1007/s003480050202. URL: https://link.springer.com/article/10.1007/s003480050202.

[15] Crimaldi, J. P. “Planar laser induced fluorescence in aqueous flows”. In: *Experiments in Fluids* 44.6 (June 2008), pp. 851–863. ISSN: 0723-4864. DOI: 10.1007/s00348-008-0496-2. URL: http://link.springer.com/10.1007/s00348-008-0496-2.

[16] Dhavaleswarapu, Hemanth K., Garimella, Suresh V., and Murthy, Jayathi Y. “Microscale Temperature Measurements Near the Triple Line of an Evaporating Thin Liquid Film”. In: *Journal of Heat Transfer* 131.6 (2009), p. 061501. ISSN: 00221481. DOI: 10.1115/1.3090525. URL: http://link.aip.org/link/JHTRAO/v131/i6/p061501/s1%7B%5C&%7DAgg=doi%20http://heattransfer.asmedigitalcollection.asme.org/article.aspx?articleid=1475093.

[17] Dillon, H. E. and Penoncello, S. G. “A fundamental equation for calculation of the thermodynamic properties of ethanol”. In: *International Journal of Thermophysics* 25.2 (2004), pp. 321–335. ISSN: 0195928X. DOI: 10.1023/B:IJOT.0000028470.49774.14. URL: https://link.springer.com/article/10.1023/B:IJOT.0000028470.49774.14.

[18] Duarte, F. J. (Frank J.) and Hillman, Lloyd William. *Dye laser principles, with applications*. Academic Press, 1990, p. 456. ISBN: 9780122227004. URL: http://www.sciencedirect.com/science/book/9780122227004.

[19] Francisco J. Duarte, ed. *High-Power Dye Lasers*. Vol. 65. Springer Series in Optical Sciences. Berlin, Heidelberg: Springer Berlin Heidelberg, 1991. ISBN: 978-3-662-13813-7. DOI: 10.1007/978-3-540-47385-5. URL: http://link.springer.com/10.1007/978-3-540-47385-5.

[20] Eckbreth, Alan C. *Laser diagnostics for combustion temperature and species*. 2nd ed. Taylor and Francis, 1996, p. 630. ISBN: 2-88449-225-9.

[21] Estrada-Perez, Carlos E., Tan, Sinchao, and Hassan, Yassin A. “Whole-Field Temperature and Velocity Measurements for Two-Phase Flow Using PIV/LIF”. In: *ASME/JSME 2011 8th Thermal Engineering Joint Conference*. Vol. 2011. 38921. ASME, 2011, T10100–T10100–11. ISBN: 978-0-7918-3892-1. DOI: 10.1115/AJTEC2011-44507. URL: http://link.aip.org/link/abstract/ASMECP/v2011/i38921/pT10100/s1%20http://proceedings.asmedigitalcollection.asme.org/proceeding.aspx?articleid=1622297.

[22] European Machine Vision Association. *EMVA Standard 1288 Standard for Characterization of Image Sensors and Cameras*. 2010. URL: http://www.emva.org/standards-technology/emva-1288/.

[23] Fenner, Andreas and Stephan, Peter. “Two dye combinations suitable for two-color/two-dye laser-induced fluorescence thermography for ethanol”. In: *Experiments in Fluids* 58.6 (June 2017), p. 65. ISSN: 0723-4864. DOI: 10.1007/s00348-017-2349-3. URL: http://link.springer.com/10.1007/s00348-017-2349-3.

[24] Fischer, Sebastian. “Experimental Investigation of Heat Transfer during Evaporation in the Vicinity of Moving Three-Phase Contact Lines”. PhD thesis. TU Darmstadt, 2015. URL: http://tuprints.ulb.tu-darmstadt.de/4396/.

[25] Funatani, S, Fujisawa, N, and Ikeda, H. “Simultaneous measurement of temperature and velocity using two-colour LIF combined with PIV with a colour CCD camera and its application to the turbulent buoyant plume”. In: *Measurement Science and Technology* 15.5 (May 2004), pp. 983–990. ISSN: 0957-0233. DOI: 10.1088/0957-0233/15/5/030. URL: http://stacks.iop.org/0957-0233/15/i=5/a=030%20http://stacks.iop.org/0957-0233/15/i=5/a=030?key=crossref.b0e7f540173f51086a9f19d04b0e7a69.

[26] Heldt, J.R. and Diehl, H. “Temperature dependence of fluorescence quantum yield, decay time and intersystem crossing activation energy of 9-acetoxy-10-acetoxyhalogenphenylanthracene derivatives”. In: *Journal of Molecular Structure* 142 (Mar. 1986), pp. 183–188. ISSN: 00222860. DOI: 10.1016/0022-2860(86)85091-8. URL: http://linkinghub.elsevier.com/retrieve/pii/0022286086850918.

[27] Hishida, K and Sakakibara, J. “Combined planar laser-induced fluorescence-particle image velocimetry technique for velocity and temperature fields”. In: *Experiments in Fluids* 29.0 (2000), S129–S140. ISSN: 0723-4864. URL: http://dx.doi.org/10.1007/s003480070015.

[28] Höhmann, C and Stephan, P. “Microscale temperature measurement at an evaporating liquid meniscus”. In: *Experimental Thermal and Fluid Science* 26.2-4 (June 2002), pp. 157–162. ISSN: 08941777. DOI: 10.1016/S0894-1777(02)00122-X. URL: http://dx.doi.org/10.1016/S0894-1777(02)00122-X%20http://linkinghub.elsevier.com/retrieve/pii/S089417770200122X.

[29] Ibrahem, Khalid et al. “Experimental and numerical investigation of evaporative heat transfer in the vicinity of the 3-phase contact line”. In: *2010 3rd International Conference on Thermal Issues in Emerging Technologies Theory and Applications*. IEEE, Dec. 2010, pp. 207–215. ISBN: 978-1-61284-268-4. DOI: 10.1109/THETA.2010.5766400. URL: http://ieeexplore.ieee.org/lpdocs/epic03/wrapper.htm?arnumber=5766400.

[30] Ibrahem, K. et al. “Experimental investigation of evaporative heat transfer characteristics at the 3-phase contact line”. In: *Experimental Thermal and Fluid Science* 34.8 (Nov. 2010), pp. 1036–1041. ISSN: 08941777. DOI: 10.1016/j.expthermflusci.2010.02.014. URL: http://linkinghub.elsevier.com/retrieve/pii/S0894177710000622.

[31] Ibrahem, K. et al. “Experimental Investigation of Micro-Scale Heat Transfer at an Evaporating Moving 3-Phase Contact Line”. In: *2010 14th International Heat Transfer Conference, Volume 3*. ASME, Jan. 2010, pp. 783–790. ISBN: 978-0-7918-4938-5. DOI: 10.1115/IHTC14-22280. URL: http://proceedings.asmedigitalcollection.asme.org/proceeding.aspx?articleid=1620298.

[32] Jones, B. J. “Fundamental studies of thermal transport and liquid-vapor phase change using microscale diagnostic techniques”. Ph.D. Purdue University, 2010. URL: http://docs.lib.purdue.edu/dissertations/AAI3444576/.

[33] Kim, H.J., Kihm, K.D., and Allen, J.S. “Examination of ratiometric laser induced fluorescence thermometry for microscale spatial measurement resolution”. In: *International Journal of Heat and Mass Transfer* 46.21 (Oct. 2003), pp. 3967–3974. ISSN: 00179310. DOI: 10.1016/S0017-9310(03)00243-6. URL: http://linkinghub.elsevier.com/retrieve/pii/S0017931003002436.

[34] Kubin, R.F. and Fletcher, A.N. “Fluorescence quantum yields of some rhodamine dyes”. In: *Journal of Luminescence* 27.4 (Dec. 1982), pp. 455–462. ISSN: 00222313. DOI: 10.1016/0022-2313(82)90045-X. arXiv: arXiv:1011.1669v3. URL: http://linkinghub.elsevier.com/retrieve/pii/002223138290045X.

[35] Larsen, L. G. and Crimaldi, J. P. “The effect of photobleaching on PLIF”. In: *Experiments in Fluids* 41.5 (2006), pp. 803–812. ISSN: 07234864. DOI: 10.1007/s00348-006-0205-y. URL: https://link.springer.com/article/10.1007/s00348-006-0205-y.

[36] Lavieille, P. et al. “Non-intrusive temperature measurements using three-color laser-induced fluorescence”. In: *Experiments in Fluids* 36.5 (May 2004), pp. 706–716. ISSN: 0723-4864. DOI: 10.1007/s00348-003-0748-0. URL: http://link.springer.com/10.1007/s00348-003-0748-0.

[37] Lee, T.-W. *Thermal and flow measurements*. CRC Press, 2008, p. 390. ISBN: 9780849379703.

[38] Lemoine, F, Wolff, M, and Lebouche, M. “Simultaneous concentration and velocity measurements using combined laser-induced fluorescence and laser Doppler velocimetry: Application to turbulent transport”. In: *Experiments in Fluids* 20.5 (Mar. 1996), pp. 319–327. ISSN: 0723-4864. DOI: 10.1007/BF00191013. URL: https://link.springer.com/article/10.1007/BF00191013.

[39] Lemoine, F. et al. “Simultaneous temperature and 2D velocity measurements in a turbulent heated jet using combined laser-induced fluorescence and LDA”. In: *Experiments in Fluids* 26.4 (1999), pp. 315–323. ISSN: 07234864. DOI: 10.1007/s003480050294. URL: https://link.springer.com/article/10.1007/s003480050294.

[40] Melton, L. A. and Lipp, C. W. “Criteria for quantitative PLIF experiments using high-power lasers”. In: *Experiments in Fluids* 35.4 (Oct. 2003), pp. 310–316. ISSN: 0723-4864. DOI: 10.1007/s00348-003-0632-y. URL: http://link.springer.com/10.1007/s00348-003-0632-y.

[41] Migliaccio, Christopher P., Dhavaleswarapu, Hemanth K., and Garimella, Suresh V. “Temperature measurements near the contact line of an evaporating meniscus V-groove”. In: *International Journal of Heat and Mass Transfer* 54.7-8 (Mar. 2011), pp. 1520–1526. ISSN: 00179310. DOI: 10.1016/j.ijheatmasstransfer.2010.11.040. URL: http://linkinghub.elsevier.com/retrieve/pii/S001793101000654X.

[42] Nasarek, R. “Temperature Field Measurements with High Spatial and Temporal Resolution Using Liquid Crystal Thermography and Laser Induced Fluorescence”. PhD thesis. TU Darmstadt, 2010. URL: http://tuprints.ulb.tu-darmstadt.de/2096/.

[43] Natrajan, V K and Christensen, K T. “Two-color laser-induced fluorescent thermometry for microfluidic systems”. In: *Measurement Science and Technology* 20.1 (Jan. 2008), p. 015401. ISSN: 0957-0233. DOI: 10.1088/0957-0233/20/1/015401. URL: http://stacks.iop.org/0957-0233/20/i=1/a=015401?key=crossref.8e2a35672e946b8eff3b0c3e3a5250f6.

[44] Oster, Gerald and Adelman, Albert H. “Long-Lived States in Photochemical Reactions. I. Photoreduction of Eosin”. In: *Journal of the American Chemical Society* 78.5 (Mar. 1956), pp. 913–916. ISSN: 0002-7863. DOI: 10.1021/ja01586a012. URL: http://pubs.acs.org/doi/abs/10.1021/ja01586a012.

[45] Pishchik, Valerian, Lytvynov, Leonid A., and Dobrovinskaya, Elena R. *Sapphire*. Boston, MA: Springer US, 2009. ISBN: 978-0-387-85694-0. DOI: 10.1007/978-0-387-85695-7. URL: http://link.springer.com/10.1007/978-0-387-85695-7.

[46] Sakakibara, J and Adrian, R J. “Whole field measurement of temperature in water using two-color laser induced fluorescence”. In: *Experiments in Fluids* 26.1 (1999), pp. 7–15. ISSN: 0723-4864. URL: http://dx.doi.org/10.1007/s003480050260.

[47] Sakakibara, J. and Adrian, R.J. “Measurement of temperature field of a Rayleigh-Benard convection using two-color laser-induced fluorescence”. In: *Experiments in Fluids* 37.3 (July 2004), pp. 331–340. ISSN: 0723-4864. DOI: 10.1007/s00348-004-0821-3. URL: http://link.springer.com/10.1007/s00348-004-0821-3.

[48] Sakakibara, J., Hishida, K., and Maeda, M. “Measurements of thermally stratified pipe flow using image-processing techniques”. In: *Experiments in Fluids* 16.2 (1993), pp. 82–96. ISSN: 07234864. DOI: 10.1007/BF00944910. URL: https://link.springer.com/article/10.1007/BF00944910.

[49] Fritz P. Schäfer, ed. *Dye Lasers*. Vol. 1. Topics in Applied Physics. Berlin, Heidelberg: Springer Berlin Heidelberg, 1973. ISBN: 978-3-540-51558-6. DOI: 10.1007/3-540-51558-5. URL: http://link.springer.com/10.1007/3-540-51558-5.

[50] Shan, Jerry W., Lang, Daniel B., and Dimotakis, Paul E. “Scalar concentration measurements in liquid-phase flows with pulsed lasers”. In: *Experiments in Fluids* 36.2 (Feb. 2004), pp. 268–273. ISSN: 0723-4864. DOI: 10.1007/s00348-003-0717-7. URL: http://link.springer.com/10.1007/s00348-003-0717-7.

[51] Song, L. et al. “Photobleaching kinetics of fluorescein in quantitative fluorescence microscopy”. In: *Biophysical Journal* 68.6 (June 1995), pp. 2588–2600. ISSN: 00063495. DOI: 10.1016/S0006-3495(95)80442-X. URL: http://linkinghub.elsevier.com/retrieve/pii/S000634959580442X.

[52] Song, L. et al. “Influence of the triplet excited state on the photobleaching kinetics of fluorescein in microscopy”. In: *Biophysical Journal* 70.6 (June 1996), pp. 2959–2968. ISSN: 00063495. DOI: 10.1016/S0006-3495(96)79866-1. URL: http://linkinghub.elsevier.com/retrieve/pii/S0006349596798661.

[53] Song, Xudong. “Experimental investigation of evaporation-induced convection in water using laser based measurement techniques”. PhD thesis. University of Alberta, Sept. 2010. DOI: 10.1016/j.expthermflusci.2011.01.010. URL: http://linkinghub.elsevier.com/retrieve/pii/S0894177711000215.

[54] Song, Xudong and Nobes, David S. “Experimental investigation of evaporation-induced convection in water using laser based measurement techniques”. In: *Experimental Thermal and Fluid Science* 35.6 (Sept. 2011), pp. 910–919. ISSN: 08941777. DOI: 10.1016/j.expthermflusci.2011.01.010. URL: http://dx.doi.org/10.1016/j.expthermflusci.2011.01.010.

[55] Sutton, Jeffrey A., Fisher, Brian T., and Fleming, James W. “A laser-induced fluorescence measurement for aqueous fluid flows with improved temperature sensitivity”. In: *Experiments in Fluids* 45.5 (June 2008), pp. 869–881. ISSN: 0723-4864. DOI: 10.1007/s00348-008-0506-4. URL: https://link.springer.com/article/10.1007/s00348-008-0506-4.

[56] Valeur, Bernard. *Molecular Fluorescence: Principles and Applications*. Wiley-VCH, 2013, p. 569. ISBN: 3527328378.

[57] Vogt, Jan. “Development of novel Particle Image Thermometry methods for highly resolved measurements of temperature and velocity fields in fluids”. PhD thesis. TU Darmstadt, Jan. 2014. URL: http://tuprints.ulb.tu-darmstadt.de/id/eprint/3696.

[58] Wang, Hao, Murthy, Jayathi Y., and Garimella, Suresh V. “Transport from a volatile meniscus inside an open microtube”. In: *International Journal of Heat and Mass Transfer* 51.11-12 (June 2008), pp. 3007–3017. ISSN: 00179310. DOI: 10.1016/j.ijheatmasstransfer.2007.09.011. URL: http://www.sciencedirect.com/science/article/pii/S0017931007005856.

[59] Ware, William R. and Baldwin, Bernard A. “Effect of Temperature on Fluorescence Quantum Yields in Solution”. In: *The Journal of Chemical Physics* 43.4 (Aug. 1965), pp. 1194–1197. ISSN: 0021-9606. DOI: 10.1063/1.1696903. URL: http://link.aip.org/link/JCPSA6/v43/i4/p1194/s1%7B%5C&%7DAgg=doi%20http://aip.scitation.org/doi/10.1063/1.1696903.

[60] Wee, Sang-Kwon. “Microscale observables for heat and mass transport in sub-micron scale evaporating thin film”. PhD thesis. Texas A&M University, 2004. URL: http://oaktrust.

library.tamu.edu/bitstream/handle/1969.1/312/etd-tamu-2004A-MEEN-Wee-1.pdf?sequence=1%7B%5C&%7DisAllowed=y.